Performance Estimation of Oversampled Bio-inspired Velocity Estimator Based on Reichardt Correlator

by

Bin Guo

B.Eng., Northwestern Polytechnical University, China

Thesis submitted for the degree of

Master of Engineering Science

in

School of Electrical and Electronic Engineering
Faculty of Engineering,
Computer and Mathematical Sciences
The University of Adelaide, Australia

May 2010

Typeset in LaTeX 2ε

Bin Guo

to my parents

This page is blank

Contents

This page is blank

Abstract

Inspired by the insects' incredible visual capabilities, many vision motion detection systems were proposed and developed. The Reichardt Correlator, as a bio-inspired vision motion detector is commonly used for velocity estimate of objects. Traditionally, the received signals in receptors in a Reichardt Correlator are digitised at bit depths of 8 or greater and sampled at Nyquist rate. Its implementation requires relatively complicated arithmetic units to cope with the processing of the samples. This is considered as bringing heavy computation burden to the motion detection system.

In this thesis, a new approach for using oversampled, low bit depth representations for velocity estimation using the Reichardt Correlator is developed. This is achieved by considering the trade-off between oversampling ratio and bit depth, commonly found in oversampled data converters. After using real images as stimuli to the Reichardt Correlator, it was found that using lower bit depths and oversampling can retain the accurate velocity estimation performance, and at the same time, reduce the system arithmetic complexity. As a result, a sigma-delta conversion was proposed to pre-process the input signals to the Reichardt Correlator. In this approach, the image information is encoded as 1-bit oversampled representation. The long term aim is to have a scheme whereby the required system arithmetic complexity can be made simpler. In this step, three different panoramic images were used as the stimuli in simulations. The core contribution of this thesis is an investigation between the trade-off in performance and arithmetic complexity using the Reichardt Correlator as a velocity estimator in vision system, rather than elaborating the Reichardt Correlator, which can result in a more complex arithmetic implementation.

The performance of the proposed approach is evaluated by comparing oversampled results with traditional representations. The comparisons results show that the proposed approach can achieve better performance in terms of optimal velocity detection,

under reduced system arithmetic complexity. Because of the image contents, small oscillations and a slight loss in velocity estimation accuracy was observed. Since the approach can reduce system arithmetic complexity are the primary considerations, small oscillations and inaccurate velocity detection can be tolerated.

Statement of Originality

This work contains no material which has been accepted for the award of any other degree or diploma in any university or other tertiary institution to Bin Guo and, to the best of my knowledge and belief, contains no material previously published or written by another person where due reference has been made in the text.

I give consent to this copy of the thesis, when deposited in the University Library, being made available for loan, photocopying, and dissemination through the library digital thesis collection, subject to the provisions of the Copyright Act 1968.

The author acknowledges that copyright of published works contained within this thesis resides with the copyright holder of those works.

I also give permission for the digital version of my thesis to be made available on the web, via the University's digital research repository, the Library catalogue, the Australasian Digital Thesis Program (ADTP) and also through web search engines, unless permission has been granted by the University to restrict access for a period of time.

Signed

Date

This page is blank

Acknowledgments

This thesis could not have been completed without the help and support of a number of people. I would like to take this opportunity to thank them.

First, I would like to thank my supervisor Dr Said Al-Sarawi whose many ideas, guidance and enthusiasm have been a source of motivation to me. He showed me different ways to approach a research problem and the need to be persistent to accomplish any goal. Many thanks must also be given to my co-supervisor Dr Brian Ng, who provided continued support and motivation for my research. It has been so important to get his academic advice and understanding in our regular meetings. In the final step of writing thesis, his unfailing support and guidance gave me the confidence and helped me successfully accomplish my project.

This research has been carried out in the School of Electrical and Electronic Engineering School in University of Adelaide. I would like to acknowledge everyone who made available their assistance, support and advice. I would like to acknowledge Dr Tamath Rainsford for providing some of the images used in this thesis. I would like to thank my colleagues at the room of EM419, Omid Kavehei, Robert Moric, Kiet To, Kyukjin Lee, Ying Sun, for their general moral support throughout my time here, and their willingness to answer questions. I would like to express appreciation to Associate Professor Cheng Chew Lim, Mr. Matthew Trinkle, Zhonghao Hu, Ruiting Yang, Yuexian Wang, Lifang Lu for their valuable help and support.

I would like to thank my friends in Australia, Annie, Celeste, David, Chloe, Cindy, Zifang Liu, Peiqiong Lai, who provided valuable support and companionship in my time in Australia and without whom I would be much lonely in Australia.

Last but not least, I would like to thank my parents for their support throughout my degree, their consistent financial support and encouragement is the basis of my study in Australia. Their love and understanding are always the force which drives me forward.

This page is blank

Conventions

Typesetting

This thesis is typeset in Times New Roman and Sans-Serif using LaTeX2e. Referencing and citation style are based on the Institute of Electrical and Electronics Engineers (IEEE) Transaction style [1].

Spelling

English spelling in this thesis is based on Australian English.

This page is blank

Publications

Conferences

[1] B. Guo, B. W.-H. Ng, and S. Al-Sarawi, "Using sigma-delta conversion for velocity estimation in bio-inspired detection system." Kuala Lumpur, Malaysis: 2010 International Conference on Electronic Devices, Systems and Applications (ICEDSA2010), 11-13 April 2010.

[2] B. Guo, B. W.-H. Ng, and S. Al-Sarawi, "Performance estimation of oversampled low bit depth, bio-inspired motion detection system." Taichung, Taiwan: The 5^{th} IEEE Conference on Industrial Electronics and Applications (ICIEA2010), 15-17 June 2010.

This page is blank

List of Figures

This page is blank

List of Tables

This page is blank

Chapter 1

Introduction

INSPIRED by the insects' incredible visual system, many artificial vision research have focussed on the visual systems of insects to develop artificial visual motion detection systems. These initiatives have benefited from the underlying fundamental aspects of biological vision. The bio-inspired vision systems mimic the insects' visual system, which can offer several advantages in comparison to the traditional camera-processor approach, such as speed, system size and large dynamic range. Through the description of the insects' visual behaviour, the motivation and aims of this research are presented.

1.1 Motivation

The research on bio-inspired motion detection is one of the most active areas in today's engineering field. Directional motion detection demonstrates a response of visual information processing in animals [2]. Many types of biological motion detection systems in animals are used to help them catch a prey, or escape from a predator. In terms of this motion detection, the flying insects are capable of tracking and chasing objects in complex environments with remarkable speed and accuracy, despite their small size and relatively simple visual motion detection systems. Insects can estimate their own movements from the overall movement of their visual field [3]. Humans and other animals can even use the information of motion detection to complete more complex tasks, like distinguishing different objects by relative motion or estimating velocity of objects [4].

Many animals have elaborated motion detection systems as the ability to sense its dynamic environment which is very important for survival. Take flying insects as an example, their brains are very small, typically contain one hundred thousand times fewer neurons than humans [2]. Despite this, insects are capable of carrying out much more complex motion processing from visual stimuli. They can use their visual motion detection system to control flying direction [5], and to navigate and fly through obstacles [6], detect borders between objects [7], find out distance to individual object [8] and total distance moved [9]. In many aspects, insect motion detection systems are far more intelligent than the current artificial robotics systems in the task of motion detection and velocity estimation [10].

On the other hand, along with the development of mixed signal processing and very large scale integration (VLSI) techniques, a number of visual motion detection algorithms have been embedded in vision systems, by integrating photo detectors and digital signal processing elements into a single VLSI chip. One of the main targets of vision chips is achieving a reliable estimate of velocity for objects, or generally, motion detection. There is an ever-growing need for vision systems, which can detect and track targets, navigate and search objects. The applications of motion detection are comprehensive, such as blind spot overtaking monitoring, visual replacement for artificial

intelligence, collision avoidance systems, surveillance, robotics and aerial unmanned vehicles [11, 12].

The research on insect vision systems is considered to provide a key to answering many different aspects of artificial motion detection systems. Because of a large proportion of advanced species' brain is dedicated to visual information processing, the motion detection in flying insects is extremely fast and accurate, typically requiring a few milliseconds for computation [13]. This illustrates the importance of visual information in biological systems. Therefore, researching and understanding of the biological motion detection can offer new ideas to computer vision researchers for elaborating artificial vision system. In fact, through recent research on biological vision, many algorithms for motion detection have been proposed. Some of these algorithms have been structured as models, used in particular biological visual systems for motion detection [14].

The most successful and most frequently applied model amongst the bio-inspired motion detection models is the Reichardt Correlator, which was first proposed by Hessenstein, Reichardt and Varju as a model for motion detection in the beetle Chlorophanus [15]. It has gained widespread application, since a large body of evidence from visual motion experiments support the Reichardt Correlator as a visual model for motion detection in flying insects [2, 3, 13, 16–18]. Moreover, the Reichardt Correlator and its mathematical equivalents also can be applied to model human vision [19], as well as to model pigeon vision [20]. The basic concept of the Reichardt Correlator model is to correlate responses in parallel from two nearby spatial locations after delaying one of the two signals. Chapter 2 will describe the Reichardt Correlator model and its concept of operation in detail.

Currently, there are many vision systems, with inbuilt photo detectors and motion computation processing elements, to implement the task of motion detection. However, some algorithms are very complicated, and have different limitations [21]. Moreover, from system arithmetic complexity and power consumption point of view, a simpler motion computation algorithm is needed to perform fewer mathematical operations, and are consequently preferred over more complex algorithms. Therefore, the

biologically inspired motion detection system, Reichardt Correlator, is further developed in this thesis. Through the proposed approaches of using oversampled, low bit depth to represent the input stimuli for the Reichardt Correlator, to demonstrate the trade-off between system performance and arithmetic complexity.

1.2 Aims of research

In this thesis, computational and analytical approaches to investigate the basic Reichardt Correlator's performance for the task of velocity estimation are proposed. Following this, the aim is to implement the proposed approaches of using different bit depth representations, that are sampled at different oversampling rates to represent the detected stimuli. Since the lower bit depth representation can simplify the complexity of an arithmetic implementation, in order to investigate the performance of velocity estimation, the proposed approaches will be compared with the conventional approaches of using 8 bit representations and Nyquist sampling rate to represent the input signal to the Reichardt Correlator. This will be achieved by reviewing the Reichardt Correlator, using different kinds of images as stimuli in simulations. In the part of simulations, the sine grating images will be used firstly to validate the principle idea, and then, natural and panoramic images will be used to highlight the limitations of the Reichardt Correlator. After that, the proposed approaches are investigated, namely using different bit depth representations, sampling at different oversampled rates for the stimulus signal, then evaluating the correlator response for this proposed approaches. The Reichardt Correlator processing is performed on this oversampled stimuli, with reduced precision of the different bit representations providing a trade-off against increased sampling rate, with expected benefits of reduced realisation costs. At last, through the simulation results on proposed approaches to investigate the trade-off between system performance and arithmetic implementation.

Currently, there are many elaborated Reichardt Correlators published in the literature to improve its reliably in terms of velocity estimation [2, 13, 22]. The core intellectual idea behind this research is to examine the different signal representations and to understand the trade-off in performance and complexity using the Reichardt Correlator

as the velocity estimator in vision system, rather than elaborating the Reichardt Correlator to improve its performance.

1.3 Contribution of research

The focus in this thesis is to investigate the performance and complexity of the velocity estimation using the Reichardt Correlator. Using a full correlation in such estimator is impractical due to massive computational requirements, which precludes their use in hardware implementations due to power requirements. In this thesis, a velocity estimator using reduced data precision is proposed. This exploits oversampling of the input stimulus to achieve lower complexity arithmetic elements compared to full resolution implementation of the velocity estimator. It is found that the system can result in less implementation complexity without increasing a significant loss in performance.

1.4 Thesis organisation

This thesis begins with the introduction in Chapter 1. The background and literature review about the different motion detection algorithms and the Reichardt Correlator model, are presented in Chapter 2. Chapter 3 introduces the principle behind the bit depth, and oversampled representation. Chapter 4 demonstrates the results through simulating the performance of the proposed velocity estimator using real image stimuli. Chapter 5 presents the conclusion and future work.

This page is blank

Chapter 2

Background and Literature Review

MOTION detection in insects' visual system inspired researchers and resulted in numerous algorithms and models. One of these models is the Reichardt Correlator, which mimics two pixels in an insect's eyes. Some background knowledge about different motion detection algorithms and the Reichardt Correlator model will be presented in this chapter. The proposed approach in this thesis will then be presented.

2.1 Mathematical basis for motion detection

Bio-inspired artificial vision study is considered to provide most useful source of ideas for many vision systems which is intended to interact with its environment. This approach to vision research builds on bio-inspired vision by utilising some of the basic observations obtained from the development and implementation of vision algorithms [2]. When developing algorithms, arithmetic complexity issues are often completely ignored. Through review of many motion detection algorithms, Moini [21] had proposed that the driving force behind many motion detection algorithms are reliability and flexibility, for operation in real environment rather than physical implementation. As a result, many algorithms cannot run in real-time even on advanced computers.

In real-time, motion cues provide a very valuable source of visual information. Tracking a target in a cluttered environment requires extensive computational architecture. In nature, even a small housefly is adept at pursing its prey with fast and accurate speed, and so bio-mimetic algorithms are a novelty and potentially a fruitful way of looking at this problem. In order to avoid collisions or become the food source of predators, flying insects have to sense their position and ego-motion with regard to the objects in three dimensional environment that surround them. Since the objects in the environment can move, animals are also required to detect motion, which means they need to estimate the velocity of the input signals at the receptors, in the animal's motion detection system. Typically, the receptors used for motion detection system are arranged in a two dimensional array, therefore, the visual information that are available to the animal's motion analysis system relates to the projection of three dimensional velocity vectors on the two dimensional image plane of the receptor array [23]. If the motion need to be analysed, the first step is to estimate the apparent object images' motion in the image plane, or its image motion field. Then, motion field is estimated in the image plane spanned by the observer's photo receptors, and the three dimensional velocity field needs to be derived from the two dimensional motion field. After that, by combining these outputs of motion analysis with position evaluation, it will allow

an insect to estimate its ego-motion in the environment and motion of objects which is detectable by the receptor array.

In the literature, many motion detection models have been developed. There is a larger number of computational models for motion detection, all these motion field estimation needs the input of at least two image instances in time, which need to be compared with each other. According to this requirement, motion detection models can be classified into three fundamentally different groups in this identification process: intensity-based, feature-based and correlation-based. Intensity-based algorithms use some linearly-filtered version of the image brightness for motion processing [24]. In feature-based algorithms, some features in the image such as corners, edges, blobs and templates are found, and tracked over time [25]. In correlation-based algorithms, either the raw image or the processed image is correlated with the previous frame to find a movement in the image [26].

However, these approaches have their shortcomings [21]. The main problem in intensity-based algorithms is known as the aperture problem. Since it looks at localised processing without any concern about the structure of the whole image, whereby the direction of motion of an object cannot be determined uniquely, when looked at from a small aperture. Feature-based algorithms face the correspondence problem, where the feature in one frame are to be matched with corresponding features in the previous frame. A particular concern with correlation-based detection in some applications is the hefty computation requirements of computing the correlation sequences. In the following section, more details about the three motion detection approaches will be given.

2.1.1 Intensity-based motion detection

Intensity-based motion detection approach was first used in the field of computer image processing and was later developed in the modelling of biological systems [27]. This approach is an approximation of the motion fields from spatial and temporal differences in the intensity or brightness and profiles of the image frames to be compared. Two of the widely know intensity based models are: spatio-temporal gradient models [28] and spatio-temporal energy models [19].

In spatio-temporal gradient models, gradient algorithms utilise the image's spatial and temporal derivatives to estimate velocity, under the assumption of the overall intensity of the image remains constant. The intensity of the spatial and temporal gradients can be used to decide the optical flow. Horn and Schunck developed a approach for determining the optic flow from the measurements of spatial and temporal intensity gradients, based on the assumption that the brightness is constant [29]. As long as this assumption holds, the gradient algorithm measures velocity directly and independent of contrast. However, since this makes use of derivatives, the spatio-temporal gradient algorithm is susceptible to high-frequency noise [24].

In spatio-temporal energy models, motion detectors measure spatiotemporal correlations induced by moving objects or self-motion. While other motion detection models are common among the researchers in computer vision, the spatio-temporal energy models have become more popular among the physiologists and biologists [30]. Adelson [19] proposed a spatio-temporal energy model, it includes a set of detectors to measure the spatio-temporal energy of the visual field within a range of spatial and temporal frequencies, however, because of the spatio-temporal correlation is used, the spatio-temporal energy algorithms are hard to implement in hardware implementation.

As a result, this approach is more constraints and require more spatio-temporal information. The intensity-based approaches have resulted in more complex algorithms. Therefore, there are a number of difficulties in applying intensity-based models to detect image sequences. A major problem is that spatio-temporal derivatives are very sensitive to discontinuities in image intensity [23].

2.1.2 Feature-based motion detection

Feature-based motion detection, or correspondence-based approaches are used to detect the motion through tracking of salient features contained in an image. Considering the detection of motion as a change in the position of distinguishable features in an image frame, these models propose that motion detection can be accomplished by first finding features in the image and then matching the corresponding features in the next

frame [25]. In real scenes, a large number of the images may not contain useful information. Therefore, these salient features, like corners, critical points, edges and shapes can all be seen as tokens, which can provide the most useful information about the scene. Thus, feature-based approaches for motion detection can reduce the amount of information by concentrating on the displacement of feature of interest in a sequence of images. However, there are two major issues which may cause problems for feature-based motion detection [21]. Firstly, features must be reliably and accurately detected in each image frame. Secondly, the correspondence problem may confuse the process of tracking the displacement of one feature from an image to the next [31]. For dense image motion fields, it becomes difficult to decide which feature in the image at time t corresponds to which feature at time $t + \Delta t$.

The salient features such as corners, edges, lines and templates are divided into two types. The first is purely spatial feature, the spatial features are two dimensional feature, like corners and edges. Corners are mainly defined by points of high curvature in the image boundaries [32]. Edges and lines can also be used in other tasks, such as segmentation. Due to its relative structural simplicity and clear definition, edge detection is one of the most developed tasks in computer vision [33,34]. The other one is spatio-temporal features, it is a three dimensional feature like templates [35]. There have also been much research on the development of spatio-temporal algorithms [19,36–39]. However, the feature-based algorithms have the disadvantage of low reliability and often difficulties when run into dense image motion fields [23].

2.1.3 Correlation-based motion detection

In correlation based motion detection models, each frame is correlated with the previous frame. Movement in parts of the image can be detected by observing the location of maximum correlation with respect to the previous frame [21]. In intensity-based algorithms, the derivatives are involved in the processing directly. In feature-based algorithm, the derivatives are used indirectly for detecting features. In contrast, correlation-based approaches do not require any form of spatial and temporal derivatives of the intensity to compute motion, unlike the other two approaches. Due to the integrative

rather than differentiative nature of these approaches, the models that use correlation-based algorithm produce more robust output. However, the correlation-based models generally need more arithmetic operations, which can increase the computational cost [26].

The correlation-based approach is also often used as correlator, or matched-filter in communication systems, often used for detecting and estimating the time of arrival of a known pulse, obtained by correlating the known signal with a delayed version of itself. It can achieve maximum signal-to-noise ratio (SNR), under the assumption of additive Gaussian white noise [40]. Two dimensional correlation algorithms are often used in image processing. This correlation-based motion detection algorithm calculates the correlation value between two discrete time signals, we set them as $x(n)$ and $y(n)$, where $y(n)$ is a delayed signal of $x(n)$ plus an additive noise, and $y(n)$ can be written as:

$$y(n) = x(n-K) + N(n), \tag{2.1}$$

where K is a random positive integer implies the delayed discrete time, $N(n)$ is the noise, then the correlation between $x(n)$ and $y(n)$ is

$$r(n) = \sum_{m=-\infty}^{\infty} y(m)x(m+n). \tag{2.2}$$

Using Eq. (2.1) in Eq. (2.2), the correlation between $x(n)$ and $y(n)$ can be written as:

$$\begin{aligned} r(n) &= \sum_{m=-\infty}^{\infty} [x(m-K) + N(m)]x(m+n) \\ &= \sum_{m=-\infty}^{\infty} [x(m-K)x(m+n) + N(m)x(m+n)]. \end{aligned} \tag{2.3}$$

In general, $x(n)$ is not correlated with noise signal $N(n)$, so the highest value of $r(n)$ is relative to the match of $x(n)$ and $y(n)$. The property of n at which makes the $r(n)$ reach the maximum value is an estimate of delay K. The use of this feature shall be exploited for the purpose of velocity estimation.

A sequence of images are sampled at regular time intervals, τ. If the received signal is the image frame at time t, the previous image frame is at time $t - \tau$ in the images sequence. The correlation detector would reach a peak value at a spatial lag which

would correspond to the amount of image shift and the temporal sampling interval, and it follows that the velocity can be computed from a knowledge of this spatial shift and the temporal sampling interval. From Eq. (2.3), it is clear that the computations require an $O(n^2)$ complexity, where n is the length of the signals. Furthermore, from the arithmetic complexity perspective, correlation detectors will require many multiply operations, which lead to high power consumption and implementation costs.

An example of correlation-based motion detection model is the Reichardt Correlator [24], whose output is equivalent to the output of the spatiotemporal motion energy model proposed by Adelson and Bergen [19]. More details about Reichardt Correlator will be given in following section.

2.2 Biological motion detection models

2.2.1 The biological insect visual system

The research into insect vision system has offered approaches to solve the different aspects of motion detection systems. The insect visual system contains very complex neural structure, most of them are still needs more investigation. However, compared with more complex animals, insects have a visual system of intermediate complexity. This kind of visual systems can be mimicked through less complex models and algorithms and can be developed for computer vision systems. This simplicity is the secret to the effectiveness visual system in insect. In other animals, the perceived image is completely transferred to the brain and a huge neural structure processes the image. In insects, however, many of the tasks, such as the perfect recognition of objects, have either been eliminated or simplified [13]. The insects visual system has been researched for many years, it is found that motion detection plays a predominant role in the visual system of insects. Its neural structure has been partially understood, and through experimental results which match well to the neural structures, many motion detection models are proposed and used in many aspects [12, 41–43].

Figure 2.1 illustrates a cross section of the house-fly's brain and compound eyes as an example, insects have compound eyes in both sides of the head. This visual structure

has evolved to give the insect the ability of moving accurately in the same environment that other animals with much more complex vision move, but with simpler visual system. This system is composed of four neural layer: retina, lamina, medulla and lobular.

NOTE:
This figure is included on page 14
of the print copy of the thesis held in
the University of Adelaide Library.

Figure 2.1. The cross section of the house-fly's brain with the compound eyes. The insect visual system is classified into four layers, retina, lamina, medulla and lobula. Figure modified from [13]

Retina contains a large array of photoreceptor, used to sample the visual field [22]. It has been found that from the response of the photoreceptor to an input image, the retina has the function of spatial low-pass filter and some degree of temporal filtering [13]. Lamina is a curved plate beneath the retina. Laughlin [44] in his work gave the clear evidence that some kind of temporal high-pass filtering takes place in the lamina. Medulla is the most complex layer of the insect visual system. Douglass and Strausfeld experimentally found that the motion sensitive cells in medulla serve as components of an array of elementary motion detectors (EMD) [45]. Lobula contains wide field, directionally selective motion detection neurons. It receives the inputs from medullary cells and conveys the outputs to higher levels in the neural structure to perform higher level functions, such as detection of whole frame motion [13].

2.2.2 The bio-inspired Reichardt Correlator model

The Reichardt Correlator model was first proposed by Reichardt and Hessenstein, they deduced this model for motion detection from experiments on beetle chloro-phanus [15]. This bio-inspired model is categorised under correlation-based motion detection.

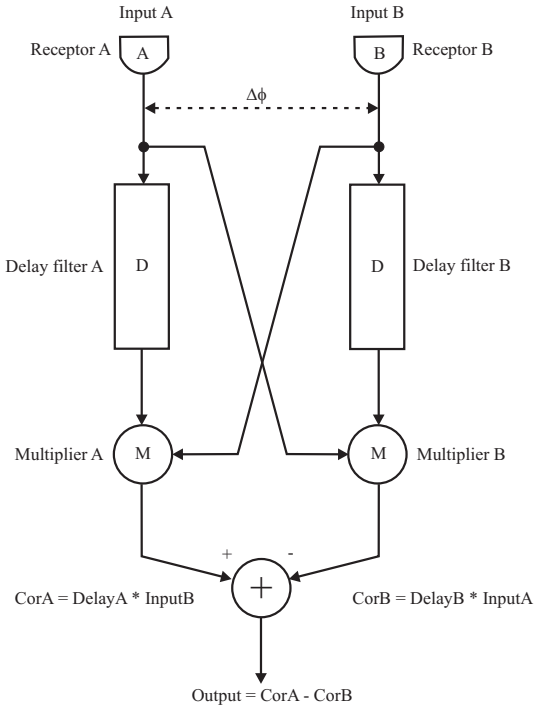

Figure 2.2. The basic Reichardt Correlator model. The Reichardt Correlator samples two input signals A and B with a fixed spatial angle $\Delta\phi$. The two time-dependent inputs passes through a delay filter (D) before multiplied by the other, undelayed, signal. Then, the two correlations CorA and CorB are subtracted to produce a output. A positive output indicates a rightward motion, a negative output indicates a leftward motion, and a zero means no motion.

A simplified model of the Reichardt Correlator is shown in Figure 2.2. It is functionally similar to the operations of insects' visual systems. Firstly, like most insect visual systems, this model has at least two receptors. They are used to sample the signals at two fields on the retina. Secondly, the arrangement between the two receptors is asymmetric to achieve directional selectivity. Finally, the interaction of the two signals is nonlinear [23]. Buchner [46] has termed the asymmetrically nonlinear interaction between two input channels as an elementary motion detector (EMD). So, the basic

structure of Reichardt correlator contains four elements: (1) Two elementary motion detectors (EMD), (2) Two linear delay filters (D), (3) Two multipliers (M) and (4) One subtracter.

The Reichardt Correlator's principle of operation is as follows: Two EMDs A and B are used to perceive the motion of objects and create two time-dependent input signals. The two EMDs need to be separated by an spatial angle $\Delta\phi$, and these signals then pass through a temporal delay (linear delay filter D) before multiplying with the non-delayed signal from the other channel, if the signal from A is delayed appropriately, the two signals will match. In order to have the similar sensitivity to both directional motion and to cancel excitation by stationary stimuli, a parallel delay and multiply operation takes place with a delay on the opposite arm. In the end, the results of two correlators are subtracted to produce a single time-dependent correlator output. A positive output signal indicates a rightward motion, a negative output signal indicates a leftward motion, and a zero output means lack of motion.

The Reichardt Correlator is simple and has low computational complexity, but it has dependencies on variations in image conditions, such as contrast, spatial frequency and velocity. Chapter 4 shows the dependence of the Reichardt Correlator on image content through simulations. Although the basic Reichardt Correlator model can obtain more meaningful responses for different image velocities, however, it suffers from two major shortcomings. First, the standard deviation of the correlator response is large relative to its mean, with relative error values ranging from 3.3 to 76 for natural images [13]. Second, the stimulated mean correlator response of the Reichardt Correlator (with $\Delta\Phi = 1.08^\circ$ and a first-order delay filter with time constant $\tau = 35ms$) for most images peaks at a velocity in the range $35^\circ - 40^\circ/sec$ [22], yet, the insects' visual systems can commonly track objects with the velocities in the range of hundreds degree per second [37]. The velocity response curves that are obtained from the simulation often have a bell-like shape. The velocity at the peak of these bell-like shape response curves is called the optimum velocity. In the range of lower or faster than the optimum velocity, the one response value correspond to two different velocities. These velocities, which are beyond the optimum velocity will be misinterpreted, therefore, the useful range of detected velocities is from zero to the optimum velocity. In

addition, the delay unit is an important element in the Reichardt Correlator. A small delay filter time constant would raise the peak response velocity, but experimentally observed time constants are not sufficiently low to account for the fact that insects may turn and track targets at velocities up to hundreds of degrees per second [37]. In order to solve these above problems, Dror [22] has elaborated the basic Reichardt Correlator which can help to overcome these problems, the response of elaborated Reichardt Correlator is raising the peak response velocity and lowering the relative error.

NOTE:
This figure is included on page 17
of the print copy of the thesis held in
the University of Adelaide Library.

Figure 2.3. The Elaborated Reichardt Correlator model. T,D,H and M are depicted temporal filters; S is represented spatial filter: ρ and ξ are saturation functions(compressive nonlinearities). The subunit subtraction may be unbalanced, with weights g_{pos} and g_{neg}. The outputs of the various EMDs undergo two-dimensional spatial integration Σ, which may be non-uniform, with weights represented by w_i. For simplicity, this figure omits a number of demonstrated nonlinear and adaptive phenomena. Figure modified from [22].

Figure 2.3 shows the elaborated Reichardt Correlator proposed by Dror, which include additional spatial and temporal prefiltering, saturation, integration, and adaptation operations that would help to improve the correlators' performance. On the other hand, these additional components would raise the implementation complexity of the

elaborated Reichardt Correlator. In this thesis, the basic Reichardt Correlator is chosen as the focus of the research. The correlator will be combined with the proposed approach of using different bit depth representations, sampling at different oversampled rates for the stimulus signal as the input to the Reichardt Correlator to bring the benefits in reducing the arithmetic implementation complexity, and at the same time, obtain accurate system performance.

2.3 Motion detection against velocity estimation

Many research works have found out that the correlation-based models are sensitive to object speed, and so affects the ability to measure velocity accurately [9, 30, 47]. If the input signal to the Reichardt Correlator is a simple sinusoid, the output response changes with velocity, contrast, and spatial frequency. The response curve obtained has a bell-like shape, starting with low velocity rising to a peak value with velocity increases and then decreasing back to zero with further velocity increases. For naturalistic images, the output responses fluctuate heavily and become much more difficult to explain. Furthermore, the Reichardt Correlator model are sensitive to velocity, as well as sensitive to the higher order derivatives of velocity [47]. Adelson and Bergern motivated by research in human psychophysics, proposed other models for motion detection, named spatiotemporal energy models [19]. However, these models can be expressed as a simple Reichardt Correlator and are equal mathematically, and so both of them experience the same problems.

It is clear that humans, and many other animals have the ability to behave and perform tasks which rely on visual velocity estimation. For example, Srinivasan found the honeybees can perform the tasks of velocity estimation from a series of behavioural experiments [9]. In view of these evidence, Srinivasan has proposed that humans and insects possess two parallel systems for velocity estimation, one is capable of correlation and the other is capable of velocity estimation [48]. Moreover, the psychophysical researchers through using the ratios of outputs of correlators with different spatial and temporal tuning to measure the velocity [19, 49].

Results from many experiments showed that statistical characteristic of natural images play an important role in associating the correlator response with motion velocity, also verified that additional physiological components of the correlator model can improve the accuracy of the Reichardt Correlator as a velocity estimator [2,50,51].

2.4 Velocity estimation performance criteria

In order to compare the performance of different velocity estimation systems, one must put them in a same quantitative standard of accuracy performance. However, establishing this kind of standard is difficult for biological visual systems. This is because in the visual field, different biological visual tasks need different information on motion. For example, when insects are chasing an object, the primary requirement is tracking a small moving object successfully, but when they are flying, insects just need to distinguish their position and judge the distance between themselves and the surrounding environment. Hence, they should have the ability to estimate local velocity. Some motion detection system can measure the local velocity accurately, and some can measure accurately in global velocity, while others can only carry out with in a particular range of velocities [17].

In view of all these different possible criteria, Dror [22] put forward two basic requirements for a good performance velocity estimation system:

- At a specific velocity, the image motion should always output the same response.
- At different velocities, the output response to motion should significantly differ from the response at other velocities.

In this thesis, these two basic requirements from the quantitative standard to investigate the Reichardt Correlator response performance for different images and different approaches will be used.

2.5 Related works

Insects are remarkably adept at manoeuvering their way with seemingly great ease and navigating themselves through complex and unpredictable environments. Research into insect vision has provided great insights into the functioning of visual processing systems. This line of research spans many different fields, including behavioral, neurophysiological and physiological sciences [22]. Insights obtained have subsequently been used to improve the motion detection approaches in real environment, it can lead effectively use in various fields to enhance the safety and quality of artificial systems.

Srinivasan et al. [52] studied the optomotor response in insect visual system which is a turning response evoked by the apparent movement of the visual environment, serves to stabilise the insect's orientation with respect to the environment. Then, they proposed new model for motion detection to improve the stability of the performance with respect to the environment.

Indiveri and Douglas [43] developed vision sensors, called neuromorphic vision sensors which are based on the fly visual systems. Neuromorphic sensors are specialised sensory processing functions implemented by analog electronic circuits that are inspired by biological systems. This computational architecture, dense processing, small size, and low power consumption of neuromorphic sensors make them attractive for constructing artificial sensor systems that attempt to emulate biological processing. They also provide qualitative processing for machine vision tasks on autonomous mobile robots.

Moini et al. [53] were inspired by the insect visual system and the template model for insect vision, built blocks of a motion detection chip in VLSI. Their model comprises two one-dimensional 64-cell arrays as well as front-end analog circuitry for visual processing and digital control circuits.

Through the elaboration, the bio-inspired motion detection can be applied to various fields. Mota et al. [11, 54] described a bio-inspired motion detection algorithm based system, which is able to efficiently segment overtaking cars using a sparse map of features from the visual field of the rear-view mirror. Reiser and Dickinson [55] have

shown the detection of expanding optic flow patterns based on bio-inspired visual system, their simple control system is a viable model for obstacle avoidance which can be used in robotic control. Moreover, Aubepart and Franceschini [12] put the optic flow sensors in Micro-Air-Vehicles (MAVs) for stabilisation and guidance purposes. Higgins [56] and Komuro [34] both described a new vision chip architecture for high-speed target tracking. The number of pixels and the processing speed are improved by the implementation of a special algorithms which utilises a property of high-speed vision and introduction of bit-serial and cumulative summation circuits.

In this thesis, the Reichardt Correlator is chosen as the velocity estimation model. Hassenstein and Reichardt [57] developed this famous motion detection model which is through mimicking the insect vision. Due to its low computational costs in estimating motion vectors, it can be realised in real-time motion detection algorithms. In fact, the architecture for many motion detection chips is based on the Hassenstein-Reichardt model [21]. However, a mass of experiments and mathematical derivations suggest that the basic Reichardt Correlator although exquisitely sensitive to motion, the output response is affected by the image condition, such as contrast and spatial frequency [23, 58]. Hence, a number of elaborations for the Reichardt Correlator are conducted to improve its accuracy and stability [22, 52].

Contrast in an image is one of the main problems which affect the performance of the basic Reichardt Correlator. Tan et al. [59], Rajesh et al. [2] have adapted different approaches to reduce the contrast effect in motion detection. Tan's approach is to reduce the dependency of contrast as early as possible in hardware and leave the actual motion detection to the digital processing part, they designed a front-end module for the pre-processing of the input. In Rajesh's paper, the contrast gain reduction is implemented by a feedback adaptive process. The gain of the EMD (elementary motion detector) inputs is reduced by a signal derived from the rectified and low-pass filtered outputs of a local EMD pool with different local preferred direction, fed back to control the gain of the EMD inputs.

Another problem that affect the performance of the basic Reichardt Correlator is frequency, which can manifest as spatial or temporal frequency. Dror et al. [58] in their

study examined the accuracy with which realistic Reichardt Correlator can provide velocity estimates in an organism's natural visual environment. Analysis and simulations suggest that processes commonly found in visual systems, such as pre-filtering, response compression, integration, and adaptation, improve the reliability of velocity estimation and expand the range of velocities coded. Rajesh et al. [2, 13] further investigated and expanded Dror's model to improve the correlator performance. Through their neurobiological experiments suggest that adaptive mechanisms decrease EMD dependence on pattern contrast and improve reliability.

After reviewing all the above related work, it can be seen that the basic Reichardt Correlator can be improved through adding components or elaborating the system. However, the system complexity is one aspect that has been often neglected in most of presented research. Adding components bring the benefit in performance, but this implies a trade-off with the system complexity. In this thesis, the core idea is not to elaborate the basic Reichardt Correlator in pursuit of accuracy velocity estimation, but instead investigates approaches to reduce arithmetic complexity of the basic Reichardt Correlator, while maintaining its level of velocity estimation performance.

Chapter 3

Proposed Methodology

THE core idea of this work is to use low bit depths and oversampling to represent the input signal to the Reichardt Correlator for velocity estimation. This chapter introduces the principle behind the approaches of low bit representation and oversampling techniques. Using theoretical arguments and simulations, it will demonstrate that using the proposed approaches an effective velocity estimation performance can be produced, while yielding potential arithmetic implementation benefits.

3.1 Introduction

In the literature, the simple Reichardt Correlator has many shortcomings as a velocity estimation system, namely its strong dependence on contrast and spatial frequency in the input signal. On the other hand, full correlation-based algorithms while less dependent on spatial frequency, have very high computation requirements. Moreover, full correlation requires a high arithmetic complexity, that can translate to high power consumption. Therefore, a particular motivation is the development of a reliable velocity estimator using relatively simple arithmetic elements. In this line of pursuit, the following approach is proposed for this thesis, Figure 3.1 shows the research block diagram:

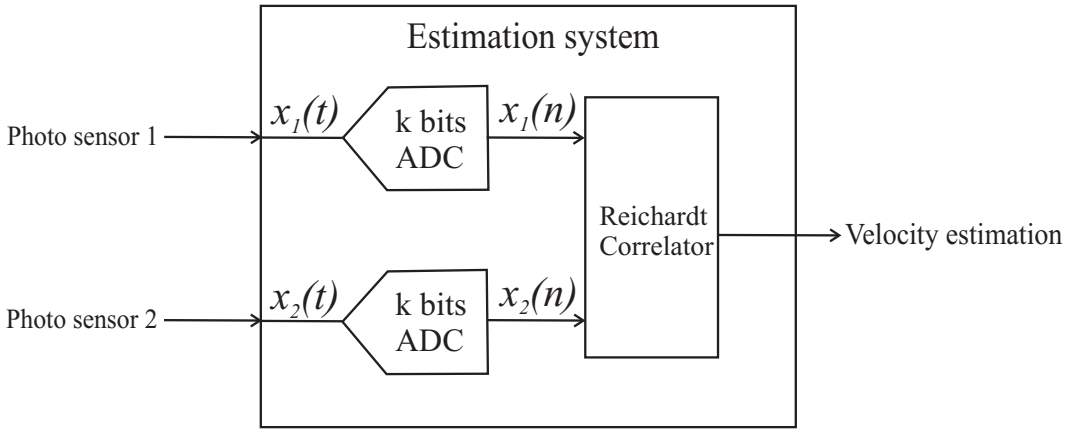

Figure 3.1. Digitisation velocity estimation system. The aim in this research is to use different bit depths and sampling rates in the Reichardt Correlator to investigate the trade-off between system performance and system arithmetic complexity.

In this research, the strategy to reducing arithmetic complexity is to use lower bit depths to represent input signals. The proposed system samples and quantises the input signals $x_1(t)$ and $x_2(t)$ to digital representations $x_1(n)$ and $x_2(n)$, respectively. The sampling rates can be Nyquist rate or oversampling rate. Compared with Nyquist sample rate, the oversampling rate is many times higher. In this thesis, the following oversampling factors are used: 16, 32 and 64 times the Nyquist rate. After quantisation and sampling, the digital signals are applied as inputs to the Reichardt Correlator, and the attained response is used to estimate the velocity.

This chapter describes the operation of proposed approaches and makes a comparison of these alterative digitisation strategies, namely the combination of different bit depths and sampling rates. The results will serve as an illustration of the trade-off between velocity estimation performance and system arithmetic complexity in the context of the Reichardt Correlator. In this spirit, three different options for the representation of the signals are investigated, corresponding to various bit depths and sampling rates.

The bit depths and sampling rates used are shown in Table. 3.1:

Table 3.1. The parameters used in the simulations. The simulations in the research uses different bit depth representations and different sampling rates to represent the input signals to the Reichardt Correlator.

Bit depths	1, 2, 3, 4, 5, 6, 7, 8
Sampling rates	Nyquist, 16x, 32x, 64x

The input signal stimuli in this work are derived from several types of images: sine grating image, naturalistic image and panoramic image. The sine grating image is chosen since it is simple and only contains a single spatial frequency. Then, naturalistic and panoramic images are used to validate the system performance as they contain multiple spatial frequencies. Throughout the simulations in this thesis, the simplifying assumption is made that all image motions are uniform and take place along the horizontal axis. This assumption avoids the need to compute two dimensional correlations, and instead only take one dimensional correlations on corresponding rows in successive frames. Since the image motion is uniform across all the rows, the overall response of velocity estimation can be calculated by taking the mean value of the estimates from all rows. The details are described in Chapter 4.

3.2 Bit depth

Bit depth is an image processing term. It describes the number of bits used to represent the value of a single pixel in a greyscale bitmapped image or video frame buffer. It

represents the number of finely defined levels of brightness that can be expressed in an image. It is proposed that lower bit depths used in the image representation can bring benefit in lowing the computational complexity, and so reduce the complexity of the arithmetic implementation.

Figure 3.2 shows a RGB model image of a person in an indoor environment, which will be used as a naturalistic image in this thesis. This image will subsequently be referred to as 'friend'.

NOTE:
This figure is included on page 26
of the print copy of the thesis held in
the University of Adelaide Library.

Figure 3.2. RGB 'friend' image. The RGB color model is a color model in which red, green and blue color are used together in various ways to reproduce a broad array of colors. In order to simplify the work, greyscale images corresponding to the luminance information of this image are used in the simulation.

The 'friend' image is chosen as the input signal since it contains numerous different spatial frequencies. Spatial frequency, in the study of visual motion, is mainly expressed as the number of cycles per degree of visual angle. Different spatial frequencies express different information about the contents on image. High spatial frequencies represent abrupt spatial changes in the image, such as edges and corners. On the other hand, low spatial frequencies represent global information about the shape, such as general orientation and proportions [60]. It has been previously established that spatial frequency greatly affects the performance of the Reichardt Correlator, this impact will be discussed in details in Chapter 4.

NOTE:
These figures are included on page 27
of the print copy of the thesis held in
the University of Adelaide Library.

(a) 8-bit representation. (b) 7-bit representation. (c) 6-bit representation.

(d) 5-bit representation. (e) 4-bit representation. (f) 3-bit representation.

(g) 2-bit representation. (h) 1-bit representation.

Figure 3.3. Naturalistic 'friend' greyscale image at various bit depths. Examples of the naturalistic images used in simulations throughout this thesis. Using the lower bit depths to reduce the arithmetic complexity which in terms of dependence on the number of bits in the data's representation.

In this thesis, in order to simplify the work, the chrominance information in the RGB images are discarded. All the images in this study are greyscale images which contain only luminance information. The greyscale digital image in computing is an image which the value of each pixel is a single sample, that is, it carries only intensity information. Images of this sort, also known as greyscale image, are composed exclusively of shades of gray, varying from black at the weakest intensity to white at the strongest [61]. The greyscale is used in bit depths, 1 to 8-bit to represent the images.

For example, an 8-bit image has an brightness that is encoded in $2^8 = 256$ different grey levels from white to black. Similarly, a 7-bit image contains $2^7 = 128$ different grey levels from white to black, 1-bit image which is also named as binary image only contains black or white. Figure 3.3 is the greyscale images of 'friend' from 8 to 1-bit.

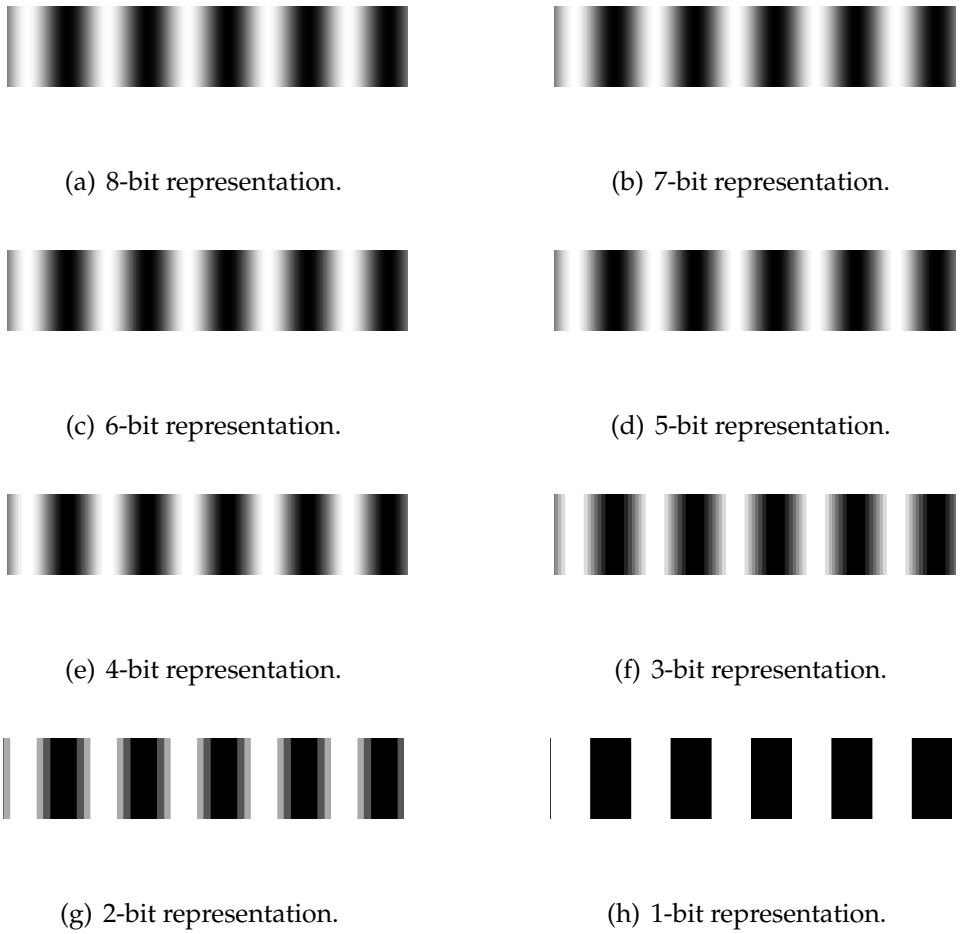

(a) 8-bit representation. (b) 7-bit representation.

(c) 6-bit representation. (d) 5-bit representation.

(e) 4-bit representation. (f) 3-bit representation.

(g) 2-bit representation. (h) 1-bit representation.

Figure 3.4. The 'sine grating' greyscale images at various bit depths. Using different bit depths to represent the 'sine grating' image, the motivation is same as 'friend'.

It is clear that the higher bit representation of images have the greater fidelity. Moving from 8 to 1-bit, the degradation in image quality is obvious. In the 8-bit image of Figure 3.3 (a), the facial features are vivid, and the different pieces of equipment in the indoor environment can be distinguished easily. However, along with the decrease in bit depth, the features in the image are increasingly more difficult to distinguish. In the 1-bit image of Figure 3.3 (h), the facial features of the person and background

environment can hardly be distinguished, since there are only two greyscale levels (black and white) to represent the information in image.

Figure 3.4 shows the sine grating images at various bit depths which will be used as input signal stimuli. These images will collectively be referred to as 'sine grating'. It can be seen that varying the bit depth has the same impact on image fidelity as for the image 'friend'.

From earlier discussion in Section 2.1.3, it is clear that a low bit depth is favourable from an arithmetic complexity perspective. The purpose of this work is to investigate the effect of different bit depths on the Reichardt Correlator's performance as a velocity estimator. Therefore, it is necessary to simulate the Reichardt Correlator response when using input stimuli encoded at different bit depths.

3.3 Interpolating

Generally, in digital signal processing technology, the original signal must be sampled at a rate which is at least twice of the highest in-band frequency. This is known as the Nyquist condition. If satisfied, this condition implies the obtained discrete time signal can be used to reconstruct the original continuous time signal without errors. The traditional sampling process is shown in Figure 3.5, which shows the use of an anti-aliasing filter to ensure the removal of all frequencies above the half sampling rate.

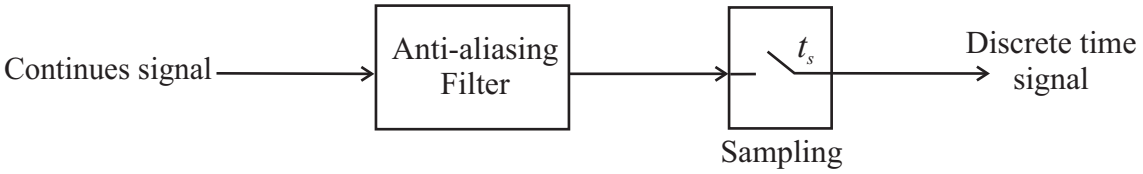

Figure 3.5. The traditional sampling process. The continuous time signal can be converted to discrete time signal throughout sampling processing. The anti-aliasing filter is used to filter out unwanted frequency components to ensure that all frequencies in the signal to be sampled are less than twice the sampling frequency.

In this thesis, all the input signals to the Reichardt Correlator are stimuli arising from moving images. For a simple signal like sinusoid, the output response can be derived

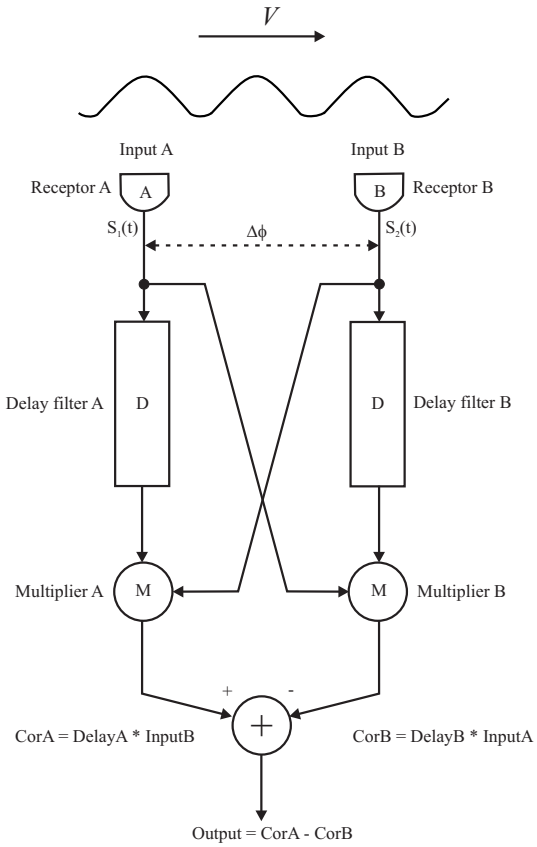

Figure 3.6. The basic Reichardt Correlator model with rightward motion input. $S_1(t)$ and $S_2(t)$ are the input in continuous time, after converted in discrete time signals, they represented as $S_1(n)$ and $S_2(n)$. This sampling process may not result in a value that is an integer multiples of sampling time.

analytically. Figure 3.6 shows the Reichardt Correlator with two input receptors A and B. The figure also shows a potential moving sinusoid signal in front of two receptors. The input signal at receptors A and B are $S_1(t)$ and $S_2(t)$, respectively. The angular distance between A and B is $\Delta\phi$, $y(x)$ is the input signal value to receptor at image's pixel x, and the image stimulus is moving from A to B at velocity v. Using these notations, the following expressions can be written at time t_0 as:

$$
\begin{aligned}
t &= t_0. \\
\text{Therefore,} \quad S_1(t_0) &= y(x_0), \\
S_1(t) &= y(x_0 + vt), \\
S_2(t) &= y(x_0 + \Delta\phi + vt).
\end{aligned}
$$

$$\text{In discrete time,} \quad t = n \cdot t_s = \frac{n}{f_s}, \tag{3.1}$$

$$S_1(n) = y(x_0 + \frac{v}{f_s} \cdot n). \tag{3.2}$$

$$\text{Then,} \quad S_2(n) = y(x_0 + \Delta\phi + \frac{v}{f_s} \cdot n). \tag{3.3}$$

where n in Eq. (3.1) indicates the sample index. Since x denotes an image pixel index, it needs to have an integer value in Eq. (3.2) and Eq. (3.3). However, the value of $\frac{v}{f_s} \cdot n$ may not result in a value that is an integer multiple of sampling time. In such cases, the exact stimulus value $y(x_0 + \Delta\phi + \frac{v}{f_s} \cdot n)$ cannot be determined. To address this issue, the linear interpolation approach is used, as illustrated in Figure 3.7.

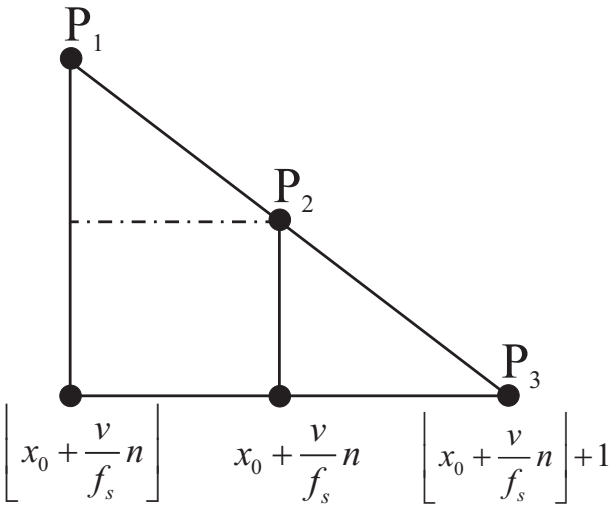

Figure 3.7. The linear interpolation. This is a method of curve fitting using first-order polynomial interpolation. It is heavily employed in mathematics and numerous applications including computer graphics. Linear interpolate is a simple form of interpolation. The symbol $\lfloor \quad \rfloor$ denotes the floor operation.

From the principle of linear interpolation, if the two known points are given by the coordinates (x_0, y_o) and (x_1, y_1), the linear interpolation is the straight line between these points. For a value x in the interval (x_0, x_1), the value y along the straight line is given by:

$$\frac{y - y_0}{x - x_0} = \frac{y_1 - y_0}{x_1 - x_0}, \tag{3.4}$$

which can be derived geometrically from Figure 3.7. Solving Eq. (3.4) for y, gives:

$$y = y_0 + \frac{y_1 - y_0}{x_1 - x_0} \cdot (x - x_0). \tag{3.5}$$

Figure 3.7 shows the process of linear interpolation, P_1 is the first sample point and P_2 is the subsequent sample point, point P_3 is the interpolated value. The symbol $\lfloor \quad \rfloor$ denotes the floor operation. So, from Eq. (3.5), the interpolated value P_3 can be calculated as an approximation of the instantaneous stimulus experienced by the receptor B.

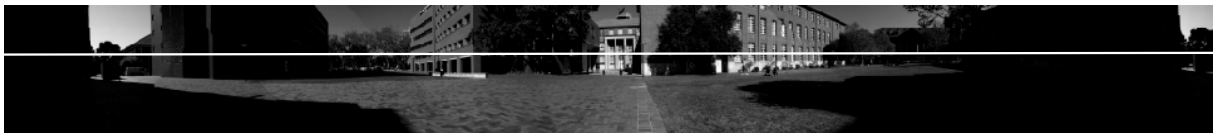

Figure 3.8. The panoramic 'scenery' image. The 30th row of 'scenery' is used to implement the linear interpolation process. The white line indictes the 30th row.

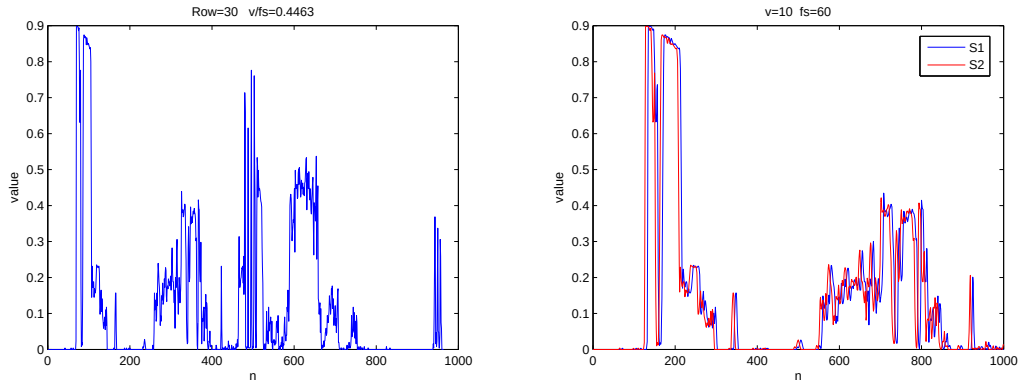

(a) (b)

Figure 3.9. Stimulated sample values at receptor A and B for velocity of 10 degrees per second, 30th row of 'scenery'. (a) shows the 30th row of 'scenery' plotted as a function of horizontal sample points. (b) shows stimulated stimuli $S_1(t)$ and $S_2(t)$ at receptors A and B, respectively.

The panoramic image in Figure 3.8 is one of the images used in this thesis, this image is subsequently referred to as 'scenery'. In this instance, its row is used to illustrate the linear interpolation process described above. For example, the 30th row of this panoramic image will be used as shown in Figure 3.9 (a). If velocity is set to 10 degrees per second, a sampling frequency of 60 Hz, and a thousand sample points are taken,

then the simulated stimuli at receptors A and B are shown in Figure 3.9 (b) (the blue curve represents the signal received by receptor A, and the red curve represents the signal received by receptor B.).

It is clear that the input at S_1 and S_2 are almost same. Indeed, from Eqs. (3.2) and (3.3), $S_2(t)$ should simply be shifted (by $\Delta\phi$) versions of $S_1(t)$. If the velocity is set to 100 degrees per second, the sampling frequency and sampled points are kept the same, then Figure 3.10 shows the stimulated stimuli with higher velocity at receptors A and B.

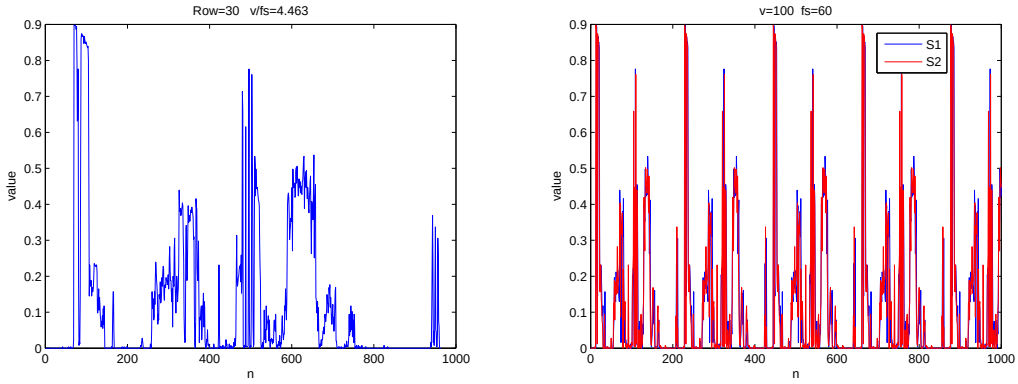

(a) (b)

Figure 3.10. Stimulated sample value at receptor A and B for velocity of 100 degrees per second, 30th row of 'scenery'. (a) shows the 30th row of 'scenery' plotted as a function of horizontal sample points. (b) shows stimulated stimuli $S_1(t)$ and $S_2(t)$ at receptors A and B, respectively.

Compared with the interpolated value at a lower velocity, the higher velocity interpolated stimuli signals has more repetitions, as a direct result of greater number of revolutions per unit of time. These results help with understanding the behaviour response of the Reichardt Correlator as discussed in details in Chapter 4.

3.4 Oversampling

Real-world image signals are analog, but it is necessary to converted the visual stimuli into the digital domain using an analog to digital converter (ADC). The analog-to-digital conversion for a signal is often described in terms of two separate operations: uniform sampling in time, and quantisation in amplitude. The Nyquist rate

ADC samples at twice the bandwidth of the signal. In order to ensure the signal is indeed band-limited to half the Nyquist sample rate, an anti-aliasing filter with a very sharp cutoff response is often needed. Once the signal is sampled, the samples must also be quantised in amplitude to a finite set of output values for processing by a digital computer. The quantised output amplitudes are usually represented by a digital code word composed of a finite number of bits. The digital code words are often said to be in pulse code modulation (PCM) format. As described, the ADC requiring an anti-aliasing filters with sharp cutoff frequency. This is necessary to maximise the use of available bandwidth without exceeding the Nyquist limit. For Nyquist rate converters, each sampled signal is quantised at the full resolution or precision of the converter. The high resolution measurement is related to the maximum ratio of signal's dynamic range. The resolution of such converters implemented on VLSI chips is limited by the fabrication process. If Nyquist rate ADC has 8-bit of resolution, the comparator is required to be able to resolve voltage better than $V_{Fs}/2^8$, where V_{Fs} is the full supply voltage used in the comparator design [59]. As a result, achieving high resolution Nyquist rate converters are extremely difficult to attain in current integrated circuit technology.

In signal processing, oversampled conversion is a technique that improves the resolution of samples, by increasing the correlation between samples, and this can be leveraged to reduce the number of bits required per sample while still maintaining the same overall conversion precision. Oversampling is the process of sampling a signal with a sampling frequency significantly higher than twice of the bandwidth or highest frequency of the signal being sampled. There are three main reasons for performing oversampling:

1. Reduce the complexity of the ADC by not requiring expensive analog anti-aliasing filters. By increasing the sample rate, the demands on the anti-aliasing filter is reduced, and so the filters have lower complexity and can be made less expensively.

2. Using this approach, the higher-resolution A/D and D/A conversion can be achieved at low cost. Since digital signal processing techniques are used in place of complex and precise analog components.

3. Noise reduction. This will be introduce in Section 3.5.

In essence, oversampling pulse code modulation (PCM) conversion changes the distribution of the quantisation noise power. This has the effect of reducing the contained quantisation noise in the signal band. On the other hand, using the technique of noise shaping in addition to oversampling will allow for high resolution conversion of relatively low bandwidth signal, and provides a trade-off between sampling and bit depth [62]. Commonly there are two types of oversampling ADC, namely error difference and sigma-delta modulator. In the next section, more details about the features of oversampling and noise shaping in sigma-delta ADC from image digitisation point of view will be discussed.

3.5 Oversampling, with noise shaping

It has been mentioned above that the oversampling PCM often integrates with noise shaping process, using 1-bit quantisation to convert an analog signal to the digital domain. This kind of ADCs were named oversampling sigma-delta A/D converter which was first proposed by Inose and Yasuda [63] in 1964. However, the sigma-delta ADC only obtained popularity after the relevant development in VLSI digital technology has matured to a certain extent.

In comparison with Nyquist rate conversion, sigma-delta conversion samples input analog signal at higher sampling rates. Therefore, the noise in signal which is the frequency component out of the needed frequency can be filtered by a simple low-pass filter, since the noise components which are closed to the sampling frequency can be aliased back into the signal band [64]. The oversampled conversion produce the same noise power with Nyquist conversion, however, due to the higher sampling rate, its frequency distribution is much reduced in band compared to the Nyquist ADC.

Figure 3.11 shows the quantisation noise power $P_e(f)$ for Nyquist sampling rate f_{s1} and oversampling rate f_{s2} with a signal band of f_B. The blue shadowed rectangular area represents the noise power produced by a Nyquist rate converter, and the unshadowed

area represents the noise power produced by an oversampling converter. The areas underneath the two rectangles are the same, but the noise power outside the signal band for the oversampling converter can be greatly attenuated with a digital low-pass filter following the conversion [62]. Such approach cannot be used with the Nyquist rate converter.

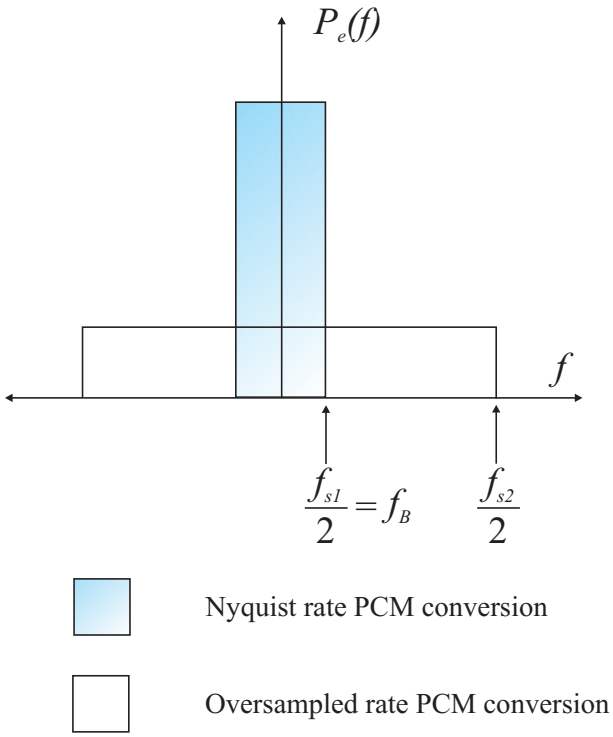

Figure 3.11. Quantisation noise power for Nyquist rate and oversampling rate. For Nyquist rate sampling, all the quantisation noise power represented by the area of the tall shadowed rectangle, occurs across the signal bandwidth. In the oversampled case, the same noise power, represented by the area of the unshadowed rectangle. The bandwidth f_{s2} is much greater than the signal bandwidth f_B.

This process can bring benefit to the design and implementation of the ADC, since it provides an alternative to realising a complex analog anti-aliasing filter. Instead, more digital signal processing is needed after the conversion. Figure 3.12 is a model of first order sigma-delta ADC. The system consists of a sigma-delta modulator, followed by a digital decimator. The sigma-delta modulator consists of a discrete time integrator, a quantiser and a DAC used to convert the digital signal back to an analog signal in the feedback path.

The principle of oversampling sigma-delta ADC is as follows: the input signal $x(t)$ is sampled at oversampled frequency, a feedback signal $y_a(t)$ from 1-bit DAC is subtracted with the $x(t)$ and the residue signal $u(t)$ is accumulated by an integrator. The output of the integrator $v(n)$ is quantised to generate a 1-bit digital bit stream. This digital output decides the sign of the feedback, if the digital output is 1, it feeds back a large negative signal to be subtracted from the input signal. This feedback loop keeps the output of the integrator small so that the output can track the amplitude of the input signal.

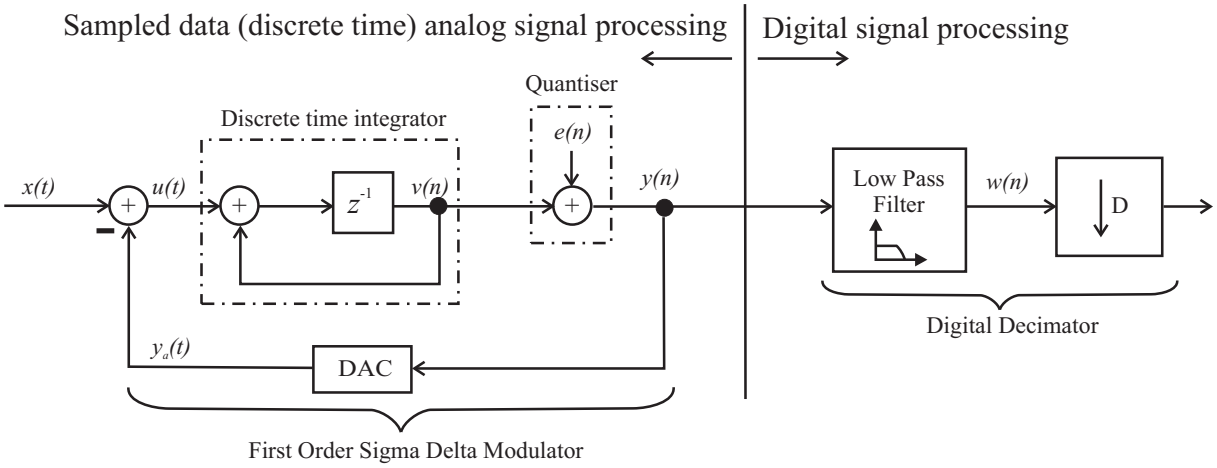

Figure 3.12. First order sigma-delta modulator A/D system. The difference signal between input $x(t)$ and the analog representation $y_a(t)$ which from the feedback loop, after through the discrete time integrator, is quantised to produce $y(n)$. Then, $y(n)$ is processed by subsequent digital signal processing.

Another important process in sigma-delta ADC is noise shaping. It is the process of nonlinear quantisation and feedback loop combined to shift some noise to frequencies beyond the input signal spectrum [62]. The integrator in sigma-delta conversion plays the role of loop filter in the modulator, the integrator in terms of playing the role of low-pass filter for the input signal, and of high-pass filter for quantisation noise. The connection for a continuous time modulator can be explained with the aid of Figure 3.13 as follows:

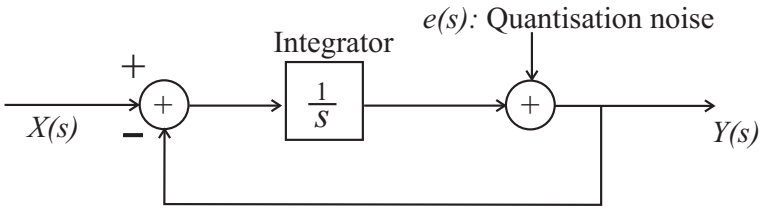

Figure 3.13. The integral process in sigma-delta conversion. The modulator can be modeled in the s domain, with an ideal integrator represented with transfer function of $\frac{1}{s}$, and the DAC in feedback loop is considered to be ideal. This is used to illuminate the important fact of noise shaping.

It can be derived from Figure 3.13, when $e(s) = 0$, the signal transfer function is:

$$\begin{aligned} Y(s) &= X(s) - s \cdot Y(s), \\ \frac{Y(s)}{X(s)} &= \frac{1}{s+1}. \end{aligned} \tag{3.6}$$

Eq. (3.6) indicates that the integrator acts as low-pass filter for input signal. When $X(s) = 0$, the noise transfer function is:

$$\begin{aligned} Y(s) &= -Y(s)(\frac{1}{s}) + e(s), \\ \frac{Y(s)}{e(s)} &= \frac{1}{1+\frac{1}{s}} = \frac{s}{s+1}. \end{aligned} \tag{3.7}$$

Eq. (3.7) shows that the integrator acts as high-pass filter for the quantisation noise.

The sigma-delta conversion is using oversampling and noise shaping to push the noise outside the band of interest. The oversampling does not change the total noise power, instead redistributes it [62]. So the input signal through sigma-delta conversion can push the noise to high frequency band, and then using digital low-pass filter to filter these noise components.

Here two sinusoids with different frequencies are used as the input signal to sigma-delta conversion, the frequencies are chosen to be 10 Hz and 100 Hz for illustration purpose. Using Matlab as simulation tool, the processes of oversampling and noise shaping are shown in Figures 3.14 and 3.15.

Figures 3.14 (a) and 3.15 (a) are the input of sinusoid curve, and (b) in Figures 3.14 and 3.15 are using oversampling and 1-bit quantisation to represent the sinusoid. In

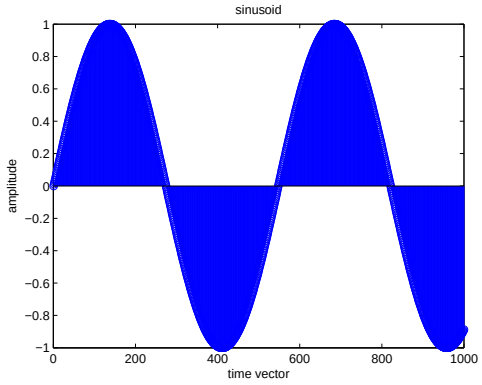

(a) The input sinusoid signal.

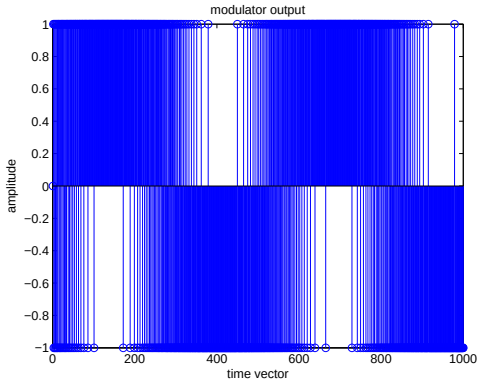

(b) The modulator output for sinusoidal input.

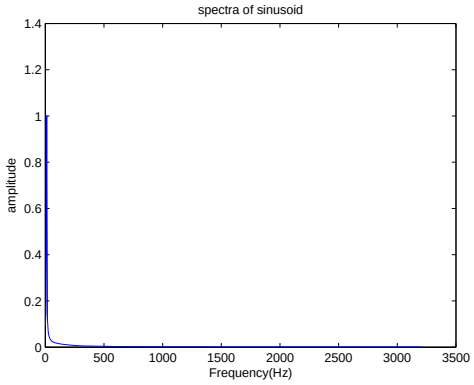

(c) The power spectra of sinusoid

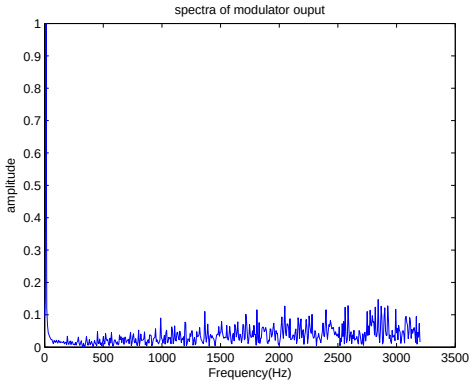

(d) Single-sided amplitude spectrum of the modulator output.

Figure 3.14. The sigma-delta conversion processing for 10 Hz sinusoidal input. (a) to (b) show the processes of quantisation and noise shaping. In subfigure (b), after quantisation, the input analog sinusoid signal (a) is represented by the values of +1 and -1. In (d), after noise shaping, the quantisation noise is pushed from the signal band to high frequencies band.

Figures 3.14 (c) and 3.15 (c), it can be observed that the two frequencies, 10 Hz and 100 Hz which contained in the two sinusoids are shown in spectra of sinusoid. In Figures 3.14 (d) and 3.15 (d), after the processing of oversampled single-bit representation and noise shaping, which can be viewed as pushing quantisation noise power from the signal band to high frequencies. Then, this part of noise can be filtered by a simple digital low-pass filter in future digital processing. However, if the high resolution conversion is needed, it will require high speed digital processing, as the sampling has

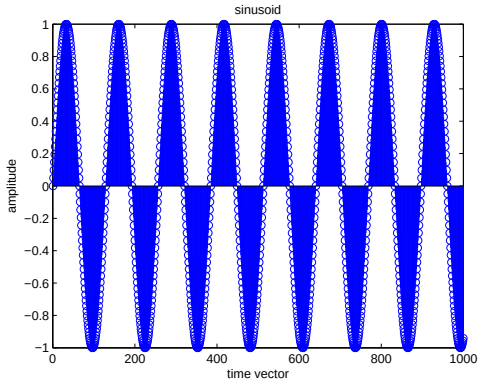

(a) The input sinusoid signal.

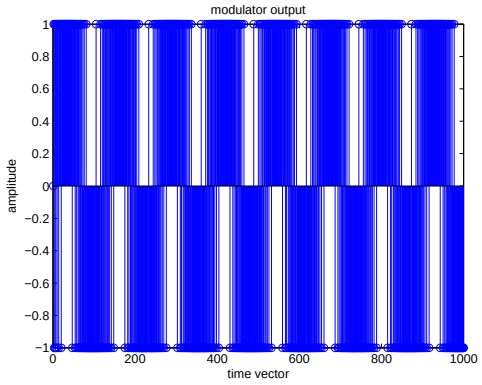

(b) The modulator output for sinusoidal input.

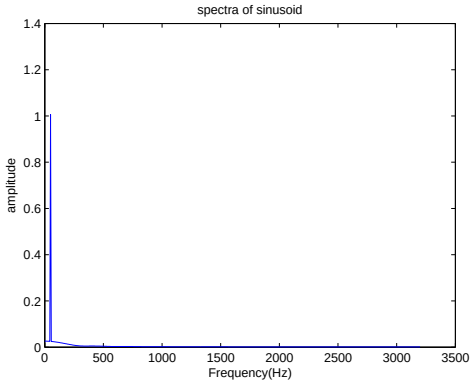

(c) The power spectra of sinusoid.

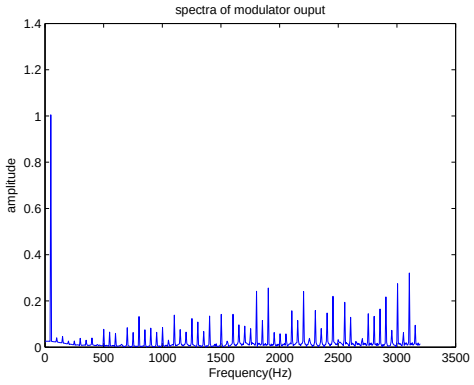

(d) Single-sided amplitude spectrum of the modulator output.

Figure 3.15. The sigma-delta conversion processing for 100 Hz sinusoidal input. These four sub-figures show the same operation as figure 3.14.

to operate at the oversampled rate. The analog circuit complexity is traded for digital circuit complexity, which is simpler to implement than analog circuit in modern VLSI technology [64].

3.6 Summary

In this chapter, in order to investigate the trade-off between the performance and arithmetic implementation using the Reichardt Correlator as velocity estimator, the theory and background of proposed approaches of bit depth, oversampling technique and

noise shaping were introduced. Through analysis and simulations, the proposed approaches can bring benefit as reducing the arithmetic operation. These approaches will be applied to the Reichardt Correlator in this thesis to provide the needed background to expand on modelling and simulations of the Reichardt Correlator in the next chapter.

This page is blank

Chapter 4

Reichardt Correlator Response

THIS chapter reports on the simulation results of the proposed velocity estimation algorithm. The investigation is conducted using proposed approaches combine with a basic Reichardt Correlator. The sampling rate and input signal bit depth are varied to examine their effects on the velocity estimation. The results show the trade-off between the accuracy of velocity estimation performance and the bit depth used to represent samples of visual stimulus signals, where the latter is strongly related to the complexity of the required arithmetical implementation.

4.1 Mathematical description of the Reichardt Correlator

Section 2.2 discussed the bio-inspired motion detection known as the Reichardt Correlator, and introduced this configuration and its operating principles in detail. It was

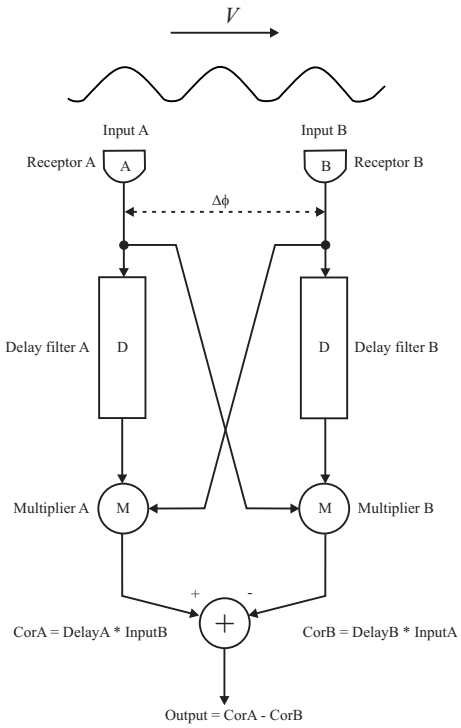

Figure 4.1. The basic Reichardt Correlator model with rightward motion input. This figure also shows a potential input signal, a sinusoid with amplitude C and spatial frequency f_s moving from left to right with velocity v.(repeat from Figure 3.6.)

discussed that the basic Reichardt Correlator of Figure 4.1 produces a bell-shaped output in response to a moving stimulus. In this section, a mathematical derivation to determine the response characteristics for sinusoidal stimulus will be presented. A sinusoid input is assumed here to simplify the derivation. Furthermore, natural signals can be decomposed into a sum of different sinusoidal components due to Fourier theory. Suppose an input sinusoid stimulus with contrast C and spatial frequency f_s (cycles/$^\circ$) is moving from left to right, (i.e. from input A to input B) with a horizontal velocity v, as shown in Figure 4.1. Then the temporal frequency of the input signal at any receptor is $f_t = f_s v$. Since the spatial angle between the receptors A and B is $\Delta\phi$, receptor A is located at $x = 0$, and receptor B is located at $x = \Delta\phi$, using x to describe the horizontal coordinate. This general sinusoidal stimulus is parameterised by

contrast, spatial and temporal frequency. As a time and space function, the sinusoidal pattern is:

$$C\cos(2\pi f_t t - 2\pi f_s x).$$

Then the signals at input A and input B are given by:

$$A(t) = C\cos(2\pi f_t t), \tag{4.1}$$

$$B(t) = C\cos(2\pi f_t t - 2\pi f_s \Delta\phi). \tag{4.2}$$

Suppose the linear delay filter has temporal frequency response $D(f_t) = X(f_t)e^{-j\theta(f_t)}$, where $X(f_t)$ indicates the amplitude of delay filter temporal frequency response and $\theta(f_t)$ indicates the phase. Therefore, the signals $A(t)$ and $B(t)$ after delay filter D are $A_D(t)$ and $B_D(t)$, which can be written as:

$$A_D(t) = CX(f_t)\cos[2\pi f_t t - \theta(f_t)], \tag{4.3}$$

$$B_D(t) = CX(f_t)\cos[2\pi f_t t - 2\pi f_s \Delta\phi - \theta(f_t)]. \tag{4.4}$$

The Reichardt Correlator computes the product of the delayed signals $A_D(t)$ and $B_D(t)$ with the original signals in the opposite branch, $A(t)$ and $B(t)$, to obtain corA and corB. These are then subtracted to produce the correlator output response $R(t)$:

$$R(t) = A_D(t)B(t) - B_D(t)A(t). \tag{4.5}$$

From Eqs. (4.1) to (4.5), and by using the two trigonometric identities:

$$\cos\alpha \times \cos\beta = \frac{1}{2}[\cos(\alpha+\beta) + \cos(\alpha-\beta)],$$

$$\cos\alpha - \cos\beta = -2\sin(\frac{\alpha+\beta}{2})\sin(\frac{\alpha-\beta}{2}).$$

Eq. (4.5) can be written as:

$$\begin{aligned}
R(t) &= A_D(t)B(t) - B_D(t)A(t) \\
&= \frac{C^2X(t)}{2}\{\cos[4\pi f_t t - 2\pi f_s\Delta\phi - \theta(f_t)] + \cos[2\pi f_s\Delta\phi - \theta(f_t)]\} \\
&\quad -\frac{C^2X(t)}{2}\{\cos[4\pi f_t t - 2\pi f_s\Delta\phi - \theta(f_t)] + \cos[-2\pi f_s\Delta\phi - \theta(f_t)]\} \\
&= \frac{C^2X(t)}{2}\{\cos[2\pi f_s\Delta\phi - \theta(f_t)] - \cos[2\pi f_s\Delta\phi + \theta(f_t)]\} \\
&= -\frac{C^2X(t)}{2}\{\cos[2\pi f_s\Delta\phi + \theta(f_t)] - \cos[2\pi f_s\Delta\phi - \theta(f_t)\} \\
&= C^2X(t)\sin(2\pi f_s\Delta\phi)\sin[\theta(f_t)].
\end{aligned} \tag{4.6}$$

Here, the delay filter is assumed to be a first order low-pass filter with impulse response $d(t) = \frac{1}{\tau}e^{-t/\tau}$ for $t > 0$, where τ is the time constant of the delay filter. In the frequency domain, the temporal frequency response of this filter is the Fourier transform of its impulse response:

$$\begin{aligned} D(f_t) &= \frac{1}{1 + j2\pi f_t \tau} \\ &= \frac{1}{\sqrt{1 + (2\pi f_t \tau)}^2} e^{-j \arctan(2\pi f_t \tau)} \\ &= X(f_t) e^{-j\theta(f_t)}, \end{aligned}$$

where

$$\begin{aligned} X(f_t) &= \frac{1}{\sqrt{1 + (2\pi f_t \tau)}^2}, \\ \theta(f_t) &= \arctan(2\pi f_t \tau), \end{aligned} \tag{4.7}$$

and

$$\sin[\theta(f_t)] = \frac{2\pi f_t \tau}{\sqrt{1 + (2\pi f_t \tau)^2}}. \tag{4.8}$$

Importing Eq. (4.7) and (4.8) into Eq. (4.6), and simplify, then the response can be written as:

$$R(t) = \frac{C^2}{2\pi\tau} \frac{f_t}{{f_t}^2 + 1/(2\pi\tau)^2} \sin(2\pi f_s \Delta\phi). \tag{4.9}$$

Eq. (4.9) is the mathematical expression for the Reichardt Correlator output under sinusoidal excitation. There have also been other derivations of this result but using different notations [16, 46]. Now, let us examine the parameters contained in Eq. (4.9) one by one:

- $R(t)$ is the output of the Reichardt Correlator, this is the value from which the moving velocity can be estimated.
- f_t is the temporal frequency of sinusoidal input.
- f_s is spatial frequency, it is a characteristic of any structure that is periodic across space. The spatial frequency is a measure of how often the structure repeats per unit of distance. For example, the sinusoid grating only contains single spatial

frequency, but natural images contain multiple spatial frequencies. For a sinusoid signal, the spatial frequency is related to f_t by: $f_t = f_s v$.

- C is the contrast or brightness. In visual perception of the real world, contrast is determined by the difference in the color and brightness of the object and other objects within the same field of view. It is the primary information used to distinguish an object from other objects and the background.

- $\Delta\phi$ indicates the spatial distance between two receptors, and represents the inter-ommatidial angle in the eyes of insects. This inter-receptor angle is found to be $\Delta\phi = 1.08^\circ$, from observations of the physiologically realistic range for flies [65].

- τ is the time constant in first order low-pass delay filter. In all simulations in this thesis, τ was set to 35ms, as this is the temporal frequency tuning matches that found experimentally in typical large flies such Calliphora, Eristalis, and Volucella [37].

From Eq. (4.9) above, it is clear that the Reichardt Correlator output is affected by all these parameters. In real environment, although the spatial angle between receptors $\Delta\phi$ and time constant τ are fixed, the output is still affected by contrast, spatial and temporal frequency, or, since $f_t = f_s v$, equivalently affected spatial frequency and velocity. There have been much research focused on attenuating the impact of contrast and spatial frequency on the Reichardt Correlator response, and experiments supported that elaborated Reichardt Correlator structures can mitigate these impact [2, 13, 22, 49, 58, 66]. However, these elaborated Reichardt Correlators are significantly more complicated and will undoubtedly increase the complexity of the arithmetic implementation. Therefore, in this thesis, the basic Reichardt Correlator is still adopted as motion detector, combined with different representations for the signal samples. The aim is to explore the resulting performance of the Reichardt Correlator under various numerical representation schemes.

4.2 Simulation of the basic Reichardt Correlator

As mentioned in Section 2.2, the output of the Reichardt Correlator is a time-dependent response. The input signals pass through delay filters, multipliers and subtracter to produce an output signal. A positive output response value indicates an object movement direction is from left to right, while a negative output response value indicates an object movement from right to left, and a zero output means a stationary object. In this manner, Figure 4.2 assumes there is a zero-mean sinusoid moving from right to left through the two receptors of the Reichardt Correlator. Using Matlab to simulate the whole process in each element of the Reichardt Correlator, the response curves are obtained and shown in Figure 4.3.

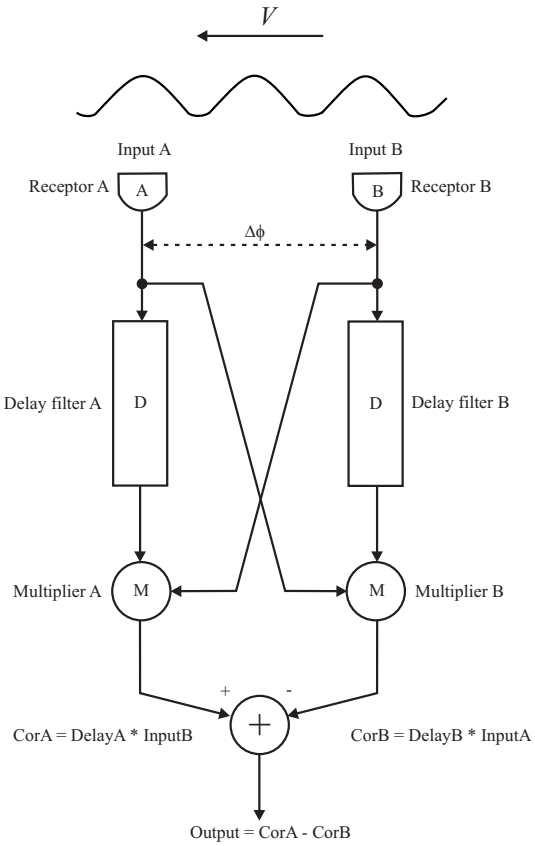

Figure 4.2. The basic Reichardt Correlator model with leftward motion input. In order to show the response in each element of the Reichardt Correlator, it assumes a potential input sinusoid signal moving from right to left.

Figure 4.3 shows the input sinusoidal response in each element of the Reichardt Correlator. The last sub-figure shows a response which is decreasing from zero to a negative

constant, hence indicating the sinusoid is moving from right to left. This result is consistent with the theoretical derivation.

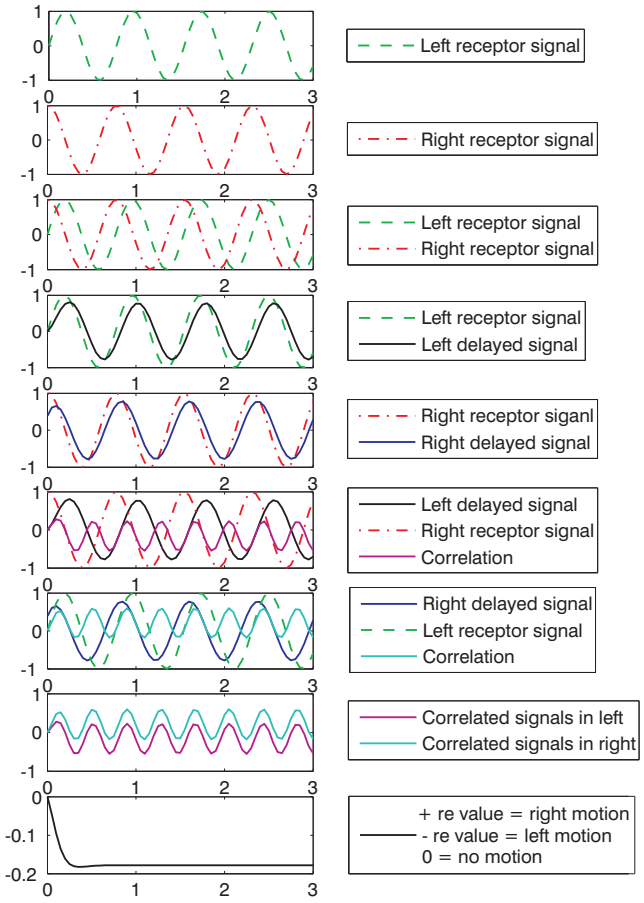

Figure 4.3. The input sinusoidal signal responses in each element of the Reichardt Correlator. It can be seen clearly that the sinusoid response in each element from input to output. It also can be concluded from negative value in response that the input signal has leftward motion.

If the direction of the moving sinusoid is changed, from left to right, the output response of the Reichardt Correlator will appear as show in Figure 4.4 (a), where the response increases from zero to a positive constant. In Figure 4.4 (b), the response curve is located at zero on the time axis, which indicates a stationary object relative to two receptors at all times.

In order to illustrate the other dependencies of the Reichardt Correlator, we return to the mathematical expression for the Reichardt Correlator in Eq. (4.9). Firstly, suppose the response value $R(t)$ in Eq. (4.9) is for the Reichardt Correlator of the form shown

in Figure 4.1, where $\Delta\phi$ between the two receptors is 1.08° and the delay filter D is a first order low-pass filter with time constant τ = 35ms. The input to the Reichardt Correlator is a zero-mean sinusoid with contrast C, spatial frequency f_s and temporal frequency f_t, is moving from left to right by velocity v degrees per second ($^\circ/s$).

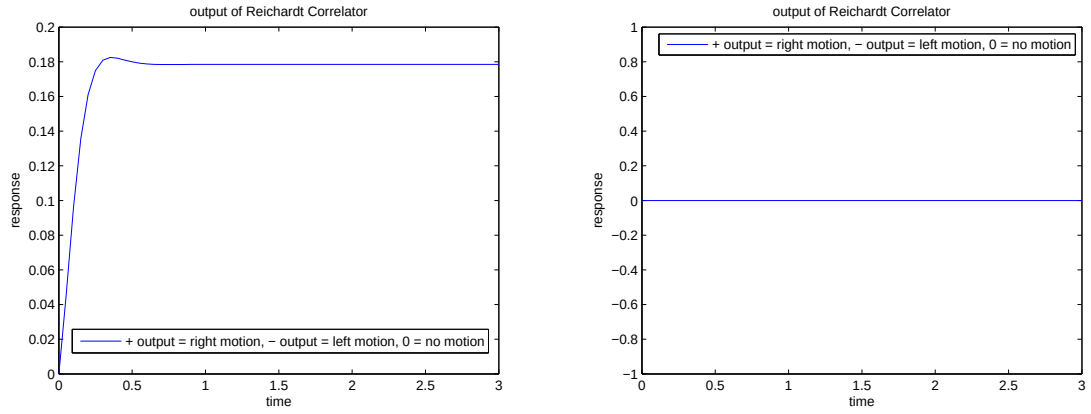

(a) (b)

Figure 4.4. The Reichardt Correlator directionally sensitive motion responses. (a) shows the positive valued response indicates rightward motion. (b) shows the zero valued response indicates no motion.

According to Eq. (4.9), the response depends on the contrast, spatial frequency and temporal frequency, but the effects are separable. The different steady-state output response curves are shown in Figure 4.5.

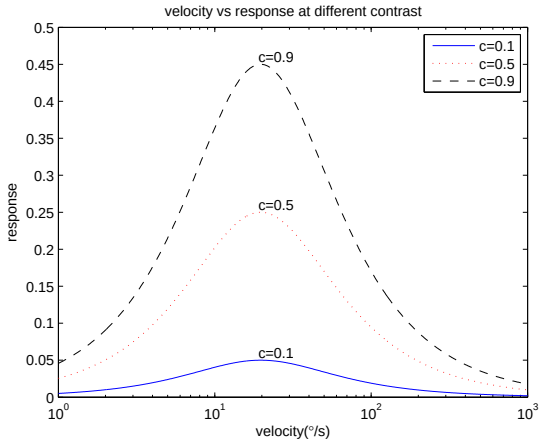

Figure 4.5. Velocity response to sinusoidal input with varying contrasts. The higher contrast has a higher response along velocity axis.

In Figure 4.5, the response strength of stimulant increase corresponds to an increase in the contrast level. In a real environment, the contrast in every signal varies inconsistently, therefore the responses of the Reichardt Correlator will vary accordingly as well. This sensitivity to contrast is generally considered to be a disadvantage of the basic Reichardt Correlator.

Figure 4.6 shows the Reichardt Correlator response as a function of spatial and temporal frequency for contrast $C = 1$. In Figure 4.6 (a), the response is negative for some sufficiently high spatial frequencies, since the inputs effectively under-sample the sinusoidal signal. This phenomenon known as spatial aliasing [22]. The response curve peaks at a lowest optimal spatial frequency of $f_{s,opt} = \frac{1}{4\Delta\phi}$, as shown in (a). This is consistent with the term $sin(2\pi f_s \Delta\phi)$ in Eq. (4.9). At a given spatial frequency, according to the identity of $f_t = f_s v$, the temporal frequency will increase along with an increase in velocity, as shown in Figure 4.6 (b). However, f_t appears in Eq. (4.9) through the term $\frac{f_t}{{f_t}^2 + 1/(2\pi\tau)^2}$, so the output will not increase monotonically with f_t. Instead, the response reaches an optimum response when $f_{t,opt} = \frac{1}{2\pi\tau}$, and then decrease monotonically as velocity increases further past this point.

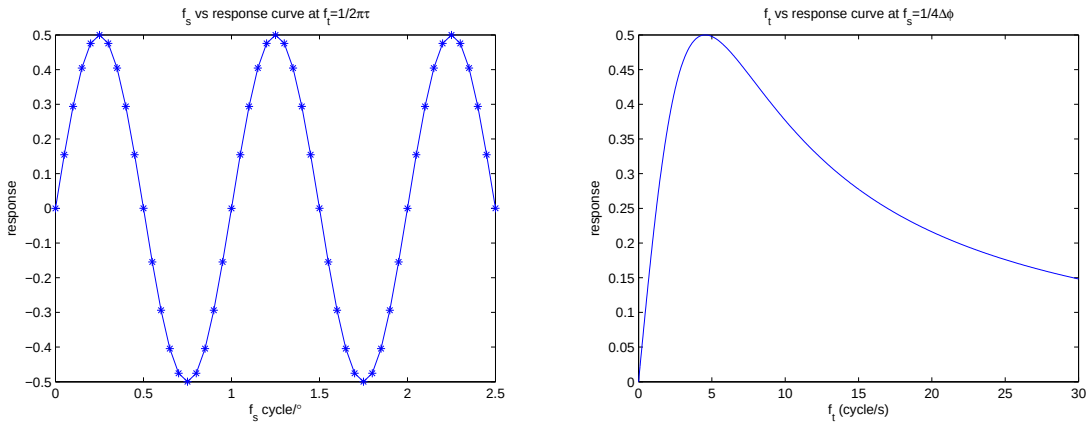

(a) (b)

Figure 4.6. Response of the Reichardt Correlator with varying spatial and temporal frequencies. (a) show the response as a function of spatial frequency for the optimal temporal frequency, $f_t = \frac{1}{2\pi\tau}$. (b) shows the response as a function of temporal frequency for the lowest optimal spatial frequency, $f_s = \frac{1}{4\Delta\phi}$.

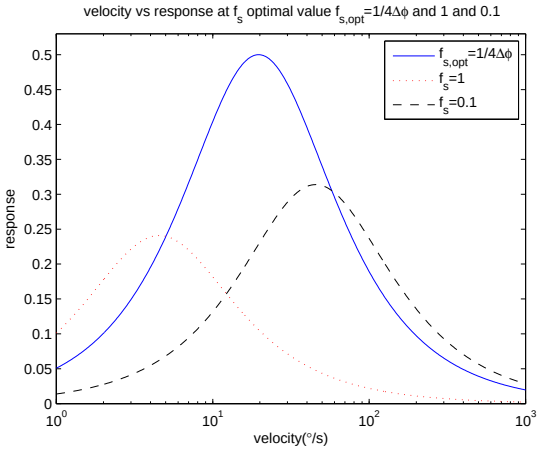

Figure 4.7. Velocity response with varying spatial frequencies. The velocity estimation varying with the spatial frequency.

Assume a sinusoidal grating with spatial frequency f_s moving with increasing velocity, the response will increase until the velocity reaches an optimum value given by:

$$v_{opt} = \frac{f_{t,opt}}{f_s} = \frac{1}{2\pi f_s \tau},$$

and then decrease gradually toward zero, as is shown in Figure 4.7. The Figure 4.7 also shows that optimal value for the velocities are different at different f_s. When the spatial frequency is set at optimal value $f_{s,opt} = \frac{1}{4\Delta\phi}$, the correlator response provides an unambiguous estimation of velocity at $19.6°/s$, which is the peak of the bell-like shape curve. When the velocity increases further than $19.6°/s$, the response values are same as the responses at velocities below $19.6°/s$. This critical velocity is named optimal velocity, which can be interpreted as the highest velocity which can be estimated unambiguously by the Reichardt Correlator.

In Section 4.1, the spatial angle $\Delta\phi$ between the two receptors was discussed. The spatial angle decides the spatial frequency tuning; varying $\Delta\phi$ changes the spatial frequency optimal value and makes the spatial frequency produce negative outputs, as shown in Figure 4.8 (a) and (b). The curves in Figure 4.8 are used as a reference only, and $\Delta\phi$ is assumed to be fixed in this chapter's simulation.

The final parameter affecting the response of the Reichardt Correlator is τ, which is the time constant in delay filter. The delay filter acts as temporal frequency tuning. In all the simulations contained in this thesis, a first order delay filter with time constant

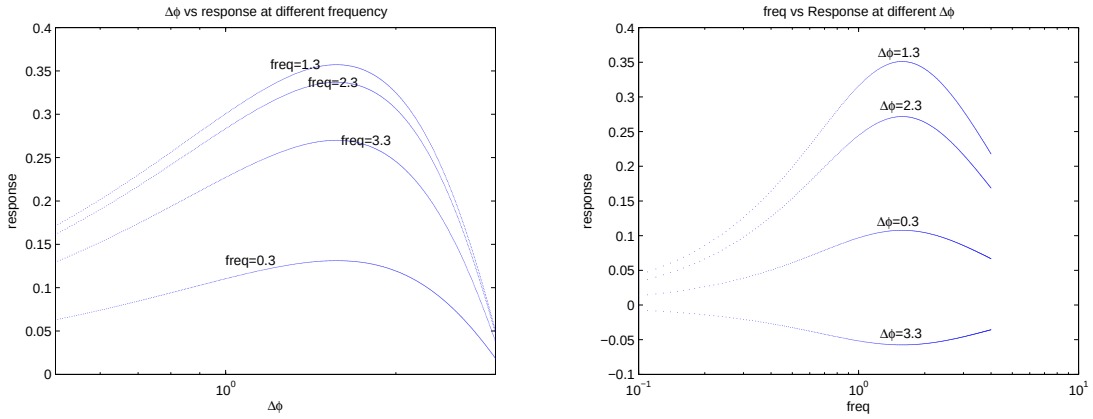

(a) (b)

Figure 4.8. Response of the Reichardt Correlator with varying spatial frequencies and spatial angles. (a) shows the responses with varying spatial frequencies. (b) shows the responses with varying spatial angles $\Delta\phi$. Even with in fixed velocity, the stimulant with different spatial frequencies keep on varying, and this is same with spatial angle.

τ=35ms is choose [37]. This value is chosen to avoid temporal aliasing, and it has been showed that other choices for τ can cause the Reichardt Correlator to produce negative output in response to certain temporal frequencies [22].

In summary, the output response of the Reichardt Correlator is highly dependent on velocity, contrast, spatial frequency and temporal frequency. However, due to its inherent simple arithmetic structure, the basic Reichardt Correlator is adopted in this thesis. In the next section, in order to investigate the performance of the Reichardt Correlator further, different types of images will be used as input signals, and then the proposed approaches of using different bit depth representation and oversampling will be elicited in more details.

4.3 Performance of the Reichardt Correlator using the Proposed Approaches

As a bio-inspired motion detector, the Reichardt Correlator has lower computational complexity than other motion detection algorithms [23], and a series of VLSI motion

sensors have adopted this model [21]. In Sections 4.1 and 4.2, the basic Reichardt Correlator model shown in Figure 4.1 was discussed. This section will investigate the performance of the Reichardt Correlator, for different input sample bit depths, with oversampling under natural image stimulation. The proposed approaches were described in Chapter 3. The aim of these approaches are to explore the performance of velocity estimation of the Reichardt Correlator under different quantisation and sampling conditions.

In this section, the spatial angle between two front receptors is $\Delta\phi = 1.08^\circ$ [65] and a first order low-pass filter with time constant τ=35ms are assumed [22, 37]. The input signals to the Reichardt Correlator will be stimulated receptor signals under stimulus from the images 'sine grating' (Figure 3.4), 'friend' (Figure 3.3), and 'scenery' (Figure 3.8). Moreover, three natural panoramic images, named 'forest', 'garden', 'building', are added, and these are shown in Figure 4.9. All the images in simulation are 8-bit greyscale. It is assumed that all images are moving from left to right in front of the two receptors of the Reichardt Correlator along the horizontal axis, at velocity v, in degrees per second ($^\circ/s$).

In order to investigate the performance of the Reichardt Correlator, from simple to complex images, the sequence of inputs into the Reichardt Correlator for each approach are:

1. 'Sine grating'. This is a simple image, and contains only a single frequency.

2. 'Friend'. This windowed image is a naturalistic image with multiple spatial frequencies. It contains objects found in an indoor environment.

3. 'Panoramic images'. Four panoramic images are used as stimuli throughout this investigation. They represent some plausible visual scenes as processed by insects. These images are 'scenery', 'forest' , 'building' and 'garden'. The 'scenery' is used firstly in panoramic image stimulation, since it is simpler than other panoramic images, and contains 964 pixels horizontally and 101 pixels vertically. In comparison, the other three panoramic images are 14659 x 1648 pixels in size.

(a) Forest in 8-bit representation.

(b) Garden in 8-bit representation.

(c) Building in 8-bit representation.

Figure 4.9. 8-bit depth representation of natural images used in the simulations as stimuli. These panoramic images are used to represent the visual scenes as processed by insects.

The larger images require more time in simulation processing, so the more complex panoramic images are only used in the last phase to thoroughly investigate the performance of the Reichardt Correlator.

All the simulations are implemented using Matlab, to take advantage of its flexible processing and toolbox capabilities.

4.3.1 General approach

In Sections 4.1 and 4.2, with single frequency sinusoid as an input to the Reichardt Correlator, we came to the following conclusions:

- The basic Reichardt Correlator has attractive implementation for its striking simplicity, and the output response is sensitive to the motion detection.
- The basic Reichardt Correlator performance is highly dependent on both the contrast and spatial frequency of the sinusoid image.

However, in the real world, moving objects that need to be detected are not simple sinusoids. In the following simulations, sine grating image and real-world images are applied to the input of the Reichardt Correlator to show the performance of the output response.

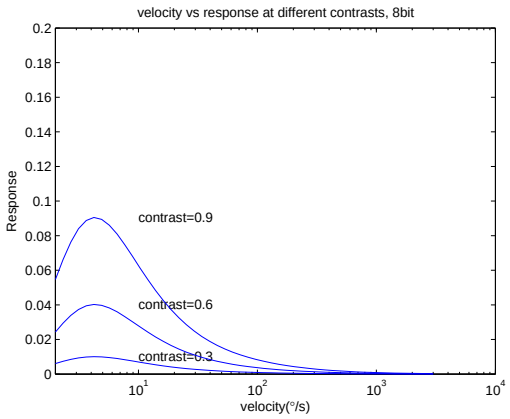

(a) Velocity responses for 'sine grating'.

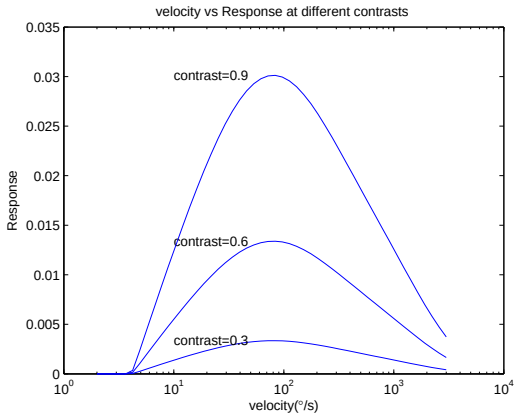

(b) Velocity responses for 'friend'.

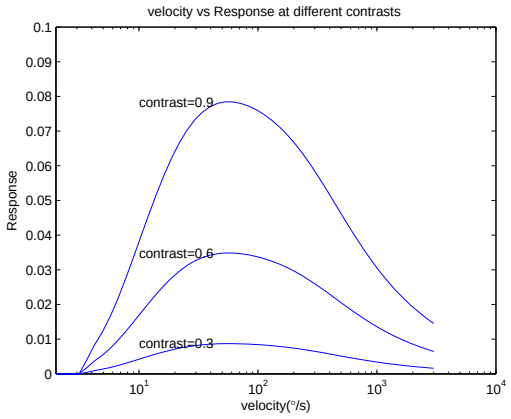

(c) Velocity response for 'garden'.

Figure 4.10. Velocity response for three images with varying contrasts. The contrast affect the response of the Reichardt Correlator, regardless of image type. Moreover, the optimal velocities are different for each image. This is considered as effect by different spatial frequencies in images.

Figure 4.10 shows the different responses of the Reichardt Correlator output for three types of image signals. It can be seen that these response curves share the same bell-like shape. As velocity increases form $0°/s$ to $3000°/s$, the response rises from zero to a maximum value, and then falls off towards zero. Three different contrasts are tested,

and it is clear that contrast has a direct impact on the output response regardless of the image. Moreover, it should be noted that the peak response value in three response curves are not same, that is, are not located at the same optimal velocity. This phenomenon is influenced by the different spatial frequencies contained in image, since these are highly variable for different types of images. It can be concluded that contrast and spatial frequency are parts of the limitations of basic Reichardt Correlator for natural images.

The simulations were conducted by firstly processing a number of rows of an images. Each row generates simulated receptor signals for different velocities. The outputs are averaged across all rows to obtain the response curves in Figure 4.10. In order to elicit the effect of spatial frequency on the Reichardt Correlator response, individual rows of the input images will be analysed.

Figure 4.11 shows how different spatial frequencies in an image affect the Reichardt Correlator output response. The 'friend' image is a windowed naturalistic image with multiple spatial frequencies, the first row represents the top line in this image when using Matlab image processing toolbox (IPT) [67] for the simulations. The $400th$ row is near the centre of the image, since 'friend' has 600 rows in total. Two black lines are used to show the 1st and 400th row in 'friend' in Figure 4.11 (a).

Figure 4.11 (a) shows that the first row only contains the background and the corner of wall, and does not have much information or changes in the greyscale representation. However, in the zone which $400th$ row passes through, there are laboratory equipment, human figure, computer and many other objects. Therefore, it is rich in information and contains rapid changes in the greyscale representation. This is exactly the reason why the curves in Figure 4.11 (c) have more accurate response curves than the curves in Figure 4.11 (b). The image motion direction is from left to right, according to the conclusion of directional response, the output response should be positive. In Figure 4.11 (b), however, the response curves for three different contrasts all indicate negative value starting from the velocity equal to $1000^\circ/s$. This negative value is caused by the first row lacking meaningful image information, with the most distinguishable feature being the edge of corner of the wall. When the image is moving at

high velocity synchronously with fewer fidelity information, the output will obtain the inaccurate response. However, this inaccurate negative value is too small to affect the mean of response, which is approximately 10^{-3} in magnitude. Since the image signal response takes the average of all rows' correlator responses, this small negative value has less influence on the overall mean response. As shown in Figure 4.10 (b), the mean response curve for 'friend' image, shows a positive response along with the velocity axis, correctly indicating the motion is from left to right.

NOTE:
This figure is included on page 58
of the print copy of the thesis held in
the University of Adelaide Library.

(a) 8-bit depth representation of 'friend' image.

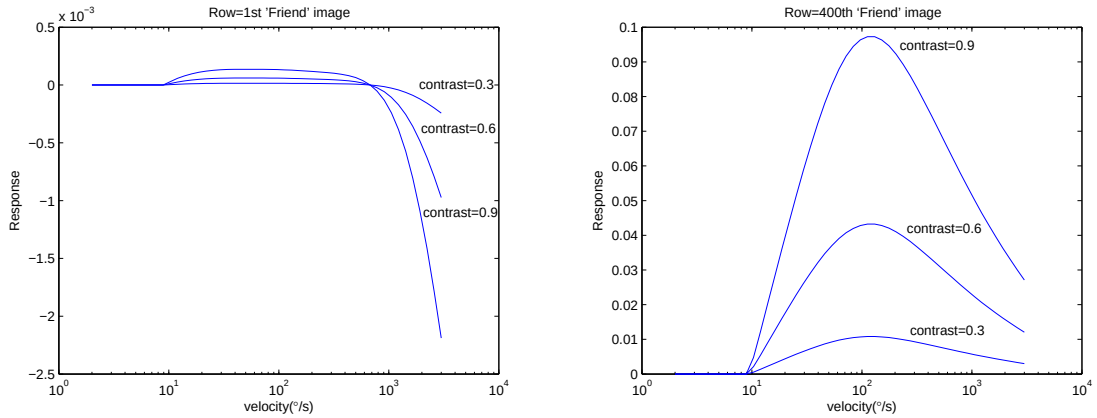

(b) Velocity responses generated by 1st row of 'friend'.

(c) Velocity responses generated by 400th row of 'friend'.

Figure 4.11. Velocity response for two fixed rows of 'friend' with varying contrasts. Compared with (b) and (c), the 400th row have more accurate velocity response than 1st row. This is caused by lacking image information in 1st row.

In this section, through using different types of input images to the basic Reichardt Correlator model, it can be concluded that the basic Reichardt Correlator is sensitive

to the motion direction for all image types, and its output response magnitude is dependent on the contrast and spatial frequency contained in the image. This limitation can be partially solved by an elaborated Reichardt Correlator [2, 13, 22, 49, 58, 66]. In Section 3.2, the approach of using different bit depths to represent image samples is proposed. Using low bit representation is mainly motivated by the pursuit of low computational complexity, as having lower bits can relieve the power consumption and complexity of arithmetic in the visual motion detection system. In the next section, the performance for different bit depths image in the input to the basic Reichardt Correlator will be studied, and from the output response we can investigate the penalty on velocity estimation performance.

4.3.2 Effect of bit depth on the Reichardt Correlator response

The images of 'sine grating', 'friend' and 'scenery' are used to investigate the effect of bit depth representations. In Section 3.2, the effect of varying bit depths for the 'sine grating' and 'friend' images, shown in Figures 3.4 and 3.3. In Figure 4.12, shows the eight different bit depth from 8 down to 1-bit representation for 'scenery'.

In the 8-bit representation of 'scenery', the visual features such as the sky, buildings, trees, shadows, and the edges between different objects are clear. As the bit depth decreases from 8-bit down to 1-bit, it becomes increasingly hard to distinguish the features such as the sky, building, trees, shadows, and the edges become increasingly unreliable. The image is visually degraded and results in a low fidelity representation at low bit depths, especially for bit depths lower than 3-bit. It has the similar impact on 'sine grating' and 'friend'. In order to show the effect of bit depth on the Reichardt Correlator response, the eight bit depth images of 'sine grating', 'friend' and 'scenery' will be input as stimulus to investigate the system performance.

Figure 4.13 shows the output responses for different bit depth representations of 'sine grating'. It can be seen that all bit depth representations are all equally affected by contrast, with high contrasts achieving high responses. Since the 'sine grating' is moving from left to right, all response curves have positive values, and the response curves

(a) 8-bit representation.

(b) 7-bit representation.

(c) 6-bit representation.

(d) 5-bit representation.

(e) 4-bit representation.

(f) 3-bit representation.

(g) 2-bit representation.

(h) 1-bit representation.

Figure 4.12. Eight different bit representations 'scenery' used in the simulation as stimuli.

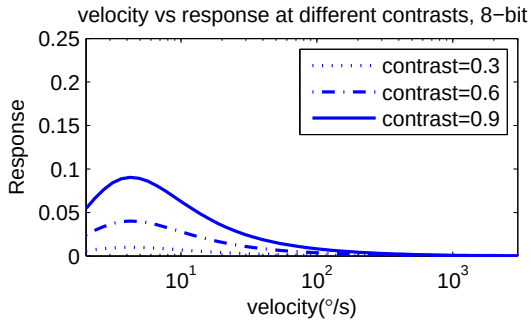

(a) 8-bit response.

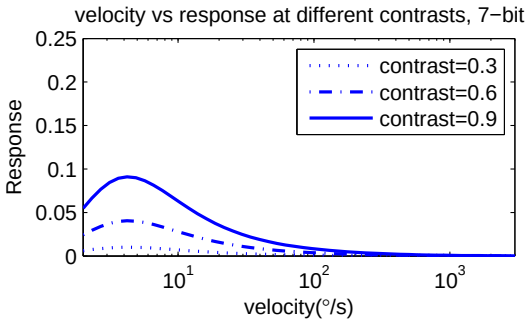

(b) 7-bit response.

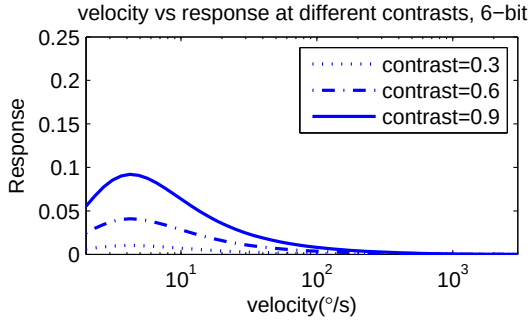

(c) 6-bit response.

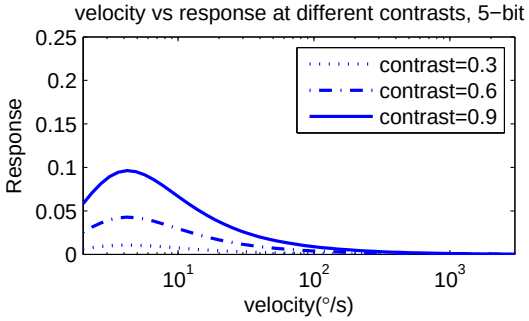

(d) 5-bit response.

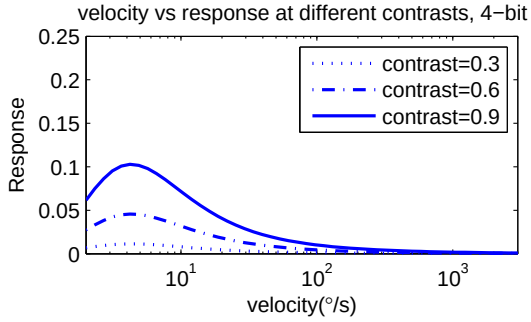

(e) 4-bit response.

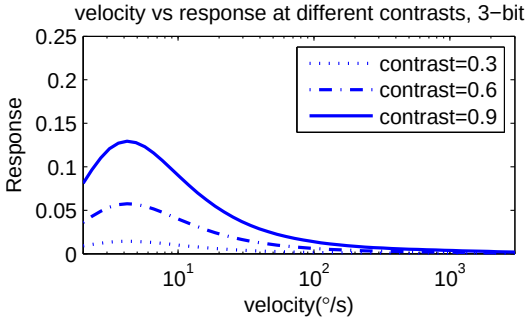

(f) 3-bit response.

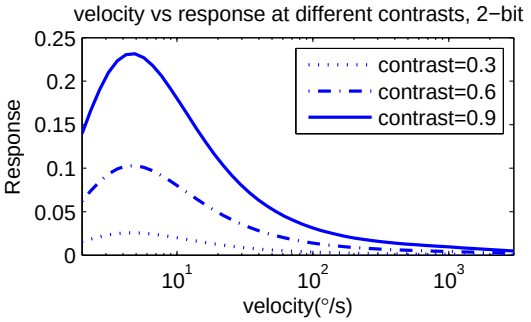

(g) 2-bit response.

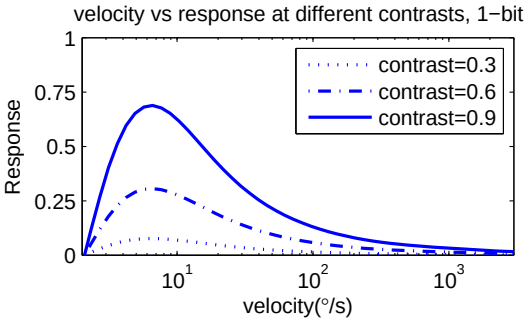

(h) 1-bit response.

Figure 4.13. Velocity estimates for 'sine grating' in eight bit depths with varying contrasts. From 8 to 2-bit, the response axis changed scales as 0 to 0.25, the 1-bit response axis is 0 to 1. It indicates the lower bit has higher response along velocity axis.

increase until the velocity reaches the optimal value and then, decrease gradually toward zero. It is also can be seen that, for the same set value of contrast, the lower bit representations have higher optimal velocity responses. However, the same optimal velocity is shared by all bit depths. It can be concluded that the proposed technique of using low bit representations can raise the dynamic range of output response for 'sine grating' stimuli, while preserving the same optimal velocity.

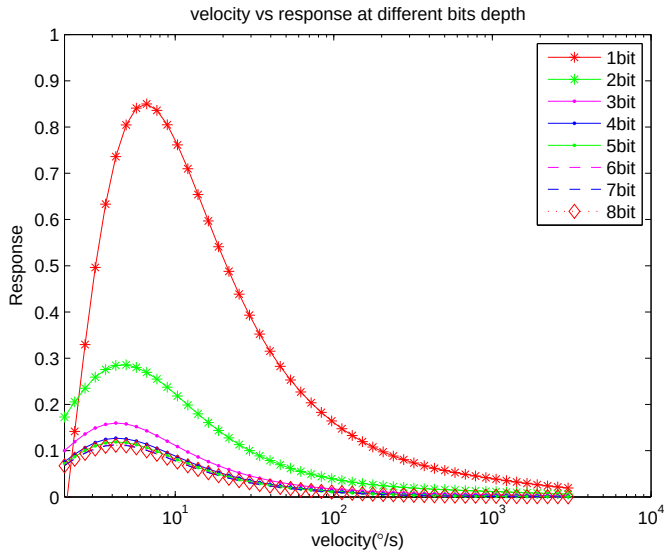

Figure 4.14. Effect of eight different bit depth representations for 'sine grating'. The eight curves for different bit depth in the same axis can clearly show the lower bit representation have higher velocity response.

Figure 4.14 shows the response of different bit depths from 8 to 1-bit for 'sine grating' images on the same axis. There is a set of curves near the bottom velocity axis, which are the 8 to 3-bit representation curves. They all have low response values, and it is particularly hard to distinguish the curves from 8 to 4-bit representations. The green line with asterisk corresponds to the 2-bit representation response, which is easy to distinguish from higher bit representation response curves, and have relative high dynamic range in response values. However, the 2-bit representation response curve, like the higher bit depth curves, retains almost the same response value from the velocity of $100^\circ/s$ to $3000^\circ/s$. The red line with asterisk curve is the 1-bit representation response, and it has the highest dynamic range of response performance. It can be seen from 1-bit representation curve that the response value at each velocity from 0 to $3000^\circ/s$ are

more distinguishable than other curves, and it has the highest response value. In this instance, it is clear that lower bit depth representations have better response curves for velocity estimation.

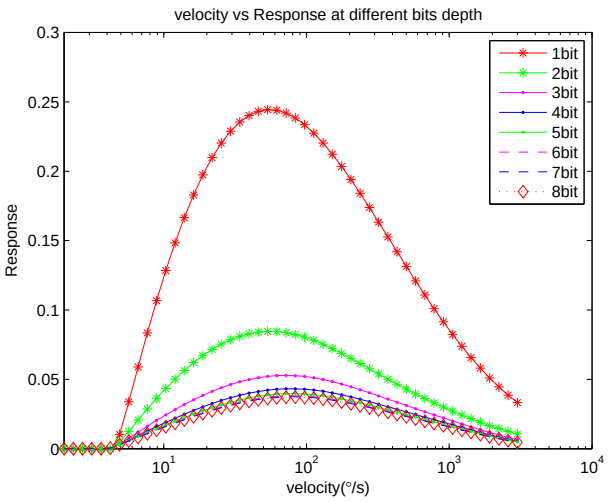

Figure 4.15. Effect of eight different bit depth representations for 'friend'. This effect is same as the 'sine grating'. The 1-bit representation has the higher velocity response than the other seven bit representations.

In order to further investigate the performance of the Reichardt Correlator on natural images, the 'friend' and 'scenery' images will be used respectively at different bit depth representations. Figure 4.16 shows the response curves for different bit depth representation of the 'friend' image. From 8 to 1-bit, it shows broadly the same behaviour as for 'sine grating': the response curves are highly affected by contrast, and the lower bit depths have higher dynamic ranges in their responses. Setting the full contrast curves on the same axis in Figure 4.15, three sets of curves are also emerged. The first set of curves correspond to 8 to 3-bit representation curves which are hard to distinguish from each other. The second set of curve is 2-bit representation curve (green line with asterisk) which has a higher dynamic range of response than the first set of curves. The red line with asterisk is the 1-bit representation curve, which has the highest dynamic range performance among all the curves. Thus, the same conclusions can be drawn as for the 'sine grating'.

Figure 4.17 shows the different bit depth representation response curves for the 'scenery' image signal. Comparing the response curves for the different bit depths, the output

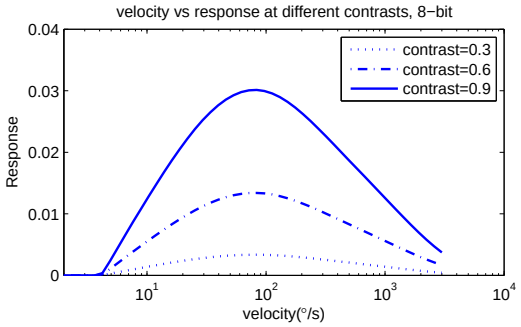

(a) 8-bit response.

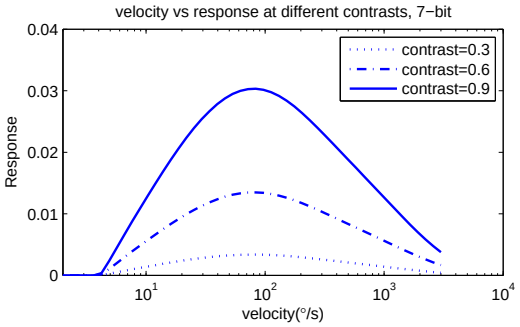

(b) 7-bit response.

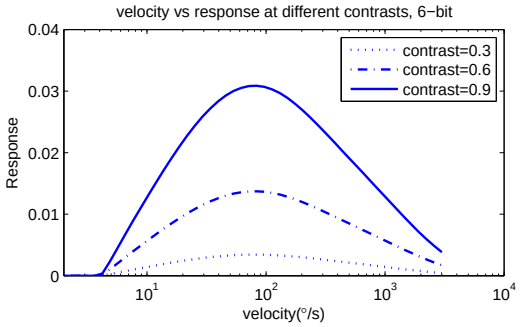

(c) 6-bit response.

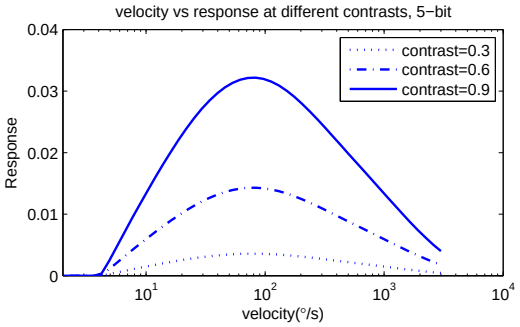

(d) 5-bit response.

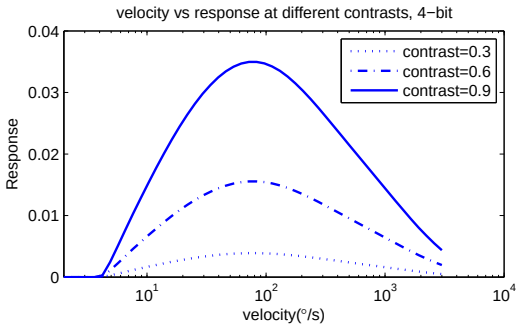

(e) 4-bit response.

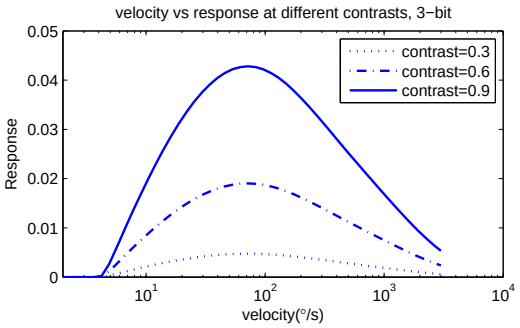

(f) 3-bit response.

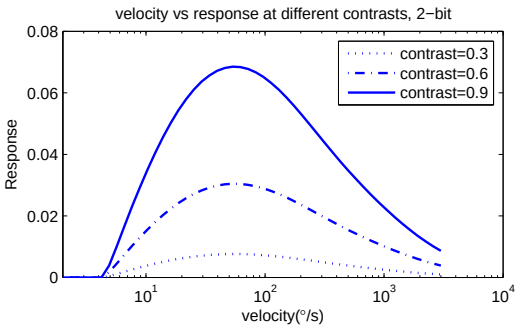

(g) 2-bit response.

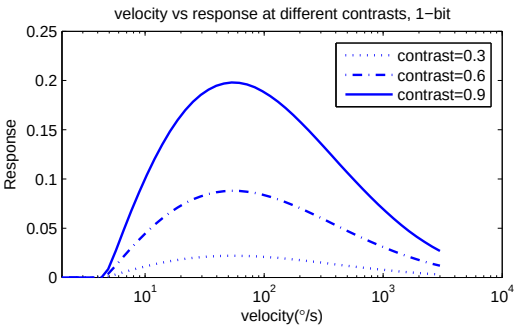

(h) 1-bit response.

Figure 4.16. Velocity estimates for 'friend' in eight different bit depths with varying contrasts. It should be notices that from 8 to 4-bit, the response axis changed scales as 0 to 0.04, the 3 to 1-bit response have larger scales in response axis.

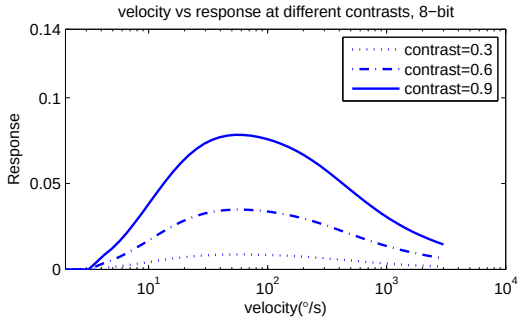

(a) 8-bit response.

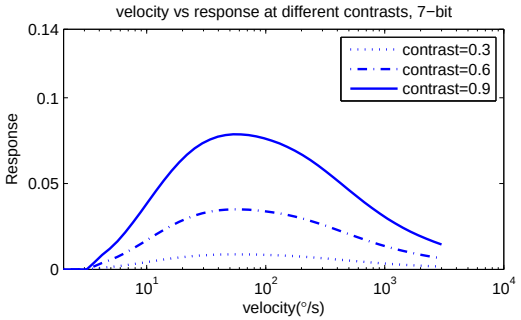

(b) 7-bit response.

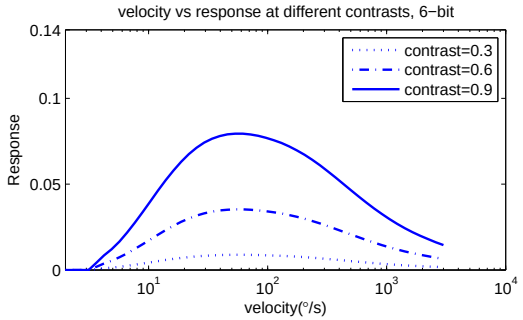

(c) 6-bit response.

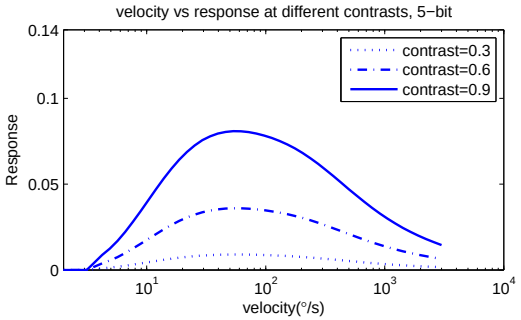

(d) 5-bit response.

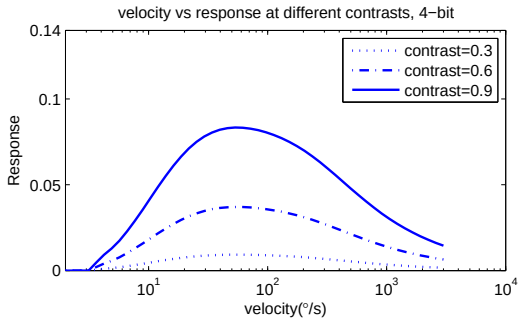

(e) 4-bit response.

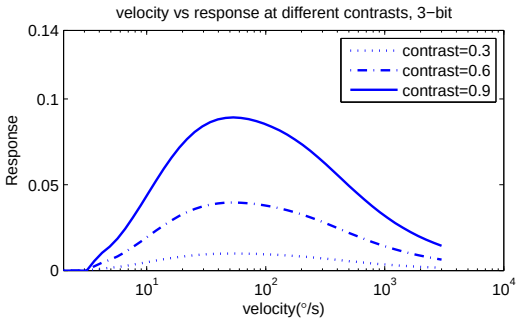

(f) 3-bit response.

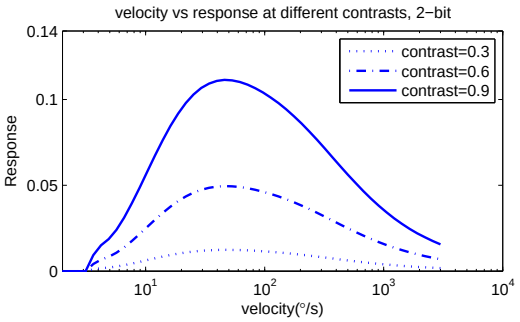

(g) 2-bit response.

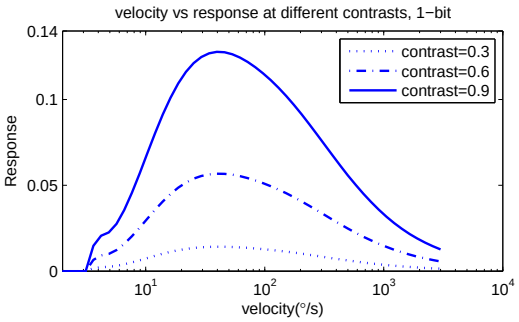

(h) 1-bit response.

Figure 4.17. Velocity estimates for 'scenery' in eight bit depths with varying contrasts. From 8 to 1-bit, the response axis in the same scale as 0 to 0.14, however, it can be clearly seen that the 1-bit response curves have higher optimal response than 8 to 2-bit.

response performance shows the same influences from contrast and bit depth representation, as for the 'sine grating' and 'friend'. Applying full contrast and putting the different bit depth representation response curves on the same axis, Figure 4.18 shows the similar performance to the 'sine grating' and 'friend' (in Figure 4.14 and Figure 4.16, respectively).

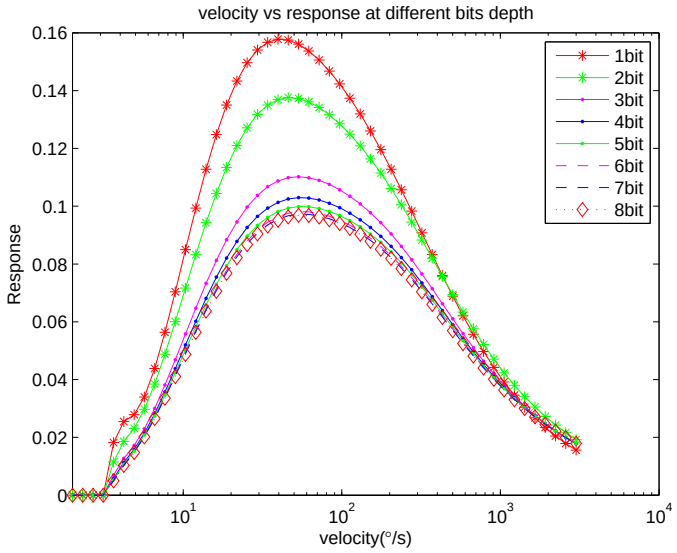

Figure 4.18. Effect of eight different bit depth representations for 'scenery'. The bit depth have the same effect on the different bits 'scenery', the behaviour is same as 'sine grating' and 'friend'.

From the above simulations, it can be seen that all these response curves share the same bell-like shape. It should be noted that despite the response curves of 'sine grating', 'friend', 'scenery' having the same shape, the response values for any given velocity are not the same. This is caused by differences in the image details.

Figures 4.19 (a) and 4.19 (b) show the response of the Reichardt Correlator for first row of 'friend' image, but at 8-bit and 1-bit representations respectively. Obviously, the 1-bit response curve has better velocity estimation characteristics than the 8-bit response. Since this simulation has assumed the motion is from left to the right, the response should show positive values. The suspected reason for the misleading Reichardt Correlator response at 8-bit is the mainly slow gradual changes in the wall failing to register large correlator outputs. In contrast, the binary 1-bit representations will introduce abrupt signal changes which would cause large correlator responses.

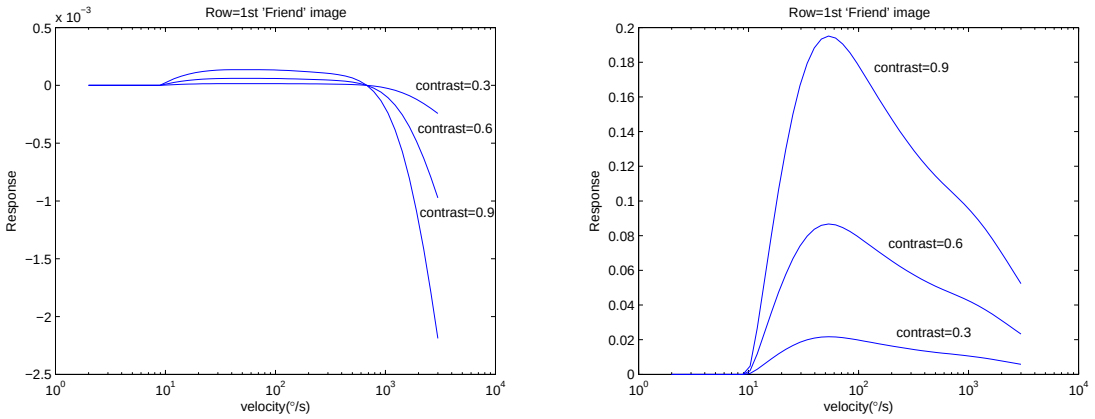

(a) 8-bit response for the 1st row.

(b) 1-bit response for the 1st row.

Figure 4.19. Velocity response of different bit depth representations for single row in 'friend' with varying contrasts. Compared with (a) and (b), it can be seen that using 1-bit representation, the velocity response of 1st row have more accurate performance than 8-bit.

One may notice that although 8-bit response in Figure 4.19 (a) has negative values, the response of the whole 8-bit 'friend' in Figure 4.16 (a) has positive response values. This is due to the whole response being the mean of all row responses. The tiny contribution from row 1 (10^{-3}) does not affect the accuracy of the overall response.

In the current section, through investigation of the different bit depth representations for image samples, it can be concluded that using lower bit depths represent the input signal to the Reichardt Correlator, the output response have better velocity estimation performance curve, and lower bit depth representations can partially mitigate the influence of spatial frequency. In the next section, using oversampling to raise sample rate is proposed and investigated through simulations.

4.3.3 Effect of oversampling on the Reichardt Correlator response

Sampling is a necessary step to capture an analog signal to a digital from suitable for processing on a computer. In this process, an analog-to-digital conversion is used to perform the sampling to convert the continuous time signal to discrete time signal. In Section 3.4, the definition of Nyquist sample rate and oversampling rate have been

given. Sampling signals at Nyquist rate, which is a sample frequency twice the signal's maximum in-band frequency, is the fundamental requirement to reconstruct original signal from sampled signal. Through the investigation in reduction in different bit depth representation, it can be concluded that using lower bit depth to represent the input signals to the Reichardt Correlator, does not affect the Reichardt Correlator's peak response. Using 1-bit representation yields the highest response among various bit depths, and this reduction in word length is tremendously advantageous from an arithmetic implementation viewpoint. However, when using lower bit depths, a large amount of signal information will be lost, but this loss can be traded-off against an increase in sampling rate. In next section, the response of the Reichardt Correlator for different sampling rates will be studied, and from the output response, we investigate the impact of varying sampling rate on the performance of the Reichardt Correlator.

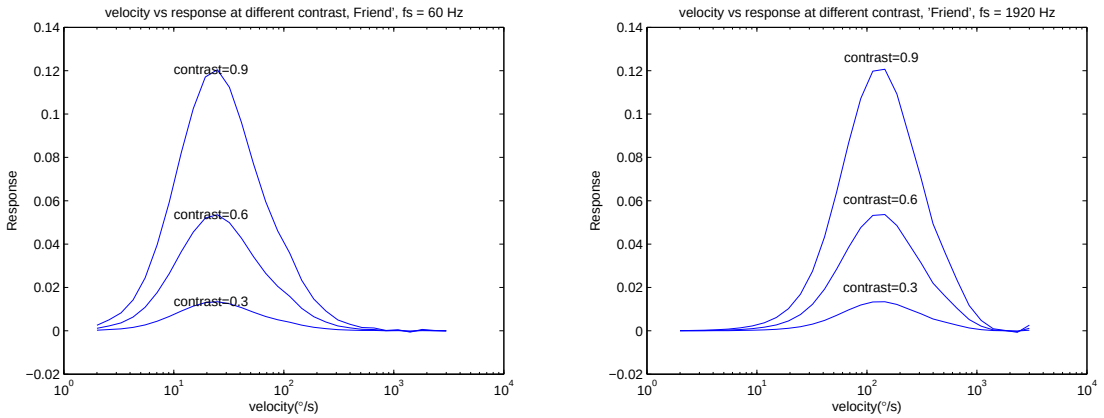

(a) Sampled at Nyquist sampling rate 60 Hz. (b) Sampled at 32X oversampling rate 1920 Hz.

Figure 4.20. Velocity response of 8-bit 'friend' for different sampling rates with varying contrasts. The curves in (a) and (b) for the same contrast have the same response dynamic range. However, the oversampling rate has the higher optimal velocity, which is $105^\circ/s$, compared $20^\circ/s$ when sampled at Nyquist rate.

At first, the 8-bit 'friend' image in Figure 3.2 will be used as input signal, sampled at Nyquist rate. Since experiments on human vision show that humans can distinguish frequencies up to 30 Hz [68], therefore, 60 Hz is chosen as the Nyquist rate in this work. For comparison, sampling is also performed at 1920 Hz, which corresponds to

a 32 times oversampling. These two different sample signals are fed into the Reichardt Correlator to obtain the different response curves shown in Figure 4.20.

In Figure 4.20, the two graphs show the response of two different sampled signals with different contrasts. For each graph, it can be seen that the contrast affects the response at both sampling rates. When Nyquist rate sampled signal is used, the response curves are shown in Figure 4.20 (a). Compared with the response curves of the oversampled signal in Figure 4.20 (b), the optimum velocity shifts from $20°/s$ (for f_s = 60 Hz) to the $105°/s$ (for f_s = 1920 Hz). Besides, for each different contrast signal, the differently sampled signals have the same peak responses. Therefore, sampling rate does not affect the shape of the Reichardt Correlator response, although higher sampling rates are more suited to the detection of higher velocities. However, contrast factor still plays a major role in all responses.

Figure 4.21 shows the Reichardt Correlator responses at the different sampling rates on 8-bit 'scenery' image.

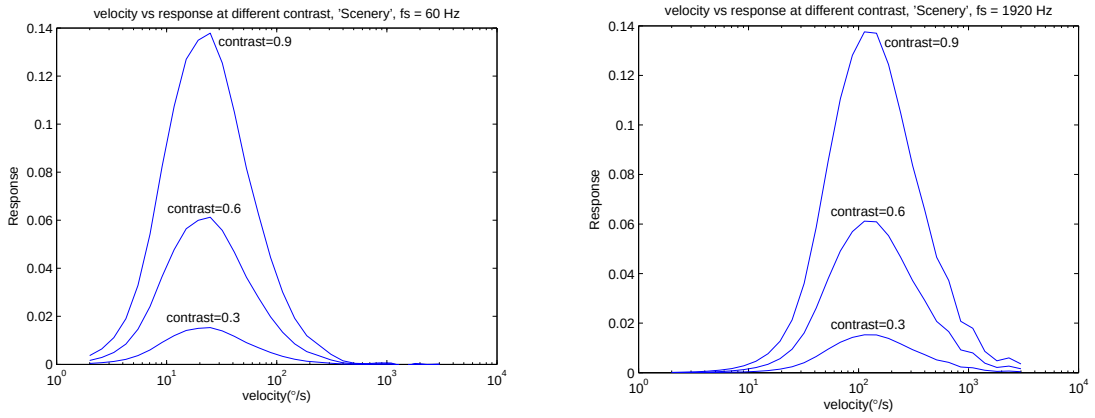

(a) Sampled at Nyquist sampling rate.

(b) Sampled at 32X oversampling rate.

Figure 4.21. Velocity response of 'Scenery' for different sampling rates with varying contrasts. The different sampling rates have the same effect as 'friend'. Sampling at oversampling rate has higher optimal velocity.

From Figure 4.21, the same conclusions can be drawn as for the response of 'friend': oversampled input almost has the same performance as Nyquist rate input and for each contrast; the different rate of sampled signal has the same peak response. The same shift in optimal velocity is observed for 'scenery', which suggests that higher f_s

is suitable for detecting higher velocities. There is one point should be noticed that in Figure 4.21 (b), the response curve oscillates for velocities faster than $1000°/s$. However, this oscillation does not affect the result of velocity estimation. Since the response curve has a bell-like shape, when the detected velocity is greater than the optimum velocity, the response curve begin to fall off, and cause aliasing with a lower velocity. It is for this reason that responses for velocities greater than optimum velocity are not considered.

In Section 4.3.2, the approach of using fewer bits to represent input signal is proposed. It shows better velocity estimation performance and can bring simpler arithmetic implementation. In this section, the simulated image samples that have full contrast images are used, with different bit depths ranging from 8 to 1-bit and sampled at two different sampling frequencies, which are Nyquist rate (60 Hz) and 32 times oversampling rate (1920 Hz).

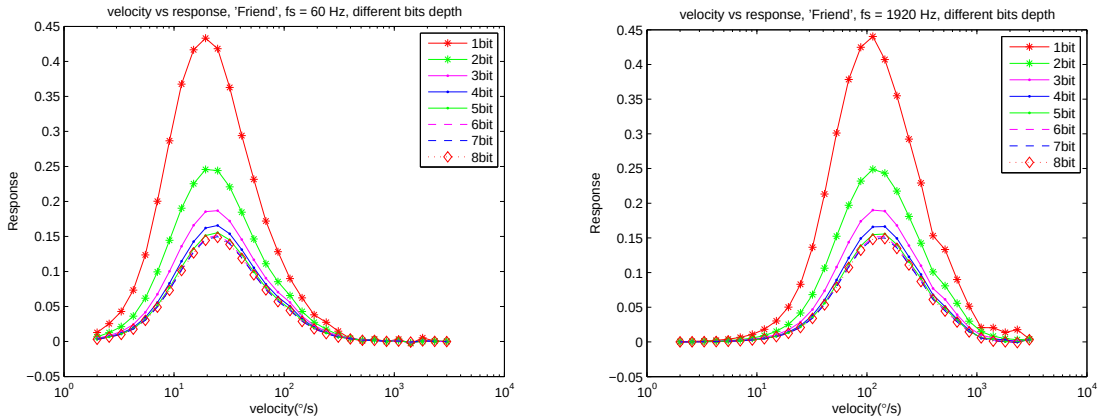

(a) Sampled at Nyquist sampling rate with different bit depths.

(b) Sampled at 32X oversampling with different bit depths.

Figure 4.22. Velocity response of 'friend' for different sampling rates with different bit depths representation. For the different bit depths, the sampling rate has the same effect on the velocity response.

Figure 4.22 shows the simulations of different bit depths with different sampling rates for the 'friend' image. For each sampling rate, the different bit depth curves show the same performance trend as in Figure 4.15: lower bit depths achieves higher responses for the same velocity. Comparing the curves between the two sampling rates with

same bit depth representation, the optimal velocity is shifted. In Figure 4.22 (a), the optimal velocity is located in $15°/s$ (for f_s = 60 Hz). When sampled at oversampling rate, the optimal velocity shifts to $105°/s$ (for f_s = 1920 Hz). Figure 4.23 shows the response curves for 'scenery' image under the same approach, the same conclusions can be obtained.

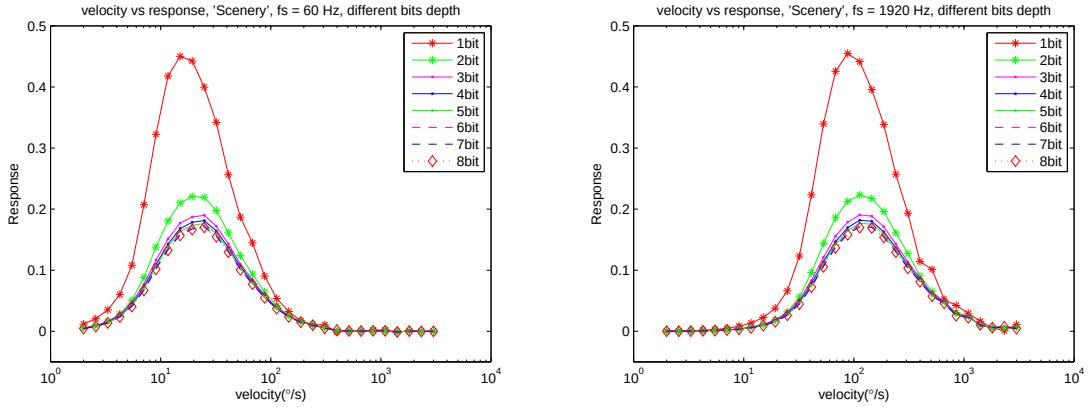

(a) Sampled at Nyquist sampling rate with different bit depths.

(b) Sampled at 32X oversampling with different bit depths.

Figure 4.23. Velocity response of 'Scenery' for different sampling rates with different bit depths representation. These curves have the same velocity response performance as 'friend'.

From the above simulations, the 1-bit representation with oversampling rate shows excellent velocity estimation performance. In the next section, the approach of using single bit, with oversampling rate and noise shaping to process the input signal will be proposed, this is discussed in Section 3.5, where a sigma-delta modulator is used.

4.3.4 Effect of oversampling with noise shaping on the Reichardt Correlator response

From the results of earlier investigations, the combined basic Reichardt Correlator and noise shaping interface is shown in Figure 4.24.

The receptors A and B capture signals, that are sampled and quantised for processing. While most converters capture signals at relatively high bit depth and Nyquist rate, the

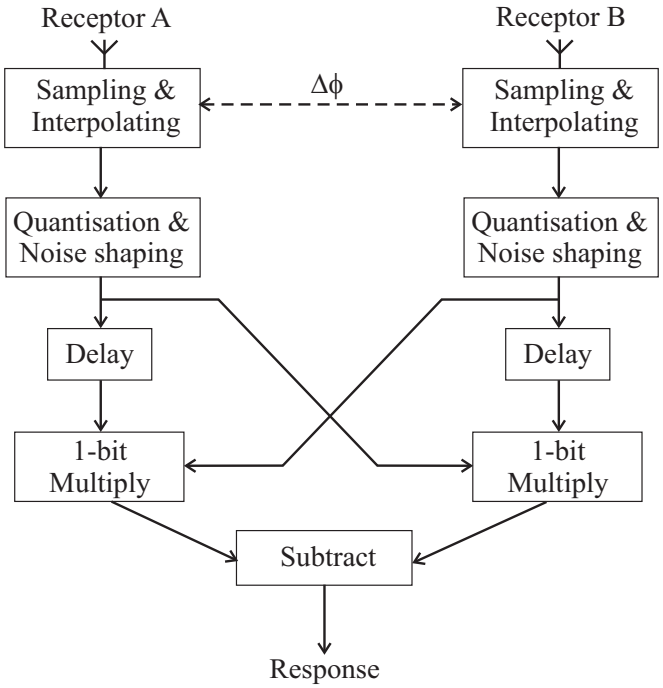

Figure 4.24. The combined Reichardt Correlator and 1-bit oversampling interface. Instead of the signal applied to the Reichardt Correlator directly, the system first performs high sampling rate conversion on the image sequence along the time dimension, to achieve oversampled time series for each pixel. Then, the oversampled series is subjected to quantisation to 1-bit samples. Finally, the 1-bit samples are input to the Reichardt Correlator as stimulus. Since the 1-bit samples are used, the multiplies in each branch can be replaced as 1-bit XOR operations, which can greatly reduce the arithmetic complexity.

sigma-delta conversion operates by using single bit quantisation, trades-off sampling rate with bit depth. Figure 4.25 shows a first order sigma-delta modulator used in the following simulations.

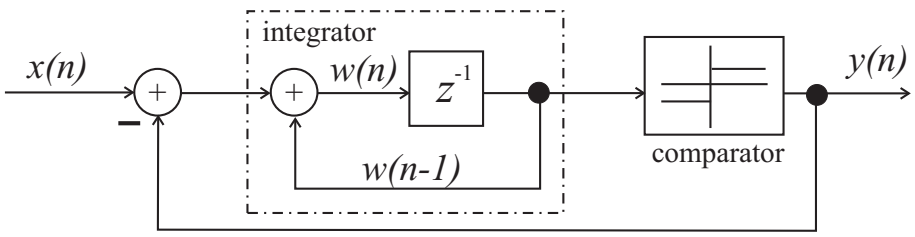

Figure 4.25. The first order Sigma-Delta digital converter. The input digital signal $x(n)$ is subjected to this sigma-delta digital converter to generate the output digital signal $y(n)$ after processed by using 1-bit oversampling rate with noise shaping processing.

The signal $x(n)$ is an sampled time signal, which is then subjected to a sigma-delta digital modulator. The modulator contains a subtractor, an integrator, and a comparator to generate 1-bit samples with a feedback loop. Using this approach, the original image signal is represented as single bit digital signal, which is only represented by +1 and -1 values. The resultant digital signal is input to the Reichardt Correlator to produce a response. This processing is supposed to bring later benefit of simplified arithmetic, since compared with some traditional analog to digital conversion, the sigma-delta modulator operating with oversampling and single bit representation has demonstrated low cost and high performance conversion. It is accepted that with advances in digital microelectronics and mixed signal techniques, the Reichardt Correlator is significantly simplified under 1-bit operation. In this section, we use this approach to simulate the Reichardt Correlator and analyse the output response, to examine its velocity estimation performance.

(a) Forest in 5 strips.

(b) Garden in 5 strips.

(c) Building in 5 strips.

Figure 4.26. Panoramic images cut into five strips. These shorter strips is used for analysis of the system performance based on image content.

The images used in the simulations are panoramic images of outdoor scenes, chosen to have different overall brightness, contrast and spatial frequency content. They are

named as 'forest', 'garden' and 'building', shown in Figure 4.9 (a), (b) and (c) respectively. There is one aspect which is different with the previous simulation: in order to investigate the qualitative effects of image content on the motion estimation algorithm, the three panoramic images are divided into 5 horizontal strips with each strip containing approximately 35 rows. The divided images are shown in Figure 4.26. These strips are then subjected to identical processing, and their results are compared.

In the following simulations, the received signals by two receptors in front of the Reichardt Correlator are converted rows in each image individually, with the direction of velocity from left to the right. The velocity is varied from 1 degree per second to 3000 degrees per second. Two sets of comparison are used to investigate the performance of the proposed approach: firstly, using single bit samples, different oversampling rates with noise shaping are applied to the received signals. In order to investigate the response effect of the proposed scheme, three different sampling rates are set: 960 Hz, 1920 Hz, and 3840 Hz, which represent 16 times, 32 times and 64 times of Nyquist sampling rate of 60 Hz, respectively. After that, a comparison of output response from two different signal representation will be put together in one axis for each strip of each image. One is using single bit, 1920 Hz sampling rate with noise shaping to represent signal while the other one is the conventional received signal representation in receptor in a Reichardt Correlator, which is digitised at 8-bit depth and sampled at Nyquist rate. This approach was implemented in Matlab to examine whether the proposed approach can achieve an accurate response.

The first set of comparisons with different oversampling rates with noise shaping, are shown in Figures 4.27, 4.28 and 4.29 for each strip of 'forest', 'garden' and 'building', respectively. The second set of comparisons are shown in Figures 4.30, 4.31 and 4.32, which uses two different signal representations: single bit sampled at 1920 Hz sampling rate with noise shaping and conventional 8-bit sampled at Nyquist rate. The simulations were drawn on the same axis to facilitate direct comparison of the responses.

Figures 4.27, 4.28 and 4.29 show the velocity responses when using the oversampling scheme with single bit representation with noise shaping for 'forest', 'garden', 'building' images, respectively. From all the sub-figures contained in these three figures, it

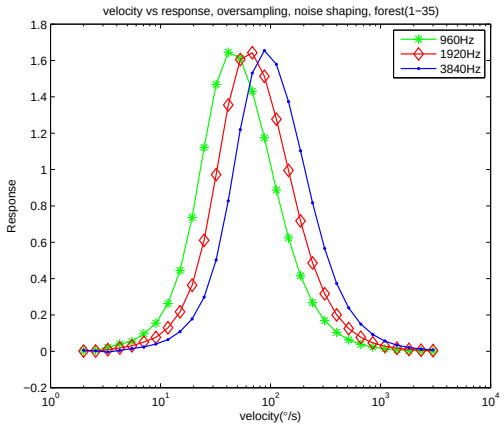

(a) Strip 1 (1-35).

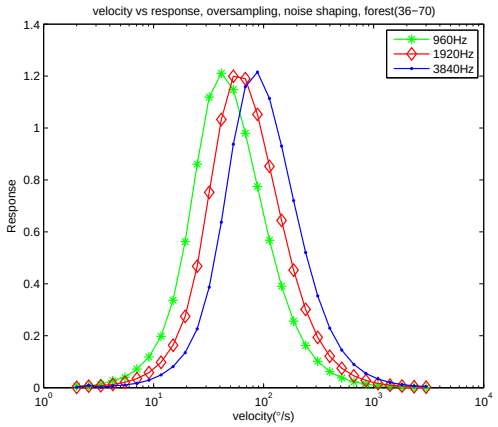

(b) Strip 2 (36-70).

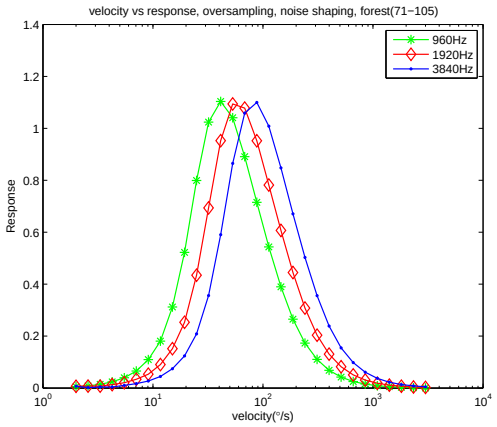

(c) Strip 3 (71-105).

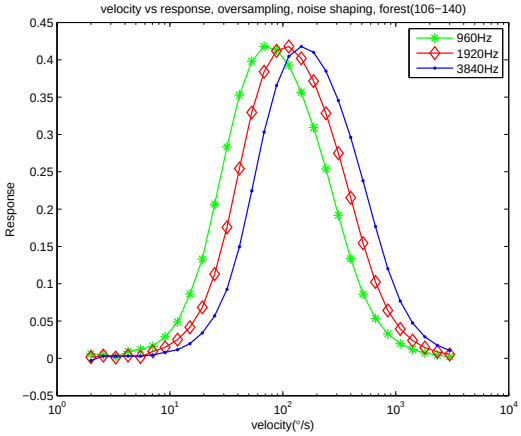

(d) Strip 4 (106-140).

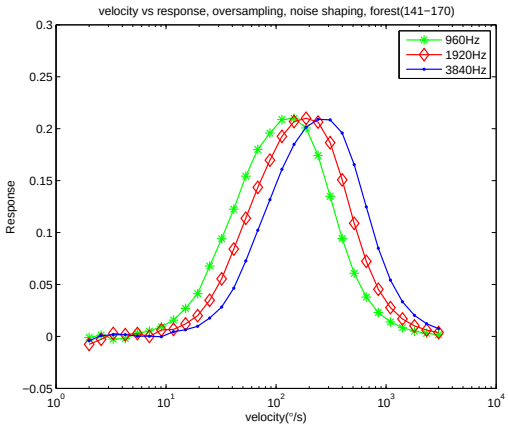

(e) Strip 5 (141-170).

Figure 4.27. The velocity estimation curves for 'forest' strips at different over-sampling rates. Through the five graphs, it can be seen that sample at higher rate, the optimum velocity which corresponds to highest response is moving to right along with the velocity axis.

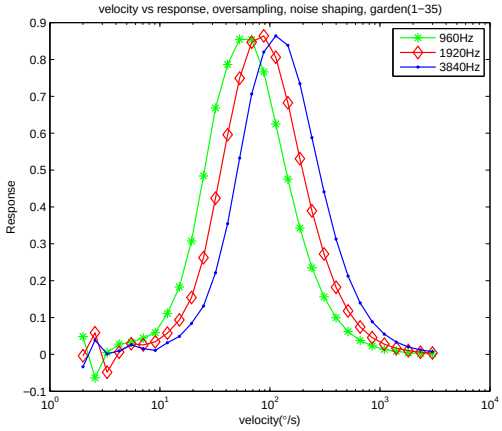

(a) Strip 1 (1-35).

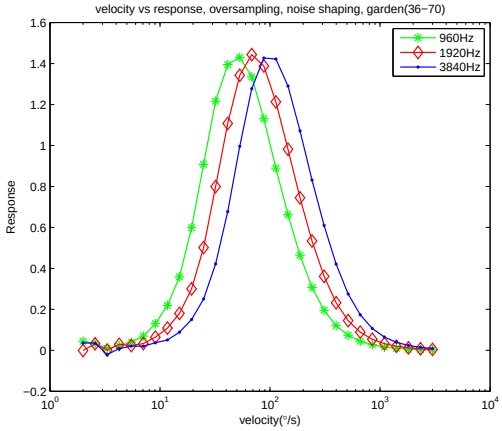

(b) Strip 2 (36-70).

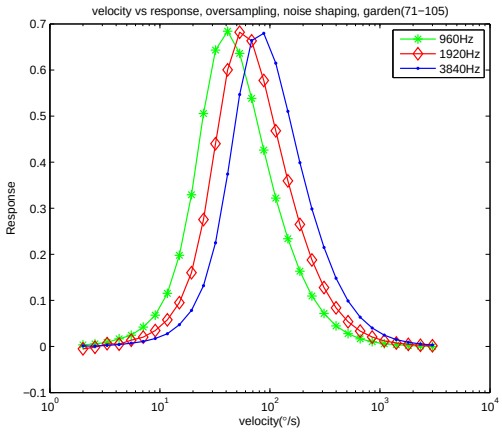

(c) Strip 3 (71-105).

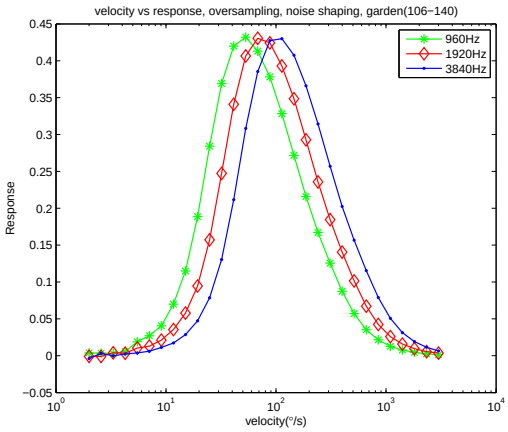

(d) Strip 4 (106-140).

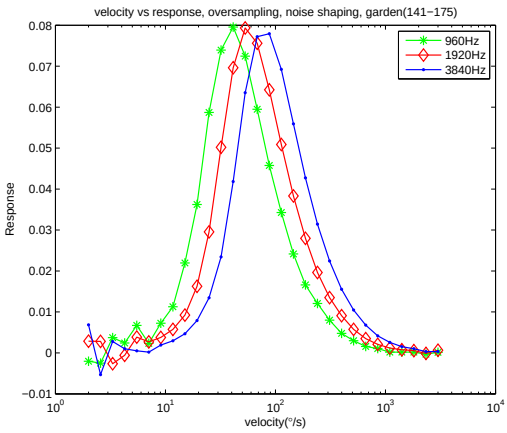

(e) Strip 5 (141-170).

Figure 4.28. The velocity estimation for 'garden' strips at different over-sampling rates. These five strips perform the same response curves like 'forest', as the over-sampling rate is changed.

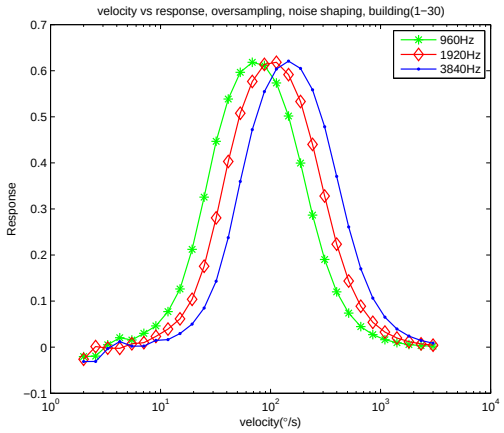

(a) Strip 1 (1-35).

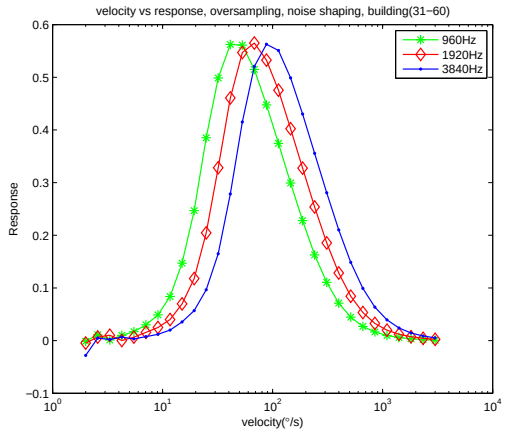

(b) Strip 2 (36-70).

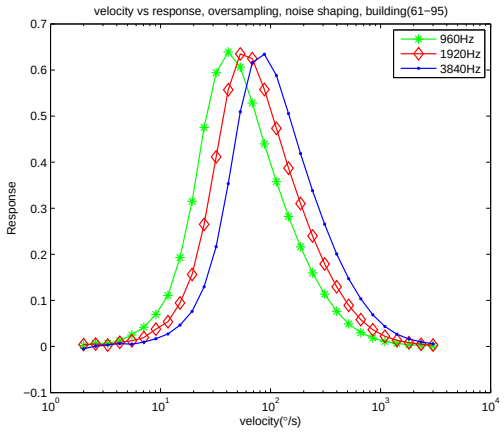

(c) Strip 3 (71-105).

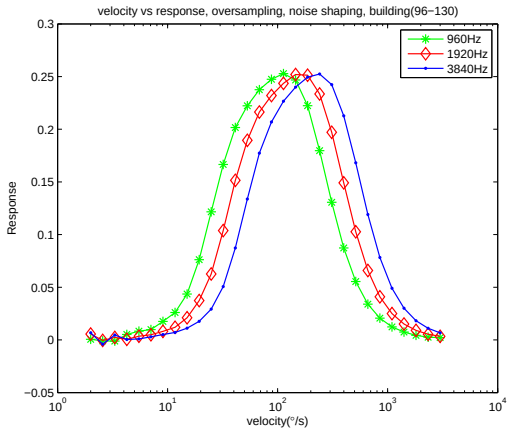

(d) Strip 4 (106-140).

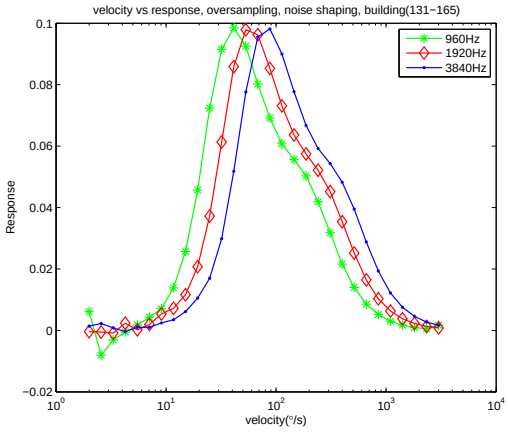

(e) Strip 5 (141-170)

Figure 4.29. The velocity estimation for 'building' strips at different over-sampling rates. The same effect on response curves when changing the over-sampling rate can still be seen from these five graphs.

can be seen see that all the curves have bell-like shape, and for velocity from $1^\circ/s$ to $3000^\circ/s$, the output responses rise from zero to a peak value and then decreasing to zero gradually. Since the simulation is aimed at objects moving from left to right, all the mean output responses have positive values. For the different images but at the same sampling rate, the responses share almost the same optimal velocity, corresponding to the same peak response. When sampling rate is 960 Hz, the optimal velocities are expressed in green line with asterisk and found to be in the range of $40^\circ/s$ to $50^\circ/s$. For 1920 Hz, the optimal velocities are expressed in red line with diamond and found to be in the range of $60^\circ/s$ to $70^\circ/s$, and for 3840 Hz, the optimal velocities are expressed in blue line with dot and found to be in the range of $100^\circ/s$ to $110^\circ/s$. In other words, when higher sampling rates are adopted, higher velocities can be detected. However, some oscillations can be observed in the responses, such as Figure 4.28 (e), and Figure 4.29 (d). This inaccurate performance lead to inaccurate velocity estimates in the low velocity range ($v < 10^\circ/s$). These inaccuracies are caused by the lack of image feature contain in image. Since the images are divided into five strips, it is observed that the inaccuracy often occurs in the simulation for bottom or top strips. For example, 'garden' image, the top and bottom strips contain mostly information for the sky or ground, in contrast to the middle strips, which contains mostly trees. After using 1-bit depth representation in these strips, the top and bottom strips are represented by white and black, and do not show many significant changes along the strips. Furthermore, at high oversampling rates, the sampling interval is much reduced, so, for slow motion, entire strips show few differences between successive frames, and it is often impossible to compute any meaningful response. That is the reason which causes the output response of the Reichardt Correlator to have inaccurate performance. (i.e. oscillations for low v)

After investigation into the performance of using 1-bit depth with oversampled representation and noise shaping, the velocity estimation effectiveness by the Reichardt Correlator of the proposed scheme will be simulated under two different settings: first scheme is simulation under the input samples is 8-bit representation sampled at Nyquist rate. Second scheme is simulation under the proposed scheme of using 1-bit, oversampled in 1920 Hz (32 times Nyquist rate) with noise shaping for input samples.

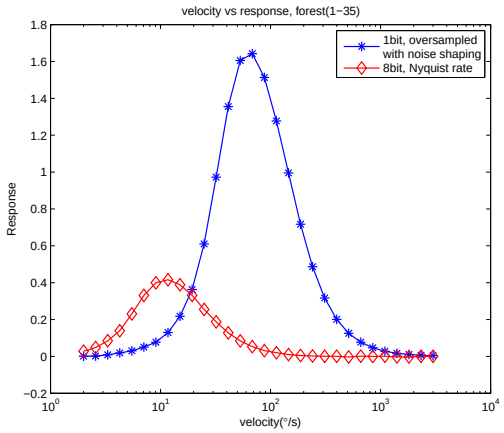

(a) Strip 1 (1-35).

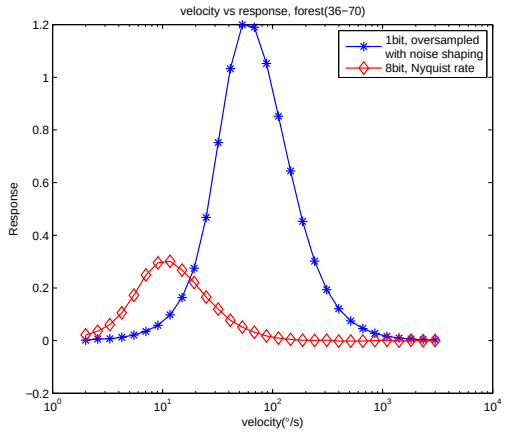

(b) Strip 2 (36-70).

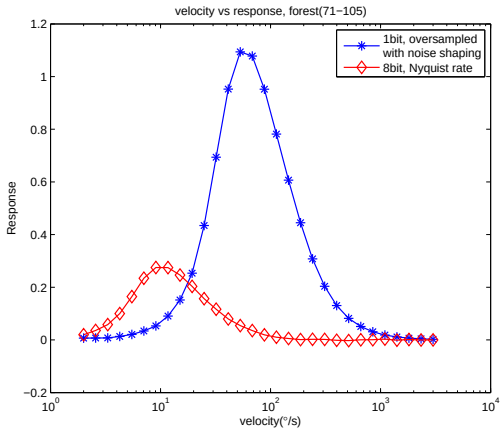

(c) Strip 3 (71-105).

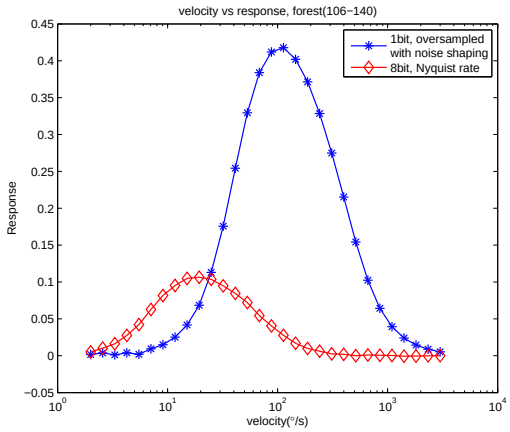

(d) Strip 4 (106-140).

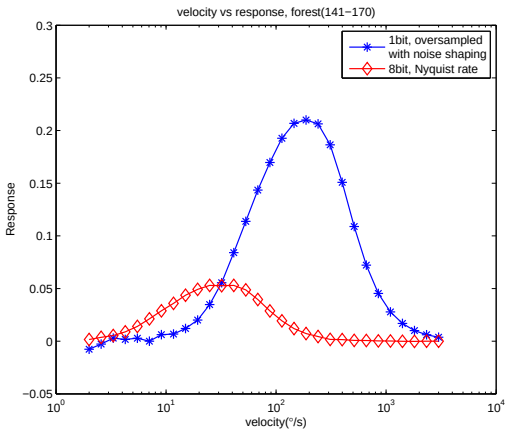

(e) Strip 5 (141-170).

Figure 4.30. The velocity estimation curves for 'forest' strips with different signal representations. These five graphs show the response curves for single bit representation with oversampling rate and 8-bit response with Nyquist rate.

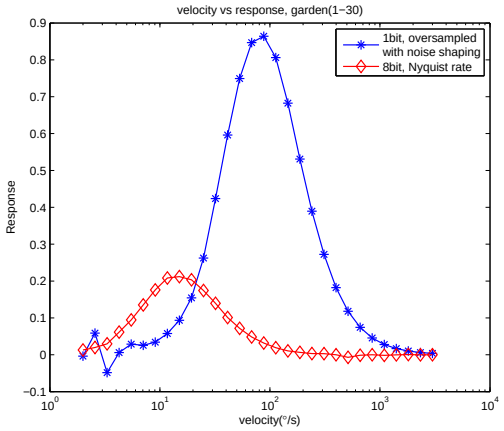

(a) Strip 1 (1-35).

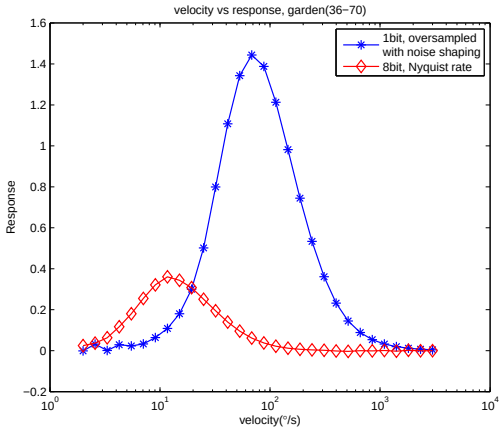

(b) Strip 2 (36-70).

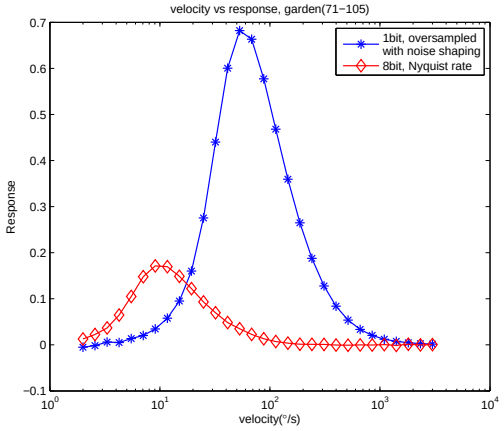

(c) Strip 3 (71-105).

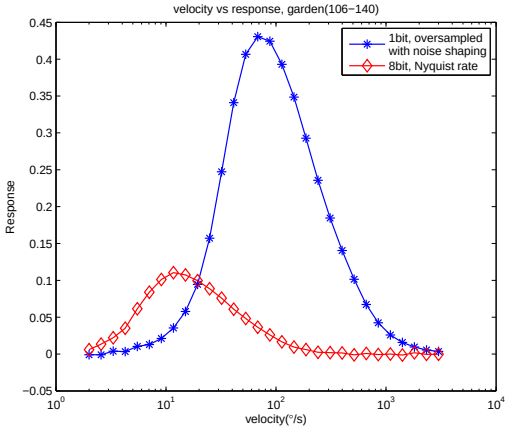

(d) Strip 4 (106-140).

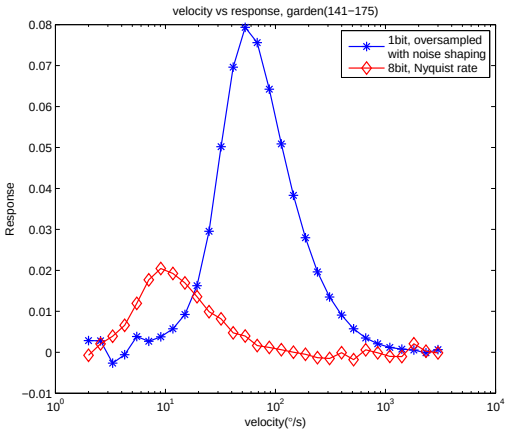

(e) Strip 5 (141-170).

Figure 4.31. The velocity estimation for 'garden' strips with different signal representations.

The same performance as 'forest'.

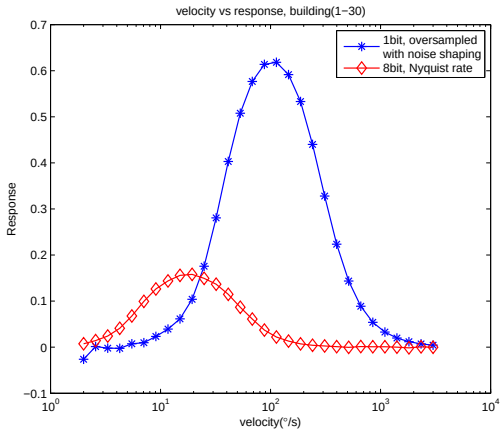

(a) Strip 1 (1-35).

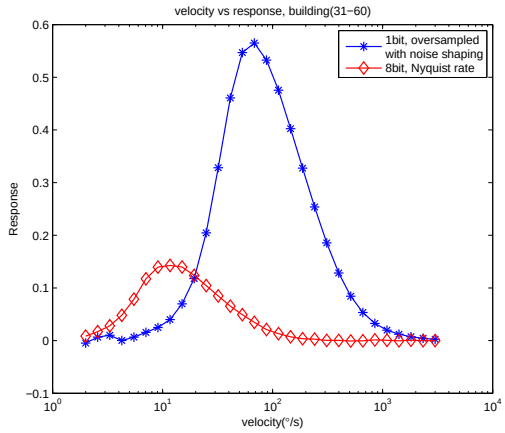

(b) Strip 2 (36-70).

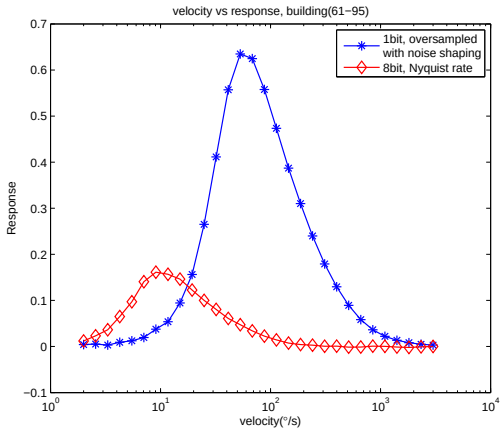

(c) Strip 3 (71-105).

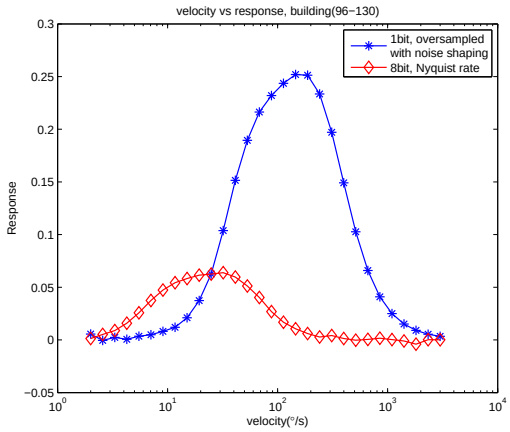

(d) Strip 4 (106-140).

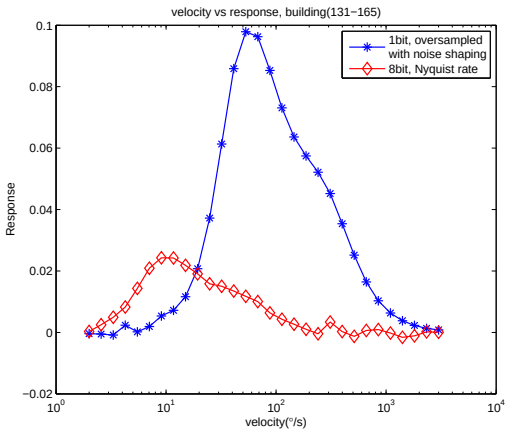

(e) Strip 5 (141-170).

Figure 4.32. The velocity estimation for 'building' image strips with different signal representations. It can be seen that the different 'building' strips are performed accurate response curves as 'forest' and 'garden'.

The responses from the two settings will be presented on one axis for each strip of images.

Figures 4.30, 4.31 and 4.32 show the velocity estimation under two different settings for the five strips of 'forest', 'garden' and 'building' images. From the three figures, we can see that all the response curves have bell-like shape and positive mean values as an accurate velocity estimation, regardless of the representation approach used. It can be seen that the red line with diamond, which corresponds to 8-bit, Nyquist rate sampled signals, the Reichardt Correlator provides lower responses than the blue line with asterisk which corresponds to the 1-bit, oversampled representation. The optimal velocities for 8-bit, Nyquist rate representation are located in the range between $10^\circ/s$ to $15^\circ/s$. However, the degradation is occurring in the low range of velocities. When using the 1-bit, oversampled representation, for low velocities ranging from $1^\circ/s$ to $20^\circ/s$ approximately, the corresponding responses are almost same. In addition, in this velocity range, the 8-bit, Nyquist sampling rate representation has the more accurate velocity estimation performance.

4.4 Summary

This chapter has presented the Reichardt Correlator response for velocity estimation from mathematical description to simulation results. In order to simplify the arithmetic complexity, we attempted to reduce the bit depth to represent the digital signals, and use oversampling to sample the digital signals. From the simulation results, the performance of the basic Reichardt Correlator which under the proposed approach of using oversampled 1-bit representation for velocity estimation is investigated, and found to offer accurate performance despite a large reduction in complexity. In the next and final chapter, we will summarise and discuss the work presented and then suggest future research directions.

Chapter 5

Conclusions and future directions

THIS chapter presents a summary of the key findings and their significance. Then the conclusions will be discussed. The thesis will conclude with recommendations for future research.

5.1 Summary

This thesis has represent a lower bit depths at oversampled signals representation study based on the bio-inspired motion detector of the Reichardt Correlator. The lower bit depths with oversampled representation is considered to be a means to reducing the arithmetic complexity in computational implementation, and at the same time, achieving the accurate velocity estimation performance.

The background knowledge about different motion detection algorithms and the Reichardt Correlator model have been studied in Chapter 2. The proposed approaches which are using lower bit depths and oversampled representation were presented in Chapter 3. The simple 'sine grating' image, naturalistic 'friend' image and panoramic 'scenery' image were used as stimuli to implement the proposed approaches. After that, the sigma-delta conversion which operating at 1-bit oversampled representation with noise shaping was proposed to combine with the Reichardt Correlator have been studied in Chapter 3. The simulations and analysis of the proposed approaches combined with the Reichardt Correlator, and the results from the comparison between proposed and conventional representations were reported in Chapter 4.

5.2 Conclusions

Conventionally, the input signals to the Reichardt Correlator are often digitised at bit depths of 8 or greater and sampled at Nyquist rate. Its implementation requires relatively complicated arithmetic units to copy with the processing of the sample. In this thesis, we developed a different approach of signal representation that is using 1-bit, oversampled with noise shaping to compare with the conventional approach of 8-bit representation with sample at Nyquist rate. The approach of this thesis differs from many Reichardt Correlator modelling studies. Instead of improving the complex components into the basic Reichardt Correlator to elaborate it as more accuracy motion detector, the aim of this work is to devise a scheme whereby the required complexity arithmetic units can be made simpler. Therefore, the main aim of the project is not to attempt to improve the Reichardt Correlator performance, but to understand the

trade-off in performance using the Reichardt Correlator as the velocity estimator in the vision system.

The performance of the developed approaches are evaluated using Matlab simulation. The input signals sampled as 8-bit at Nyquist rate are defined as the baseline to compare with which the proposed representation of 1 bit and for oversampled signals. Simulation results show that proposed approaches outperformed the conventional approach. Compare with the conventional representation, under the reduction in arithmetic complexity, the velocity estimation results from the 1-bit oversampled representation have higher dynamic range in velocity response. Moreover, the estimation of optimal velocity is higher than the conventional approach, the optimal velocity in the approach of 1-bit oversampled representation is $100^\circ/s$ to $110^\circ/s$ compared with $10^\circ/s$ to $15^\circ/s$ of optimal velocity estimation in 8-bit at Nyquist rate. However, the higher optimal velocity estimation is trade-off against the accurate estimation in the lower velocity range of $1^\circ/s$ to $20^\circ/s$. From the consideration of reducing system arithmetic complexity and achieving the accurate motion detection performance, the proposed approach is shown that a 1-bit oversampled representation can obtain accurate velocity estimation performance when combined with the basic Reichardt Correlator.

5.3 Future work

The approach of using 1-bit oversampled representation for the input signal to the basic Reichardt Correlator offered reasonable performance in velocity estimation. The analysis and simulation results show that the approach outperforms than the 8 bit, Nyquist sampled rate signal. However, some aspects of the approach still need to be improved.

Firstly, the reliability of the proposed system performance is still affected by the image conditions. For applications where the image contains multiple spatial frequencies, or the contrast is changing, the system can occasionally yield unreliable performance. In this case, the output responses are often different with the same velocity. Therefore, developing an adaptive algorithm for suitable the different image conditions need to be done in the future work.

In addition, when using 1-bit oversampled representation, the faster velocities can be detected. However, this comes with it a trade-off against the low velocities' range detected. Moreover, for low velocities, the 8 bit, Nyquist rate representation has accurate and reliable performance. Future work can be conducted to address this concern, with perhaps further elaboration of the Reichardt Correlator model.

The 1-bit oversampled signal representation combined with the Reichardt Correlator can not only provide the reduction in system arithmetic complexity, but also obtain the accurate velocity estimation performance. It is anticipated that more and more bio-inspired vision detection systems can utilise 1-bit oversampled representations and novel applications will arrive. However, there are still many challenges in bio-inspired vision detection system, and future work should be carried out to make this technology really progress beyond laboratory demonstrations.

Appendix A

Matlab Code

IN the course of this thesis, I performed repeated simulations of the Reichardt Correlator responses to images in Matlab. The Matlab code which is used to simulate the performance of the combined Reichardt Correlator (Figure 4.24) is attached in the appendix.

A.1 Matlab code 1: first order Sigma-Delta conversion

```
%-------------------------------------------------%
%-------first order Sigma-Delta conversion-------%
%-------------------------------------------------%

function y = sigma_delta_1st(x)

x=(double(x)-128)/128;  %used to make the value x between -1 and +1
y=zeros(size(x)); w1=y; y(1)=-1; for idx = 2:length(x)
    ytmp=w1(idx-1);
    y(idx) = 2*(ytmp>=0)-1;
    w1(idx)=x(idx)-y(idx)+w1(idx-1);
end y=int8(y);
```

A.2 Matlab code 2: the combined Reichardt Correlator with 1-bit oversampling interface

```
%-------------------------------------------------%
%-------the combined Reichardt Correlator-------%
%-------------------------------------------------%
clc;
clear;
tic;

%--------------variable declaration--------------%
tau=0.035;   %time constant in first order low-pass filter 35ms
delphi=1.08;   %spatial distance between two receptors (degree units)

%-----loops the contrasts to get Velocity response for each contrast-----%
%for contrast=0.3:0.3:1; %contrast vary from 0 to 1
```

```
contrast=1;
velocity_vector=logspace(log10(2),log10(3000),30);   %degrees per second
Response=[];%an empty cell array to store total responses for each velocity
i=1;%used to increase the Response array so that every addition to it will
    %be at the end of the array

%--------LOOPS THROUGH THE VELOCITY VECTOR--------%
for loop_counter=1:length(velocity_vector)
    velocity = velocity_vector(loop_counter);
    disp(['Iteration: v= ' num2str(velocity)])

%--------Reads an image into data using imread--------%
Image_data = imread('forest.png'); %input image
w=length(Image_data);  %in pixel units
pixels_per_degree = w/360;  %panoramic image
v=velocity*pixels_per_degree;  %velocity in pixels per second

%-------Nyquist rate & oversampling rate declaration--------%
%        fs=60;    %Nyquist rate  'b--'
%        fs=960;   %16x  'k'
        fs=1920;  %32x    'b'
%        fs=3840;  %64x   'r'

%        variable=v/fs;
       dist=round(delphi*pixels_per_degree); %distance in pixel units
       x0=1; %starting point
       n=1:1:floor(w /(( 2*pixels_per_degree) / fs ));

%----------Correlates first row of the data----------%
       R=1;
       disp(['Iteration: ' num2str(R)])
```

```
       data=Image_data(R,:);  % image data to read in the current row only


%----------------linear interpolation in s1----------------%
s1t=x0+(v/fs).*n;
  if floor(s1t)<w
     w1_s1=double(data(floor(s1t)));
     w2_s1=double(data(floor(s1t)+1));
     a_s1=s1t-floor(s1t);
     s1=(1-a_s1).*w1_s1+a_s1.*w2_s1 ;   % if data_data is not integer
  else
     s1t=mod(floor(s1t-1),w)+1;
     w1_s1=double(data(floor(s1t)));
     w2_s1=double(data(floor(s1t-1)+1));
     a_s1=s1t-floor(s1t);
     s1=(1-a_s1).*w1_s1+a_s1.*w2_s1 ;  % if data_data is not integer
  end
     S1=double(s1);


%----------------quantisation----------------%
        s11=mat2gray(S1)*255;
%        s11 = mat2gray(floor(s11/128)); %1bit
%        s11 = mat2gray(floor(s11/128)); %2bit
%        s11 = mat2gray(floor(s11/128)); %3bit
%        s11 = mat2gray(floor(s11/128)); %4bit
%        s11 = mat2gray(floor(s11/128)); %5bit
%        s11 = mat2gray(floor(s11/128)); %6bit
%        s11 = mat2gray(floor(s11/128)); %7bit
%        s11 = mat2gray(floor(s11/1)); %8bit


%----------------sigma-delta conversion----------------%
%   s1s=s11*contrast;   % no sigma-delta conversion 'rd'
```

```
    s1s=double(sigma_delta_1st(s11));  % sigma-delta conversion 'b*'

%----------------linear interpolation in s2----------------%
s2t=x0+(v/fs).*n+dist;
  if floor(s2t)<w
     w1_s2=double(data(floor(s2t)));
     w2_s2=double(data(floor(s2t)+1));
     a_s2=s2t-floor(s2t);
     s2=(1-a_s2).*w1_s2+a_s2.*w2_s2 ;  % if data_data is not integer
  else
     s2t=mod(floor(s2t-1),w)+1;
     w1_s2=double(data(floor(s2t)));
     w2_s2=double(data(floor(s2t-1)+1));
     a_s2=s2t-floor(s2t);
     s2=(1-a_s2).*w1_s2+a_s2.*w2_s2 ;  % if data_data is not integer
  end
     S2=double(s2);

%----------------quantisation----------------%
        s22=mat2gray(S2)*255;
%        s22 = mat2gray(floor(s22/128)); %1bit   'r*-'
%        s22 = mat2gray(floor(s22/128)); %2bit
%        s22 = mat2gray(floor(s22/128)); %3bit
%        s22 = mat2gray(floor(s22/128)); %4bit
%        s22 = mat2gray(floor(s22/128)); %5bit
%        s22 = mat2gray(floor(s22/128)); %6bit
%        s22 = mat2gray(floor(s22/128)); %7bit
%        s22 = mat2gray(floor(s22/1)); %8bit   'r:d'

%----------------sigma-delta conversion----------------%
%       s2s=s22*contrast;   %no sigma-delta conversion
```

```
        s2s=double(sigma_delta_1st(s22));   % sigma-delta conversion

%----------low-pass filter butterworth----------%
%-------uses convolution with Butterworth filter-------%
sample_rate=v;   % pixels per second
cutoff=1;
order=1;   % order of the filter
Wn=cutoff/(sample_rate/2);
[b,a]=butter(order,Wn);   % Butterworth IIR filter
s1d=filter(b,a,s1s);   %signal delayed by filter
s2d=filter(b,a,s2s);   %signal delayed by filter

%--------output of correlator--------%
corA=25.*s1d.*s2s;
corB=25.*s2d.*s1s;
totalCor=corB-corA;   %prepares an array for concatanation of other rows

%--------correlation for the rest of rows--------%
 for  R=2:35
      disp(['Iteration: ' num2str(R)])
      data = Image_data(R,:);  % image data to read in the current row only

%----------------linear interpolation in s1----------------%
s1t=x0+(v/fs).*n;
  if floor(s1t)<w
     w1_s1=double(data(floor(s1t)));
     w2_s1=double(data(floor(s1t)+1));
     a_s1=s1t-floor(s1t);
     s1=(1-a_s1).*w1_s1+a_s1.*w2_s1 ;  % if data_data is not integer
  else
     s1t=mod(floor(s1t-1),w)+1;
```

```
    w1_s1=double(data(floor(s1t)));
    w2_s1=double(data(floor(s1t-1)+1));
    a_s1=s1t-floor(s1t);
    s1=(1-a_s1).*w1_s1+a_s1.*w2_s1 ;  % if data_data is not integer
  end
    S1=double(s1);

%----------------quantisation----------------%
       s11=mat2gray(S1)*255;
%        s11 = mat2gray(floor(s11/128)); %1bit
%        s11 = mat2gray(floor(s11/128)); %2bit
%        s11 = mat2gray(floor(s11/128)); %3bit
%        s11 = mat2gray(floor(s11/128)); %4bit
%        s11 = mat2gray(floor(s11/128)); %5bit
%        s11 = mat2gray(floor(s11/128)); %6bit
%        s11 = mat2gray(floor(s11/128)); %7bit
%        s11 = mat2gray(floor(s11/1)); %8bit

%----------------sigma-delta conversion----------------%
%    s1s=s11*contrast;  %no sigma-delta conversion
    s1s=double(sigma_delta_1st(s11)); %sigma-delta conversion

%----------------linear interpolation in s2----------------%
  s2t=x0+(v/fs).*n+dist;
  if floor(s2t)<w
    w1_s2=double(data(floor(s2t)));
    w2_s2=double(data(floor(s2t)+1));
    a_s2=s2t-floor(s2t);
    s2=(1-a_s2).*w1_s2+a_s2.*w2_s2 ;  % if data_data is not integer
  else
    s2t=mod(floor(s2t-1),w)+1;
```

```
    w1_s2=double(data(floor(s2t)));
    w2_s2=double(data(floor(s2t-1)+1));
    a_s2=s2t-floor(s2t);
    s2=(1-a_s2).*w1_s2+a_s2.*w2_s2 ;  % if data_data is not integer
  end
    S2=double(s2);

%----------------quantisation----------------%
       s22=mat2gray(S2)*255;
%        s22 = mat2gray(floor(s22/128)); %1bit   'r*-'
%        s22 = mat2gray(floor(s22/128)); %2bit
%        s22 = mat2gray(floor(s22/128)); %3bit
%        s22 = mat2gray(floor(s22/128)); %4bit
%        s22 = mat2gray(floor(s22/128)); %5bit
%        s22 = mat2gray(floor(s22/128)); %6bit
%        s22 = mat2gray(floor(s22/128)); %7bit
%        s22 = mat2gray(floor(s22/1)); %8bit   'r:d'

%----------------sigma-delta conversion----------------%
%       s2s=s22*contrast;   %no sigma-delta conversion
        s2s=double(sigma_delta_1st(s22));  %sigma-delta conversion

%----------low-pass filter butterworth----------%
%-------uses convolution with Butterworth filter-------%
sample_rate = v;   % pixels per second
cutoff=1;
order = 1;   % order of the filter
Wn = cutoff/(sample_rate/2);
[b,a] = butter(order,Wn);   % Butterworth IIR filter
s1d = filter(b,a,s1s);   %signals delayed by filter
s2d = filter(b,a,s2s);
```

```
%--------output of correlator A,B (half correlator)--------%
corA=25.*s1d.*s2s;
corB=25.*s2d.*s1s;
Cor=corB-corA;%prepares an array for concatanation of other rows of arrays

totalCor=cat(1,totalCor,Cor);  %concantantes all rows into one array
 end

%---------------response vs velocity---------------%
MeanCor=mean(totalCor,2);   %means the response
MeanCor2=mean(MeanCor);
Response{1,i}=MeanCor2;   %stores the repsonse in the array
i=i+1;   %increases i to increase array position


end   %end of velocity_vector;

Response1 = cell2mat(Response);%convert cell array to single matrix
semilogx(velocity_vector,Response1);%plots veloctiy versus response
xlabel('velocity(\circ/s)');%x lable
ylabel('Response');%y lable
title('velocity vs response, forest')
hold on;%holds figure to plot repeatedly on same figure
toc;
% end  % end of contrast loop
```

A.3 Brief instruction on the Matlab code

The Matlab version is v7.6 or later versions. Matlab code 1 is implemented the Sigma-Delta conversion, which is used to quantise the input signal value between -1 and

+1. Matlab code 2 is implemented the combine Reichardt Correlator with 1-bit oversampling interface. As shown in Figure 4.24, the code is contained the functions of apperceive the signal, sampling and interpolating, quantisation and noise shaping, delay, 1-bit multiply, subtract, and plot the response curves. The different input images can be input in the syntax of Image_data=imread('input image'), different oversampling rates are listed in the sampling rate declaration, the responses and velocities are semilogarithmic plotted using syntax of semilogx(velocity_vector, Response1).

Bibliography

[1] M. Shell. (2007) How to use the ieeetran bibtex style. IEEE.

[2] S. Rajesh, D. O. Carroll, and D. Abbott, "Man-made velocity estimator based on insect vision," *Smart Mater. Struct*, vol. 14, pp. 413–424, 2005.

[3] K. Hausen and M. Egelhaaf, *Facets of Vision*, N. mechanisms of visual corse control in insects. In D. G. Stavenga and R. C. Hardie, Eds. Springer-Verlag, Heidelberg, 1989.

[4] J. Gibson, *The Perception of the visual world*. Boston: Greenwood Pub Group, 1950.

[5] H.Schöne, "Optokinetic speed control and estimation of travel distance in walking honeybees," *J. Comp. Physiol*, vol. A,179, pp. 587–592, 1996.

[6] M. V. Srinivasan and S. Venkatesh, *From Living Eyes to Seeing Machines*, M. V. Srinivasan and S. Venkatesh, Eds. Oxford University Press, 1997.

[7] R. Kern, M. Egelhaaf, and M. V. Srinivasan, "Edge detection by landing honeybees: behavioural analysis and model simultions of the underlying mechanism," *Vision Research*, vol. 37, pp. 2103–17, 1997.

[8] M. Lehrer, M. V. Srinivasan, S. W. Zhang, and G. A. Horridge, "Motion cues provides the bee's visual world with a third dimension," *Nature*, vol. 332, pp. 356–7, 1988.

[9] M. V. Srinivasan, S. W. Zhang, M. Lehrer, and T. S. Collett, "Honeybee navigation en route to the goal: visual flight control and odometry," *J. Exp. Biol*, vol. 199, pp. 237–44, 1996.

[10] N. Franceschini, J. M. Pichon, and C. Blanes, "From insect vision to robot vision," *Phil. Trans. Roy. Soc. Lon.*, vol. B,337, pp. 283–94, 1992.

[11] S. Mota, E. Ros, E. M. Ortigosa, and F. J. Pelayo, "Bio-inspired motion detection for blind sopt overtaking monitor," *Int. J. Robot. Autom.-Special Issue of Neuromorphic system*, vol. 19, no. 4, p. 2713, 2004.

[12] F. Aubpart and N. Franceschini, "Bio-inspired optic flow sensors based on fpga: Application to micro-air-vehicles," *Microprocessors and Microsystems*, vol. 31, no. 6, pp. 408 – 419, 2007, special Issue on Sensor Systems.

[13] S. Rajesh, D. C. O'Carroll, and D. Abbott, "Elaborated reichardt correlators for velocity estimation tasks," *Proceedings of SPIE*, vol. 4937, pp. 241–253, 2002.

[14] M. Egelhaaf and A. Borst, "Transient and steady-state response properties of movement detectors," *J. Opt. Soc. Am*, vol. A, 6, pp. 116–27, 1989.

[15] W. Reichardt, *Autocorrelation, a principle for the evaluation of sensoty information by the central nervous system*, A. Rosenblith, Ed. New York: MIT Oress and John Wiley and Sons, 1961, vol. in Sensory Communication.

[16] M. Egelhaaf, A. Borst, and W. Reichardt, "Computational structure of a biological motion-detection system as revealed by local detector analysis in the fly's nervous system." *J. Opt. Soc. Am.*, vol. A, 6, pp. 1070–87, 1989.

[17] D. C. O. Carroll, S. B. Laughlin, N. J. Bidwell, and E. J. Warrant, "Insect motion detectors matched to visual ecology," *Nature*, vol. 382, pp. 63–6, 1996.

[18] A. Borst, C. Reisenman, and J. Haag, "Adaptation of response transients in fly motion vision. ii: Model studies," *Vision Research*, vol. 43, pp. 1331–1324, 2003.

[19] E. H. Adelson and J. R. Bergen, "Spatiotemporal energy models for the perception of motion," *J. Opt. Soc. Am.*, vol. A, 2, pp. 284–99, 1985.

[20] F. Wolf-Oberhollenzer and K. Kirschfeld, "Motion sensitivity in the nucleus of the basal optic root of the pigeon," *J. Neurophysiology*, vol. 71, pp. 1559–73, 1994.

[21] A. Moini, *Vision Chips*. Kluwer Academic Publishers,Massachusett, 2000, part I.

[22] R. O. Dror, "Accuracy of visual velocity estimation by reichardt correlator," A thesis for the degree of Master of Philosophy, University of Cambridge, August 1998, chapter 2.

[23] S. Al-Sarawi, T. Rainsford, and A. Bender, "Review of bioinspired real-time motion analysis systems," *in Proc. SPIE, BioMEMS and Nanotechnology II*, vol. 6036, pp. 237–251, 2005.

[24] R. R. Harrison and C. Koch, "A robust analog VLSI reichardt motion sensor," *Analog Integrated Circuits and Signal Processing*, vol. 24, pp. 213–229, 2000.

[25] J. Wang, "A theory of image matching." Proc, 3rd IEEE Int. Conf. Computer Vision, 1990, pp. 200–209.

[26] S. Bohrer, H. Bulthoff, and H. Mallot, "Motion detection by correlation and voting," *Parallel Processing in Neural Systems and Computer*, pp. 471–474, 1990.

[27] C. L. Fennema and W. B. Thompson, "Velocity determination in scenes containing several moving objects," *Computer Vision, Graphics, and Image Processing*, vol. 9, pp. 301–315, 1992.

[28] R. A. Deutschmann and C. Koch, "Compact real-time 2d gradient-based analog vlsi motion sensor," T. M. Bernard, Ed., vol. 3410, no. 1. SPIE, 1998, pp. 98–108.

[29] B. K. Horn and B. G. Schunck, "Determining optical flow," *Artificial Intelligence*, vol. 17, no. 1-3, pp. 185 – 203, 1981.

[30] A. Borst and M. Egelhaaf, "Princples of visual motoin detection," *TINS*, vol. 12, pp. 297–306, 1989.

[31] R. M. Haralick and L. G. Shapiro, *Computer and Robot Vision*, 1st ed. Boston, MA, USA: Addison-Wesley Longman Publishing Co., Inc., 1992, vol. 1.

[32] S. Smith and J. Brady, "Susan-a new approach to low level image processing," *International Journal of Computer Vision*, vol. 23, pp. 45–78, 1997.

[33] L. A. Spacek, "Edge detection and motion detection," *Image Vision Comput.*, vol. 4, no. 1, pp. 43–56, 1986.

[34] T. Komuro, I. Idaku Ishii, M. Ishikawa, and A. Yoshida, "A digital vision chip specialized for high-speed target tracking," *IEEE Transactions on Electron Devices*, vol. 50, pp. 191–199, Jan. 2003.

[35] G. A. Horridge, "A template theory to relate visual processing to digital circuitry," *Proceedings of the Royal Society of London. Series B, Biological Sciences*, vol. 239, no. 1294, pp. 17–33, 1990.

[36] C. Clifford and K. Langley, "A model of temporal adaptation in fly motion vision," *Vision Research*, vol. 36, pp. 2595–2608, 1996.

[37] R. A. Harris, D. C. O'Carroll, and S. B. Laughlin, "Adaptation and the temporal delay filter of fly motion detectors," *Vision Research*, vol. 39, pp. 2603–13, 1999.

[38] M. J. M. Lankheet, A. J. van Doorn, and W. A. van de Grind, "Spatio-temporal tuning of motion coherence detection at different luminance levels," *Vision Research*, vol. 42, no. 1, pp. 65 – 73, 2002.

[39] A. Spinei, D. Pellerin, and J. Hérault, "Spatiotemporal energy-based method for velocity estimation," *Signal Process.*, vol. 65, no. 3, pp. 347–362, 1998.

[40] J. G. Proakis and M. Salehi, *Communication Systems Engineering*. Prentice Hall, 1994.

[41] S.-C. Liu, "A neuromorphic avlsi model of global motion processing in the fly," *Circuits and Systems II: Analog and Digital Signal Processing, IEEE Transactions on*, vol. 47, no. 12, pp. 1458–1467, Dec 2000.

[42] R. Etienne-Cummings, "Biologically inspired visual motion detection in vlsi," *Int. J. Comput. Vision*, vol. 44, no. 3, pp. 175–198, 2001.

[43] G. Indiveri and R. Douglas, "Neuromorphic vision sensors," *Science*, vol. 288, no. 5469, pp. 1189–1190, May 2000.

[44] S. B. Laughlin, "Matching coding, circuits, cells and molecules to signals: general principles of retinal design in the fly's eye," *Progress in Retinal Research*, vol. 13, pp. 165–195, 1994.

[45] J. K. Douglass and N. J. Strausfeld, "Visual motion detection circuits in files: peripheral motion computaion by identified small-field retinotopic neurons," *Journal of Neuronscience*, vol. 15, pp. 5596–5611, 1995.

[46] E. Buchner, "Elementary movement detectors in an insect visual system," *Biol. Cybern.*, vol. 24, pp. 85–101, 1976.

[47] M. Egelhaaf and W. Reichardt, "Dynamic response properties of movement detectors: theoretical analysis and electrophysiological investigation in the visual system of the fly," *Biol. Cybern.*, vol. 56, pp. 69–87, 1987.

[48] M. V. Srinivasan, M. Lehrer, W. H. Kircher, and S. W. Zhang, "Range perception through apparent image speed in freely flying honeybees," *Visual Neuroscience*, vol. 6, pp. 519–35, 1991.

[49] J. Allik and A. Pulver, "Contrast response of a movement-encoding system," *J. Opt. Soc. Am.*, vol. A, 12, pp. 1185–97, 1995.

[50] E. Nakamura, M. Ichimura, and K. Sawada, "Fast global motion estimation algorithm based on elementary motion detectors," in *Image Processing. 2002. Proceedings. 2002 International Conference on*, vol. 2, 2002, pp. II–297–II–300 vol.2.

[51] R. O. Dror, D. C. O'Carroll, and S. B. Laughlin, *The role of natural image statistics in biological motion estimation*, ser. Lecture Notes in Computer Science. Springer Berlin / Heidelberg, May 2000, vol. 1811.

[52] M. V. Srinivasan, M. Poteser, and K. Kral, "Motion detection in insect orientation and navigation," *Vision Research*, vol. 39, no. 16, pp. 2749 – 2766, 1999.

[53] A. Moini, A. Bouzerdoum, K. Eshraghian, A. Yakovleff, X. T. Nguyen, A. Blanksby, R. Beare, D. Abbott, and R. Bogner, "An insect vision-based motion detection chip," *Solid-State Circuits, IEEE Journal of*, vol. 32, no. 2, pp. 279–284, Feb 1997.

[54] S. Mota, E. Ros, E. M. Ortigosa, R. Agis, and R. Carrillo, "Real-time visual motion detection of overtaking cars for driving assistance using fpgas," *Lecture Notes in Computer Science*, vol. 3203, pp. 1158–1161, 2004.

[55] M. B. Reiser and M. H. Dickinson, "A test bed for insect-inspired robotic control," *Royal Society of London Philosophical Transactions Series A*, vol. 361, pp. 2267–2285, Oct. 2003.

[56] C. Higgins and V. Pant, "A biomimetic vlsi sensor for visual tracking of small moving targets," *Circuits and Systems I: Regular Papers, IEEE Transactions on*, vol. 51, no. 12, pp. 2384–2394, Dec. 2004.

[57] B. Hassenstein and W. Reichardt, "Systemtheoretische analyse der zeit-, reihenfolgen- und vorzeichenauswertung bei der bewegungsperzeption des rsselkfers chlorophanus," *Zeitschrift fr Naturforschung B*, vol. 11, no. 9, pp. 513–524, 09 1956.

[58] R. O. Dror, D. C. O'Carroll, and S. B. Laughlin, "Accuract of velocity estimation by reichardt correlators," *J. Opt. Soc. Am. A*, vol. 18, pp. 241–52, 2001.

[59] X. J. Tan, S. Chong, T. Rainsford, and S. Al-Sarawi, "Motion detection with a view toward vlsi implementation," S. F. Al-Sarawi, Ed., vol. 6414, no. 1. SPIE, 2006, p. 64141S.

[60] M. Bar, "Visual objects in context," *Nature Reviews Neuroscience*, vol. 5, pp. 617–620, August 2004.

[61] S. Johnson, *Stephen Johnson on Digital Photography, Chapter 2*. O'Reilly, 2006.

[62] P. Aziz, H. Sorensen, and J. vn der Spiegel, "An overview of sigma-delta converters," *Signal Processing Magazine, IEEE*, vol. 13, no. 1, pp. 61–84, Jan 1996.

[63] H. Inose and Y. Yasuda, "A unity bit coding mentod by negative feedback," *Proc. IEEE*, vol. 51, pp. 1524–1535, 1963.

[64] V. Madisetti and D. B. Williams, *The digital signal processing handbook, Chapter 3*. CRC Press, 1998.

[65] M. F. Land and H. M. Eckert, "Maps of the acute zones of fly eyes," *J. Comp. Physiol. A*, vol. 156, pp. 525–538, 1985.

[66] R. A. Harris and D. C. O'Carroll, "Contrast gain reduction in fly motion adaptation," *Neuron*, vol. 28, pp. 595–606, 2000.

[67] R. C. Gonzalez, R. E. Woods, and S. L. Eddins, *Digital Image Processing Using MATLAB*. Upper Saddle River, N. J. : Pearson Prentice Hall, 2004.

[68] Y. Jiang, K. Zhou, and S. He, "Human visual cortex response to invisible chromatic flicker," *Nature Neuroscience*, vol. 10, no. 5, pp. 657–662, 2007.